Aalto University
School of Engineering

Aleksi Mäki

Demand response of space heating using model predictive control in an office building

Master's Thesis
Aalto University
School of Engineering
Department of Energy Technology

Thesis submitted as a partial fulfillment of the requirements
for the degree of Master of Science in Technology

Espoo, 7.11.2018
Supervisor: Professor Risto Kosonen
Advisor: D.Sc. Juha Jokisalo

Aalto University
School of Engineering

Aalto University, P.O. BOX 11000, 00076 AALTO
www.aalto.fi

Abstract of master's thesis

Author Aleksi Mäki

Title of thesis Demand response of space heating using model predictive control in an office building

Degree programme Energy Technology

Major HVAC Technology **Code** K3008

Thesis supervisor Professor Risto Kosonen

Thesis advisor D.Sc. Juha Jokisalo

Date 7.11.2018 **Number of pages** 106+1 **Language** English

Decreasing the CO_2 emissions of building stock plays a remarkable role in the mitigation of global warming. The share of building sector from both the global final energy use and CO_2 emissions is about 30%. Demand response of electricity and district heating provides one tool for decreasing emissions in the whole energy system. In demand response the buildings energy use is controlled so that the peak-load consumption in the energy grid decreases and the consumption profile stabilizes. CO_2 emissions are reduced since the need for emission-intensive peak-demand generation decreases. The building owners benefit from the energy cost savings and the energy producers from the higher grid efficiency and decreased investments for peak-demand power plants.

The main objective of this thesis was to define the potential of space heating demand response in the perspective of local thermal comfort, cost savings and energy flexibility. Demand response was implemented using a model predictive control algorithm (MPC) that optimized and controlled the space heating temperature setpoints. The MPC algorithm was tested with dynamical simulation model of an educational office building located in Aalto University campus area. The second research question was to examine how the demand response of space heating affects the local thermal comfort of occupants. The draught risk during the demand response was investigated by thermal manikin measurements in workstations near windows. To prevent the draught risk, a window surface temperature restriction was implemented in the MPC control algorithm and its influence on the demand response potential was investigated with different properties of windows.

The thermal comfort measurements showed that the draught risk increased in workstations adjacent to windows during the decreased heating power. The increase in draught risk was noticed when the window surface temperature dropped below 15 °C while the heating was turned OFF. The influence from the window surface temperature restriction on the demand response potential was found to be small. With energy efficient windows, the influence was negligible and with non-energy efficient windows the demand response potential was affected only when unnecessary high power requirements were set. Using the MPC algorithm, the annual heating cost of the case building could be decreased 4.7%. The highest energy flexibility obtained was 14%.

Keywords Demand response, thermal comfort, model predictive control, thermal manikin, multi objective optimization

Aalto-yliopisto
Insinööritieteiden korkeakoulu

Aalto-yliopisto, PL 11000, 00076 AALTO
www.aalto.fi

Diplomityön tiivistelmä

Tekijä Aleksi Mäki

Työn nimi Tilalämmityksen kysyntäjousto mallipohjaisella algoritmilla toimistorakennuksessa

Koulutusohjelma Energiatekniikka **Koodi** K3008

Työn valvoja Professori Risto Kosonen

Työn ohjaaja Tekniikan tohtori Juha Jokisalo

Päivämäärä 7.11.2018 **Sivumäärä** 106+1 **Kieli** englanti

Rakennusten hiilidioksidipäästöjen vähentämisellä voidaan edistää merkittävästi ilmastonmuutoksen torjumista, sillä rakennusten osuus kokonaisenergiankulutuksesta (ja hiilidioksidipäästöistä) maailmassa on noin 30%. Sähkön ja lämmön kysyntäjousto rakennuksissa on yksi keino koko energiajärjestelmän kasvihuonepäästöjen vähentämiseen. Kysyntäjoustossa kuluttajat muuttavat kulutustaan siten, että energiaverkon huipputehon tarve laskee ja kulutuksesta tulee stabiilimpaa. Kysyntäjousto vähentää kasvihuonepäästöjä, sillä energia- ja päästöintensiivisiä huippuvoimalaitosten käyttötarve vähenee. Kysyntäjoustosta on hyötyä rakennusten omistajille kustannussäästöjen muodossa ja energiayhtiöille investointitarpeen pienenemisenä sekä verkon hyötysuhteen paranemisena.

Tämän tutkimuksen tavoitteena oli tutkia tilojen lämmityksen kysyntäjoustopotentiaalia kustannussäästöjen, energiankäytön joustavuuden ja lämpöviihtyvyyden näkökulmasta. Lämmityksen kysyntäjousto toteutettiin tilojen lämmitystä ohjaavan mallipohjaisen algoritmin avulla. Algoritmia testattiin Aalto yliopiston kampusalueella sijaitsevaan opetusrakennukseen dynaamisen simulointityökalun avulla. Toisena tutkimuskysymyksenä oli selvittää millainen vaikutus lämmityksen kysyntäjoustolla on lokaaliin lämpöviihtyvyyteen. Tässä työssä kysyntäjouston vaikutusta vetoriskiin tutkittiin kokeellisesti lämpönuken avulla työpisteissä, jotka sijaitsivat ikkunoiden lähellä. Kylmistä ikkunapinnoista johtuvan vetoriskin välttämiseksi kysyntäjoustolle asetettiin rajoite mallipohjaisessa algoritmissa, jonka vaikutusta kysyntäjoustopotentiaaliin tutkittiin erilaisilla ikkunoiden ominaisuuksilla.

Kokeelliset lämpöviihtyvyysmittaukset osoittivat, että vetoriski ikkunoiden lähellä sijaitsevissa toimistopisteissä kasvaa, kun pattereiden tehoa lasketaan kysyntäjouston aikana. Vetoriskin huomattiin kasvavan, mikäli ikkunan pintalämpötila laski alle 15 °C, kun patterit eivät olleet päällä. Vetoriskin pienentämiseksi tehdyn rajoitteen vaikutus kysyntäjoustolla saavutettaviin kustannussäästöihin sekä energiajoustavuuteen huomattiin olevan pieni. Energiatehokkailla ikkunoilla vaikutus kysyntäjoustopotentiaaliin oli mitätön, ja huonoilla (U-arvo = 2,6 W/m^2K) ikkunoilla potentiaali laski vasta tarpeettoman suurilla lämmitystehon korotuksilla. Mallipohjaisen algoritmin avulla tutkitun toimistorakennuksen vuotuisia lämmityskustannuksia pystyttiin vähentämään noin 4.7%. lämmityksen joustavuudeksi saatiin parhaassa tapauksessa 14%.

Avainsanat Kysyntäjousto, lämpöviihtyvyys, ennustava ohjaus, lämpönukke, monitavoiteoptimointi

Preface

The building energy simulations, optimization and energy efficiency have been one of my greatest interest during my master's studies in Aalto University. For that reason, I was really excited about my master's thesis topic. The objective in demand response is to enhance the efficiency of the district heating network by decreasing the peak power demand and thus making the peak load heating plants run more seldom. This benefits the society by decreasing the emissions, heat producers by cutting off investment costs and resulting in higher network efficiencies and building owners by heat energy cost savings.

The master's thesis was part of Business Finland's REINO research project, which was founded to investigate the intelligent control strategies in the sustainable building energy systems. The REINO project involves the following co-operators Fourdeg, Granlund, Leanheat, City of Helsinki, SRV, Residentia and Energy Finland. I would like to thank the Business Finland for funding my thesis and the co-operators for interesting discussion in the meetings and in the seminar. I direct special thanks to Granlund Consulting for giving me the time to finish my thesis.

Additionally, I would like to thank people who made the master's thesis and my graduation possible. I would like to impress my greatest gratitude to my advisor D.Sc. Juha Jokisalo and my supervisor professor Risto Kosonen for their advice and support during the whole thesis process. I would like to also thank the entire HVAC team in Sähkömiehentie 4. The working atmosphere was amazing from the start and I could ask help at any time I needed. I would also like to thank Mika Vuolle and Erkki Karjalainen from Equa simulation for advising me in IDA ICE simulation program. In addition, the help I got from my friend and college from Granlund Consulting, Kristian Martin, has been invaluable.

Finally, I would like to thank my family and friends for all the support during my university studies. Above all, I want to thank my loving wife Lotta for help, listening and understanding throughout the thesis project.

Espoo 7.11.2018

Aleksi Mäki

Table of Contents

Symbols

A	$[m^2]$	window area
C	[W]	heat exchange by convection
C_a	[J/K]	heat capacitance of the air node point
C_m	J/K	heat capacitance of the mass node point
E	[W]	rate of heat exchange by evaporation
H_{ae}	[W/K]	conductance of the windows and leakage air
H_{am}	[W/K]	conductance between mass node and indoor air node point
H_{ams}	[W/K]	conductance between indoor and outdoor air node points
H_{av}	[W/K]	heat capacity flow through ventilation
H_{ms}	[W/K]	conductance between mass node and outdoor air node point
K	[W]	heat exchange by conduction
M	[W]	rate of metabolic heat production
P_n	[W/m]	radiator model and height dependent nominal power
P_{pb}	$[W/m^2]$	heating power of the body part
R	[W]	heat exchange by radiation
RES	[W]	rate of heat exchange by respiration
R_t	$[m^2K/W]$	clothing thermal resistance
S	[W]	rate of heat storage
T_a	[°C]	air temperature node point
$T_{a,ff}$	[°C]	free-floating room air temperature
$T_{a,local}$	[°C]	local air temperature
T_{ari}	[°C]	room air temperature in calibration model
T_e	[°C]	outdoor air temperature
T_{eq}	[°C]	equivalent temperature
T_{eq}	[°C]	equivalent temperature of the body part
T_h	[°C]	room air temperature
T_i	[°C]	indoor air temperature
T_m	[°C]	inlet water temperature
T_m	[°C]	mass temperature node point
T_p	[°C]	outlet water temperature
T_{pb}	[°C]	surface temperature of the body part
T_{ref}	[°C]	reference temperature according to Finnish indoor climate
T_{si}	[°C]	inner window surface temperature
T_{sk}	[°C]	skin temperature
T_{sp}	[°C]	temperature setpoint
Tu	[%]	local turbulence intensity
T_v	[°C]	supply air temperature node point
U	$[W/m^2K]$	U-value
W	[W]	rate of mechanical work accomplished
h_{pb}	$[W/m^2,K]$	heat transfer coefficient of the body part
n	[-]	radiator specific exponent/length of the prediction horizon
n_c	[-]	number of decision variables

t	[s]	time
v_{al}	[m/s]	local mean air velocity
w	[m]	radiator width
ΔT_n	[°C]	nominal over temperature
$\emptyset_{hc}$	[W]	zone heating/(cooling) power
$\emptyset_c$	[W]	convective heat loads
$\emptyset_r$	[W]	radiative heat loads

Abbreviations

ACH	Air changes per hour
AHU	Air handling unit
BAS	Building automation system
CAV	Constant air volume
CHF	Constant heat flux
CHP	Combined heat and power
CST	Constant surface temperature
DH	District heating
DHW	Domestic hot water
DR	Demand response
DSM	Demand side management
EA	Evolutionary algorithm
EV	Electric vehicle
FF	Flexibility factor
GHG	Greenhouse gas
HDHP	Hourly district heating price
HOB	Heat only boiler
HVAC	Heating ventilation and air conditioning
KPI	Key performance indicator
MOO	Multi-objective optimization
MPC	Model predictive control
MTV	Mean thermal vote
PID (controller)	Proportional-integral-derivative (controller)
PMV	Predicted mean vote
PPD	Predicted percentage of dissatisfied
RC-model	Resistance-capacitance-model
RES	Renewable energy source
SH	Space heating
TES	Thermal energy storage
TRY	Test reference year (weather data)
U.S.	United States of America
VAV	Variable air volume

1 Introduction

1.1 Background

Mitigation of the global warming is one of the greatest challenges in human history. Building sector, as one of the most remarkable energy consumers, needs to participate in decreasing of the greenhouse gas (GHG) emissions. Globally the building sector consumes over 30% of the total final energy consumption and it produces nearly 30% of the global CO_2 emissions (IEA 2015). The corresponding metrics in EU are 40% and 35%, respectively (European Commission 2017). In addition, the trend in buildings energy consumption is rising due to the population growth, increasing demand of building services and comfort and growth in the time spent indoors (Pérez-Lombard et al. 2008).

The building sector can decrease the GHG emissions in numerous ways. Demand response (DR) is one possibility which both decreases the CO_2 emissions in energy production and allows increased introduction of RES in the energy system. In demand response, building's energy demand (load) is regulated for example according to the dynamic energy price. The demand may be shifted to cheaper time periods, the expensive peak demand may be cut, or the demand may be increased during the off-peak periods when the energy is cheaper. All previous DR actions lead to more stable load in the energy grid. As a result, more intermittent RES may be introduced in both electrical and thermal grids since the demand response helps the energy network to stabilize the load and production. Without the DR, the intermittent energy generation from RES would rarely match the energy load in the network.

Decreased peak power demand reduces the need for auxiliary power plants. Since the auxiliary power plants often produce the high peak demand by combusting fossil fuels, the decreasing peak load usage decreases the CO_2 emissions. In addition to decreased peak power demand and increased possibility to utilize RES, demand response benefits the energy system by minimizing the risk of energy shortages and enhancing the efficiency and cost effectiveness of the entire network (Alimohammadisagvand et al. 2018, IEA 2018).

In the past, research and utilization of demand response has focused predominately in the electrical grids. Some recent studies have also examined the DR of other energy carriers such as district heating. This thesis aims to investigate the energy cost saving and energy flexibility potential of district heating in an educational office building in Finland. The scope is adhered to demand response of space heating.

Energy is required to maintain adequate state of thermal environment in buildings. HVAC systems such as ventilation, cooling and heating systems that maintain the thermal comfort, consume relatively much energy. According to (Dear et al. 2013) building sector constitutes 39% of total primary energy consumption in the US and of this even as much as 35% is used for space heating, ventilation and air-conditioning. Although effort is made to reduce the energy consumption of building sector, energy savings should not be pursued at the expense of the thermal environment conditions.

The interest in demand response in both electricity and district heating has mainly been in the economic and environmental aspects. However, the buildings are built for people and DR's influence on the indoor environment quality should have higher focus in the research. In the DR studies dealing with space heating, the influence of DR in thermal comfort has often been limited to the overall thermal comfort by determining range of allowed indoor air temperatures. The local thermal comfort issues such as draught and temperature fluctuations are often neglected. In this thesis, the influence of space heating DR to the local thermal discomfort caused by draught is investigated in the office workstations adjacent to windows.

1.2 Research objective

The main objective of this thesis was to study demand response of space heating in an educational office building heated by district heating in the perspective of local thermal comfort, cost savings and energy flexibility. The study methods composed of experimental study and demand response simulations.

In the experimental part, the local thermal comfort during the space heating demand response was investigated by thermal manikin measurements. The aim was to determine how the demand response of space heating affects the local thermal comfort of the occupant in the workstations adjacent to windows. The hypothesis was that, the convective downward airflows from the cold window surface could flow towards the occupant and cause draught. If at the same time the heating power of the water radiators below the window was low due to DR, the thermal plumes from the radiators would not block the downward airflows. During the demand response action, low heating powers are often used during the peak (high demand) hours when dynamic district heating price is high.

The results from the thermal manikin tests were extended to cover different window constructions. Reason for this was that with poor non-energy-efficient windows the downward convective airflows would occur at the higher outdoor air temperatures than with new energy efficient windows due to higher heat losses.

In the second part, a model predictive control (MPC) algorithm was developed to be used for space heating demand response control. The objective was to investigate the energy cost saving potential and energy flexibility of space heating in an educational office building. In addition, findings from the thermal manikin measurements were utilized in the MPC algorithm. The local thermal comfort was considered in the control algorithm by forcing the radiator heating to be ON if the local thermal comfort was threatened due to the draught. The influence of this local thermal comfort constraint on the energy cost savings and energy flexibility was evaluated. The influence of two different window constructions was also studied.

Demand response was chosen to be implemented using MPC algorithm since it includes features that are found to be superior compared to the other control algorithms (Afram, Janabi-Sharifi 2014, Dahl Knudsen, Petersen 2016, IEA 2018). These features include the use of system model in the control, ability to handle constraints, disturbances and uncertainties, possibility to use advanced optimization tools and ability to cope with processes with time delays.

Both the experimental part and the MPC control algorithm simulations were conducted in an educational office building in the cold climate of Finland. The case building located in the Aalto University campus area.

This thesis utilized the findings from the Kristian Martin's master's thesis (Martin 2017). Martin's thesis compared decentralized and centralized rule-based demand response actions of heating and ventilation. The case building in Martin's thesis was the same as in this thesis. Martin found out that the decentralized DR yield better cost savings and energy flexibility than centralised DR. In addition, the space heating was found to be the most effective system to utilize DR. For these reasons, this thesis focuses on decentralized demand response of space heating.

1.3 Structure of thesis

The thesis is divided into literature review of thermal comfort and district heating demand response (chapters 2 and 3, respectively), methodology of the local thermal comfort measurements and development of MPC algorithm (chapters 4-5), results and analysis from the thermal comfort measurements and MPC algorithm simulations (chapter 6) and finally discussion and conclusions (chapters 7-8). Description of the structure of each chapter is briefly presented in the following.

The concept of thermal comfort is introduced and the division to overall and local thermal comfort is presented in chapter 2. In addition, the conditions for acceptable thermal comfort prescribed and categorized in the guidelines and standards are included in this chapter. Chapter 2 ends in the preview of methods how to measure thermal comfort. Thermal manikins are discussed more in detail.

Concept and definition of demand response is presented in the beginning of chapter 3. Different DR strategies are introduced, and earlier DR studies are reviewed. Demand response is usually linked to demand response of electricity. Since in this thesis the DR of district heating is studied, the general properties of the Finnish district heating production, consumption and markets are presented. Subchapter 3.4 reviews the alternative control methods to implement DR. At first, the terminology of building system control is presented. Understanding the concept of building system control and the relevant terminology is essential in the development of new control algorithms. After this, the state-of-art control methods of DR are presented. Only the general properties of the control methods are discussed and some advantages and disadvantages in the different control methods are pointed out. Common key performance indicators (KPI) of DR are also presented in this chapter.

The methodology of the local thermal comfort measurements in the case building is presented in chapter 4. This includes the description of the thermal manikin, measurement room and measurement instruments. In chapter 5 the development of the MPC control algorithm is presented. This includes the prescription of the case building and IDA ICE building model, creation of the physical building model, calibration of the building model and finally the optimization of the controlled variable, space heating setpoints with the optimization algorithm.

Results and analysis of the performed thermal comfort measurements are presented in the beginning of chapter 6. Conclusion about how the local thermal comfort should be taken into account in the DR control algorithm is driven from the results. The results from DR simulations using the developed MPC algorithm are presented and analysed in the end of chapter 6. The focus is addressed to the local thermal comfort, energy cost savings and energy flexibility.

Finally, the findings of this thesis are discussed in chapter 7 and conclusions are driven in chapter 8.

2 Thermal comfort

Appropriate level of thermal comfort is essential because it affects occupant comfort, wellbeing and productivity. Several studies have showed that poor thermal comfort decreases student's learning outcome and employees work productivity (Maula 2017, McCartney, Humphreys 2002, Seppanen et al. 2006, Wargocki, Wyon 2017). In addition, continuous exposure to thermal environments outside the thermal comfort limits may cause health hazards and act as onset of progressive illness (Ormandy, Ezratty 2012, World Health Organization 1990).

Conditions that provide sufficient thermal comfort are stated in the national and international standards (ASHRAE 55 2004, ISO 7730 2005). National building and HVAC design guidelines and building codes give further information how the buildings should be constructed, operated and maintained in order to meet the thermal environment criteria (FiSIAQ 2008).

This chapter defines the thermal comfort concept and explains the factors influencing the thermal comfort. Methods to measure and evaluate the thermal comfort are also introduced.

2.1 Thermal comfort and human thermoregulatory system

Thermal comfort is defined as "the condition of mind which expresses satisfaction with the thermal environment" (ASHRAE 55 2004). The thermal comfort is divided to overall thermal comfort and local thermal comfort. Overall thermal comfort depicts the whole-body thermal sensation that is dependent on the body energy balance. If the energy balance between the human body and the thermal environment is fulfilled without overexertion of the human thermoregulatory system, neutral thermal sensation depicting good overall thermal comfort may be achieved. The local thermal comfort resembles the thermal sensation in different body parts. Even if the overall thermal comfort is neutral, local discomfort may be sensed in one or several body parts.

Person is in thermally neutral condition if the person would prefer neither warmer nor colder environment. However, some people may prefer conditions that are on either side of the thermal neutrality. They may regard conditions where they feel slightly cooler or warmer than the neutrality condition to be the most comfortable for themselves. Since people are physiologically and psychologically different and the clothing and activity levels may differ, it is impossible to reach conditions in single space that would satisfy everyone. Therefore, a goal for thermal comfort is not to satisfy everyone but to optimize the thermal environment such that the highest percentage possible would feel comfortable (ASHRAE 2013, Corgnati, da Silva 2011).

Sophisticated thermal environment design allows persons to adjust microenvironment close to them according to their preferences (Corgnati, da Silva 2011). These designs include for example personalized ventilation and personal heating and cooling setpoint controllers. As these kinds of personalized microenvironments are not possible to implement everywhere at least in full extend, the goal for designing thermal environments is to satisfy majority of people. Problem with existing systems is also that people may not be aware of the existence of the control possibility or they dare not to use it (Karjalainen 2008).

Humans thermoregulatory system tries to maintain the constant body core temperature of approximately 37 °C. Core temperatures over 43 °C and less than 25 °C are found to be fatal. Thermoregulatory system balances the heat lost to the environment and the heat produced by the body. Insufficient heat loss may lead to overheating (hyperthermia), and in contrast too great heat loss to reduced body temperature (hypothermia) (ASHRAE 2013). Thermoregulatory system may influence the sweating (evaporation heat transfer), the blood flows, the level of metabolism and micromovements of the body like shivering and muscle tension. If the thermoregulatory system is overstressed, the overall thermal sensation is reduced. Therefore, thermal comfort is generally reached when the body temperatures are kept within narrow range, skin moisture is low and effort from the thermoregulatory system is at minimum (ASHRAE 2013).

Average skin temperature is around 33 °C, but this value varies between people more than ±1 °C. The local skin temperature at different body parts differs from the average temperature. The skin temperature at the body extremities (limbs) is usually lower. If the body core temperature decreases, the blood flow in the hands and legs decreases by vasoconstriction (constricting blood vessels) and the local skin temperature may decrease critically (Corgnati, da Silva 2011).

The heat exchange between the human body and environment can be formulated as human body energy balance equation

$$S = M \pm W \pm R \pm C \pm K - E - RES \qquad (1)$$

where

S	the rate of heat storage [W]
M	the rate of metabolic heat production [W]
W	the rate of mechanical work accomplished [W]
R, C and K	the heat exchange by radiation, convection and conduction, respectively [W]
E	the rate of heat exchange by evaporation [W]
RES	the rate of heat exchange by respiration [W].

The terms with ± mark in equation 1 can transfer heat both in and out from human body. Exposure to constant thermal environment long enough may lead to heat balance between the environment and the body. This condition resembles neutral sensation and if thermoregulatory system is not overexerted, the overall thermal comfort is attained. In the balanced situation, the rate of heat storage is zero S = 0 W (Corgnati, da Silva 2011).

2.2 Conditions for thermal comfort

2.2.1 Overall thermal comfort

Thermal comfort is influenced by factors related to humans and factors related to environment. Human specific factors include the clothing insulation given by clo-value and the activity level described by the metabolic rate. Air temperature, mean radiant temperature, air velocity and relative humidity belong to the environment factors (Kosonen 2017).

Whole body thermal comfort may be achieved with different combinations of both environment and human induced factors. However, the number of combinations of these factors that would not cause overexertion of the body thermal regulatory system is limited. Although, climate conditions, living conditions and cultures differ around the world, it has been found out that people exposed to the same environmental condition (humidity, air flows, mean radiant temperature) with similar clothing and activity level, prefer similar air temperatures (ASHRAE 2013).

The famous thermal comfort model by (Fanger 1970) incorporates the personal factors (clothing and metabolic rate) and environmental factors (air temperature, mean radiant temperature, air velocity and relative humidity) to expression of the thermal comfort. Resulting prediction of thermal comfort is presented as predicted mean vote PMV in seven-point thermal comfort scale shown in Table 1.

Table 1. Thermal comfort scale.

+3	hot
+2	warm
+1	slightly warm
0	neutral
-1	slightly cool
-2	cool
-3	cold

PMV value can be converted to another index called predicted percentage of dissatisfied, PPD using analytical equation:

$$PPD = 100 - 95 * e^{-(0.03353*PMV^4+0.2179*PMV^2)} \quad (2)$$

The conversion is based on the assumption that the thermal comfort scale is symmetric around the neutral PMV and the PMV values +2, +3 and -2, -3 resemble people that are dissatisfied.

2.2.2 Local thermal comfort

Asymmetric or nonuniform thermal radiation is caused by nonuniform surface temperatures in the space. Asymmetric thermal radiation is defined as the difference in the average radiant temperature of the environment on opposite sides (half-spaces) of the person (Kosonen 2017). Common causes for radiant asymmetry are cold or warm windows, poorly insulated cold walls, cold or hot machinery or heating or cooling panels in walls and ceiling. Figure 1 shows the percent of dissatisfied due to radiant temperature asymmetry caused by warm ceiling, cool wall, cool ceiling and warm wall. It can be seen that the warm ceiling has the greatest effect on the comfort (ASHRAE 2013, Corgnati, da Silva 2011).

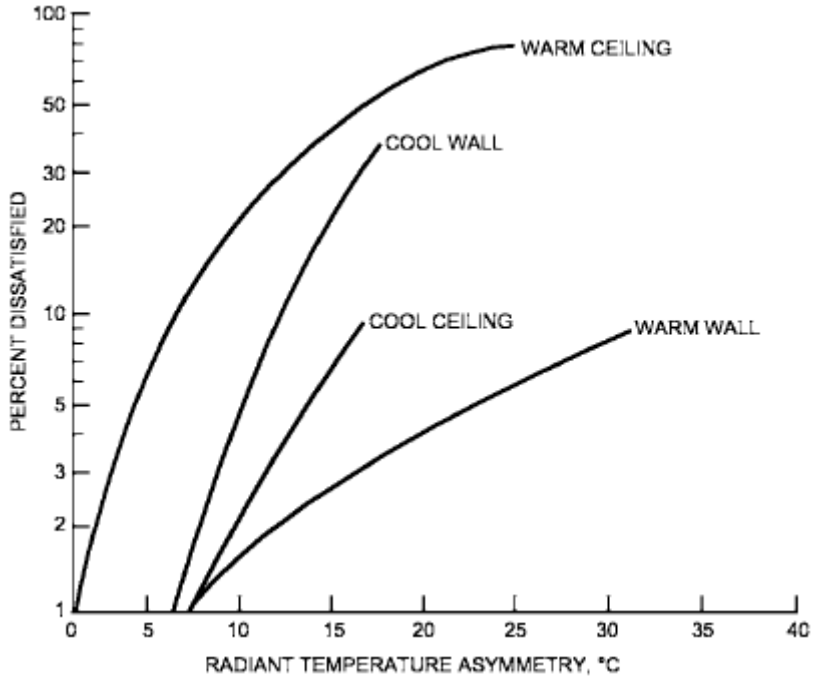

Figure 1. Percent of dissatisfied due to radiant temperature asymmetry. (ASHRAE 2013)

Draught is defined as unwanted cooling of human body part caused by air movement. The unwanted air movements may be caused by ventilation system, moving people, leaky external walls and high or low surface temperatures compared to air temperature. (Babiak et al. 2009) Draught rating is used to estimate the number of people that are dissatisfied due to draught. This index is a function of characteristic of the air movement: mean velocity, turbulence intensity and air temperature (Corgnati, da Silva 2011). Equation 3 presents the calculation of draught rate:

$$Draught\ rate = \left(34 - T_{a,local}\right) * \left(v_{al} - 0.05\right)^{0.62} * \left(0.37 * v_{al} * Tu + 3.14\right) \quad (3)$$

where

$T_{a,local}$ the local air temperature [°C]
v_{al} the local mean air velocity [m/s]
Tu the local turbulence intensity [%].

Air temperature typically increases with the height of the room. If the temperature gradient is too high, sensation of cold may occur in the feet and sensation of hot in the head, and this leads to local discomfort due to too high vertical temperature difference. Although the whole-body thermal sensation may be neutral, the nonuniform temperature sensation may cause local discomfort. Conditions where the air temperature at the head height is lower than at the heights of the other body parts have not been found to be as problematic (ASHRAE 2013, ASHRAE 55 2004).

Too cold or too warm floor may cause local discomfort in the feet. Feet is usually the only body part that is in direct contact with the environment. With bare feet the floor temperature is even more relevant. Therefore, floor temperature should be considered in design of

swimming halls, sport halls, dressing rooms and bathrooms. The construction of the floor has a great influence on its thermodynamic behaviour. Insulation thickness, connection to ground or outdoor air, floor heating and radiant heating define the thermal behaviour. In addition, the floor surface material affects how the temperature of the floor is sensed (ASHRAE 2013).

2.2.3 Thermal comfort standards

There are couple of international standards (ASHRAE 55 2004, ISO 7730 2005) about thermal comfort in addition to national guidelines, in Finland for example (FiSIAQ 2008). Here the categories given in ISO 7730 are presented.

Thermal comfort standard ISO7730 categorizes the thermal comfort according to both whole body thermal comfort criteria and criteria for the local thermal comfort (Table 2). To reach certain category, none of the limits specified for the category should be exceeded. The three categories apply only for spaces where all occupants are exposed to same indoor environment. This is since, in spaces where the occupants can control their microenvironments according to their preference, the percentage of dissatisfied decreases and the thermal comfort improves.

Table 2. Categories of thermal environment according to ISO 7730. DR stands for draught rate in this context.

Category	Thermal state of the body as a whole		Local discomfort			
	PPD %	PMV	DR %	PD % caused by		
				vertical air temperature difference	warm or cool floor	radiant asymmetry
A	< 6	− 0,2 < PMV < + 0,2	< 10	< 3	< 10	< 5
B	< 10	− 0,5 < PMV < + 0,5	< 20	< 5	< 10	< 5
C	< 15	− 0,7 < PMV < + 0,7	< 30	< 10	< 15	< 10

2.3 Evaluation of thermal comfort

Evaluation of the thermal comfort of occupants can be categorized into four methods (EN 15251 2007):

1) evaluation based on design documents
2) evaluation based on simulations
3) evaluation based on field measurements
4) evaluation based on questionnaires.

In method 1), the building design documents are reviewed, and the thermal comfort is evaluated according to the specified design values for heating and cooling season design temperatures. This method is mostly used prior to the construction of the building and as a rough estimate of the thermal environment of the building.

Building simulation programs 2) are in increasing extend used to model thermal comfort in both new and existing buildings. A performance of a building in respect of thermal comfort can be evaluated using

- simplified indicator, which requires that criteria for thermal comfort for selected category is met in most of the spaces in the building (for example over 95% of the building volume)
- hourly criteria, where the number of hours (or percentage of time) that meet the criteria during the whole simulation time is calculated
- degree hours criteria, which calculates the degree hours when the temperature is outside the set cooling or heating temperature boundary
- the overall thermal comfort criteria, where the simulation program calculates the PMV values which can be directly compared to criteria for the different indoor environment categories.

The third 3) evaluation method is field measurements where physical quantities are measured from the examined building. Measurement instruments should fulfil the requirements stated in the standard (ISO 7726 1998). Physical quantities can further be utilized to calculate the thermal comfort indicators like draught rate and PMV values. Field measurements include also measurement of the interaction between the human body and the environment by using modelled human bodies, manikins. The manikin measurements are further explained in the end of this subchapter, since manikin measurement was used in the experimental part of this thesis.

Questionnaires indicate the subjective perception of occupants to the thermal environment. When performing questionnaires, attention should be paid for the adaption time, choosing the representative group of subjective people and the proper choice of the questions. Standards and national authorities give recommendations for creating forms and procedures, for example the Berkeley survey (University of California 2017).

Thermal manikins

Manikins try to simulate the thermal and physical effects that human body experiences when it interacts with its surroundings. Different fields of research include clothing insulation, building thermal environment examination and vehicle cabin thermal inspections and evaluations. The first manikin was built in USA in 1940s for the purpose of defining the clo-value of clothing. Ever since the manikins have had a key role in research of human interaction with various surroundings (Holmer 2004, Foda, Siren 2012).

The following developments have been seen during the evolution of manikins. Number of body segments has increased. The first manikins comprised of only one body segment while the new modern manikins might have tens of body segments. Introduction of digital regulation techniques gives more possibilities. Different digital control algorithms have been developed and these allow additional measurement quantities and more precise measurements. Movability of the manikins has experienced a huge change. While the first manikins built were generally unable to move, the new ones can be modified to act in different positions. Body functions: introduction of sweating manikin provided information about evaporative heat exchange, and breathing manikin takes into account the respiration heat loss (Holmer 2004).

Recent development of manikins is twofold. One direction is towards complex, self-functioning and high-tech manikins and the another development direction is towards simple but still precise manikins that are inexpensive and easy to use. These two types of manikins serve different research problems and are thus evenly important (Holmer 2004).

Manikins are controlled in various modes. Constant skin temperature CST mode is the most used. In CST the skin surface temperature is kept constant for the whole body. Normally the skin temperature is set to somewhere around 34 °C. Constant heat flux mode CHF means that the heat flux is set constant in all the body segments. The influence of thermal environment and clothing level is seen in the skin surface temperature at different body parts. Third mode to control manikins is called comfort equation mode CE. CE represents always a neutral condition since the skin surface temperature is adjusted so that the comfort equation (Fanger 1970) is giving neutral conditions (Foda, Siren 2012).

When thermal conditions are evaluated with manikin, equivalent homogenous temperature or simply equivalent temperature is commonly used. Equivalent temperature is defined as the temperature of an imaginary space with uniform and still air conditions and equal air and radiant temperatures, where the body exchanges the same dry heat loss as in the actual environment. Dry heat loss consists of radiation and convective heat losses. The clothing, activity level and the body position of the occupant/manikin are assumed to be the same in the imaginary and actual cases (Tanabe et al. 1994, Nilsson, Holmer 2003).

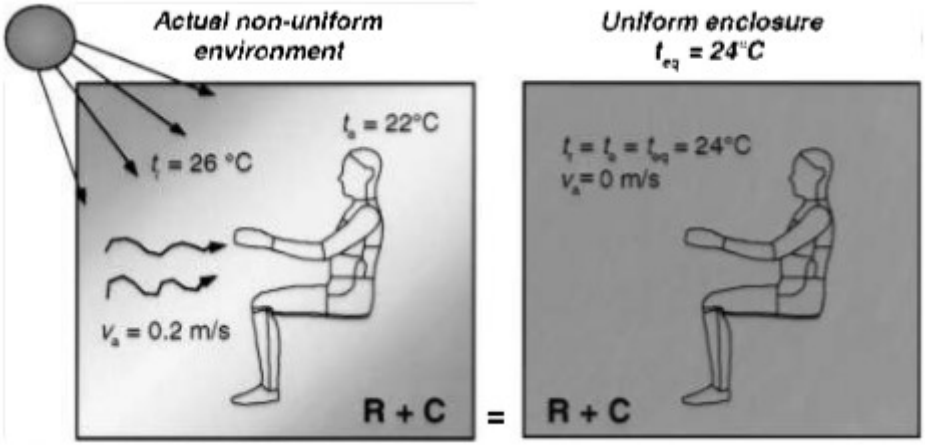

Figure 2. Equivalent temperature definition. (Nilsson, Holmer 2003)

Figure 2 illustrates the equivalent temperature definition. Equivalent temperature is defined as follows:

$$T_{eq} = T_{pb} - \left(\frac{P_{pb}}{h_{pb}}\right) \qquad (4)$$

where T_{eq} equivalent temperature of the body part [°C]

T_{pb} surface temperature of the body part [°C]

P_{pb} heating power of the body part [W/m^2]

h_{pb} heat transfer coefficient of the body part [W/m^2,K].

3 Demand response of district heating

In this chapter four specific topics about demand response of district heating are discussed. The first subchapter gives an overview of the district heating sector in Finland. The consumption, production and district heating markets are discussed. In addition, the different pricing models are introduced, and the concept smart thermal grid is presented. The second subchapter introduces the concept of demand response. In the third subchapter the earlier studies of demand response in the buildings are reviewed. The final, fourth subchapter deals with different HVAC control methods that can be used to implement DR. The main performance indicators of the DR control methods are also introduced.

3.1 District heating in Finland including demand response aspects

District heating is a common, efficient method for delivering heat (using hot water or steam as medium) to customers in dense urban areas. Heat is produced in several technologies including the most common CHP power plants and heat only boilers. The heat is delivered through district heating network that composes of transmission grid at the production side and distribution grid at the customer side of the network. The customers extract the heat by using heat exchangers which connect the distribution network to the customers heating network (IEA 2018, Dahl et al. 2017).

3.1.1 Consumption

District heating provides heat for residential, agricultural and service buildings and for industrial premises (process heat). In Finland the market share of the district heating in accordance with the heating demand of residential and service buildings was 46% in the year 2015, see Figure 3 (Finnish energy 2018). This makes district heating the most significant source of heat supply for buildings in Finland. In the EU level, the market share of district heating from the residential and service sector heat demands was 12% in 2008 (Frederiksen, Werner 2013). In Finland the market share of DH has grown during the last decades, but the growth has stabilized in recent years. One reason for the stabilized growth is that the share of heat pumps has increased considerably during the past ten years (Statistics Finland 2017, Sarvaranta et al. 2012).

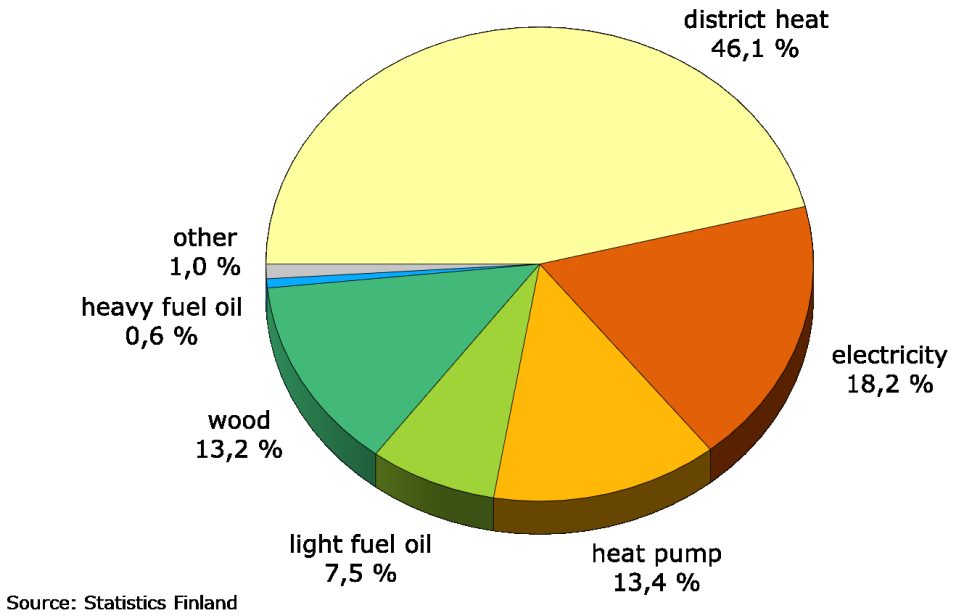

Figure 3. Market shares of space heating in residential, commercial and public buildings year 2015 (Finnish energy 2017).

Buildings use district heating for space heating (SH), heating of supply air in air handling units (AHU heating) and heating of domestic hot water (DHW heating). The share of the energy used annually for each purpose in average Finnish residential buildings are 40%, 35% and 25%, respectively (Koskelainen et al. 2006). However, the building type, age of the building and size of the building affect the shares of energy use purposes. In the old non-energy efficient buildings, the share of energy used for space heating is high whereas in the new energy efficient buildings, the share of DHW is higher since space heating demand has decreased. Older buildings may not have supply exhaust ventilation system, or the AHU may not be equipped with heat recovery unit, which both would increase the AHU heating demand.

The load in the district heating network is the result from the aggregated heat loads from the buildings and industrial premises that are connected to the district heating network. In addition, the distribution heat losses in the entire network increase the total DH load. The heat load in the DH network varies continually. The variations can be divided into seasonal, weekly and daily components. The weekly district heating load profiles for four seasonal periods in the Helsingborg DH network are presented in Figure 4 (Frederiksen, Werner 2013). The varying load profiles are the foundation of demand response actions.

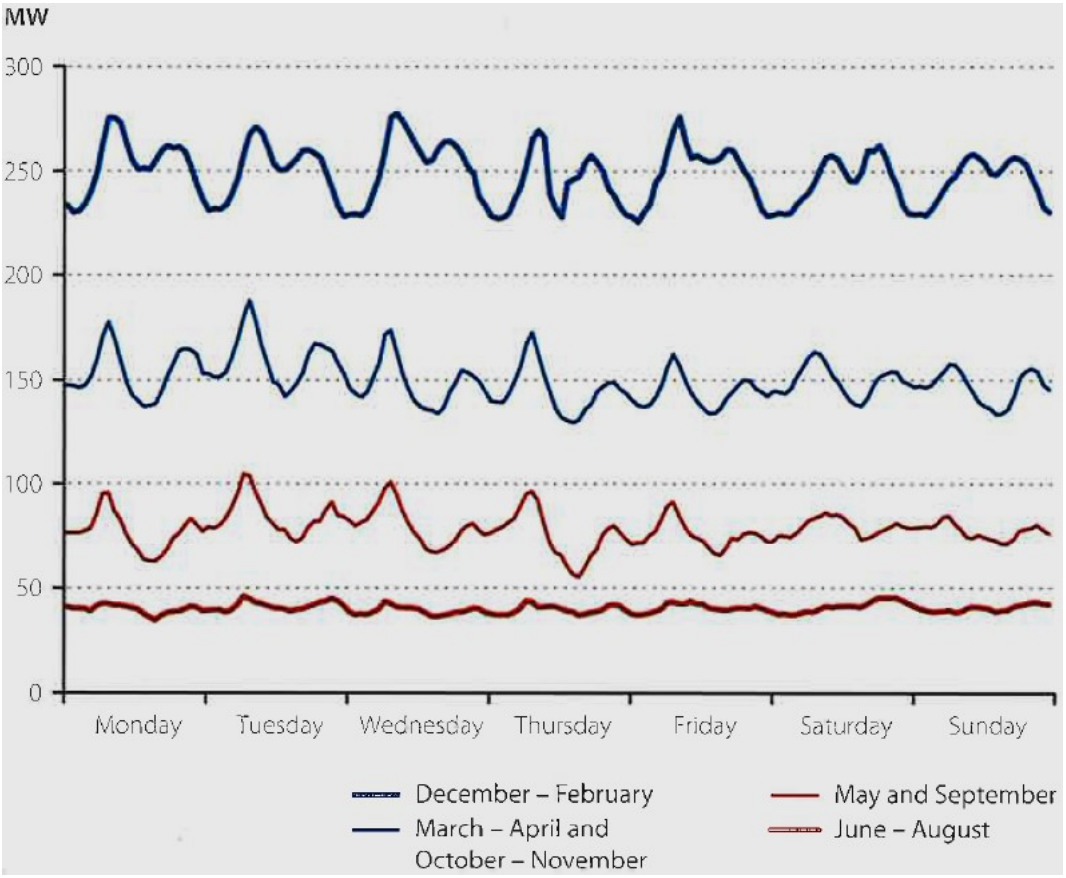

Figure 4. District heating consumption profiles showing the seasonal and weekly variations in the DH network of Helsingborg Sweden (Frederiksen, Werner, 2013).

The seasonal variation of heat load can be seen by comparing the four weekly load profiles in Figure 4. The most significant factor affecting these profiles is the weather. The space heating demand of buildings increases due to increased heat losses, when the outdoor air temperature decreases. For this reason, the peak demand in the network occurs during the cold winter days and the minimum demand during the summer days. The other weather factors affecting the load include solar radiation and wind. The solar radiation decreases the heating demand and the wind mainly provides greater heat loads by intensifying the heat losses during the cold days (Frederiksen, Werner 2013, Sarasti 2017).

The weekly and daily variations of the heating load originate from the human behaviour and weather fluctuations. The effect from the human behaviour is regarded as a social component in the heat demand. The three most significant social factors affecting the daily loads are the increased DHW consumption during the mornings and afternoons (before and after the working days), daily schedule of ventilation and the night-time set-back control of ventilation (according to the occupancy). The occupied time of the buildings and weather fluctuations also affect the demand. During the occupied time, the internal heat loads decrease the heating demand. The fluctuating solar radiation, outdoor temperature and wind during the day and night affect also the load profiles (Frederiksen, Werner 2013).

The office working days can be seen in the weekly profiles in the greater heat demand during the weekdays compared to weekends. The explanation for the difference is that the office

buildings are unoccupied during the weekends. The difference in daily and weekly loads is smaller during the summer time which may be explained by the holiday season and because the load is composed mainly from the DHW load.

3.1.2 Production

Number of technologies and various fuels are used to produce heat into the district heating network. Majority of heat supply is produced in the centralized power plants and smaller heat stations. The technologies used can be divided into technologies which produce both heat and electricity - combined heat and power plants (CHP) and to those which produce only heat - heat only boilers (HOB). Both CHP and HOB are based on the combustion of fuels. Other alternative technologies to produce district heating involve large heat pumps, geothermal heat stations, waste incineration, solar district heating, nuclear district heating and heat recycling from industrial processes (Frederiksen, Werner 2013).

The fundamental idea in the district heating is to utilize heat sources that would otherwise be wasted. For this reason, combined heat and power plants (CHP) lie in the heart of district heating production. In CHP, the condensation heat from the power plants is extracted and directed to district heating network. The overall efficiency of energy production increases compared to condensation power plants because with the same amount of fuel, greater quantity of usable energy (electricity and heat) is generated. In Finland, most of the district heating energy comes from the CHP plants. In 2016, the share of CHP in the total DH production was 68% (Statistics Finland 2017, Frederiksen, Werner 2013).

The fuel mix used to produce district heating in Finland in 2016 is shown in Figure 5. The share of biofuels (both liquid and solid fuels) has increased in previous years. The research in combustion technology has improved the combustion efficiencies of biofuel boilers in Finland. Also, the aim to mitigate climate change by incorporating more renewable fuels has increased the share of biofuels.

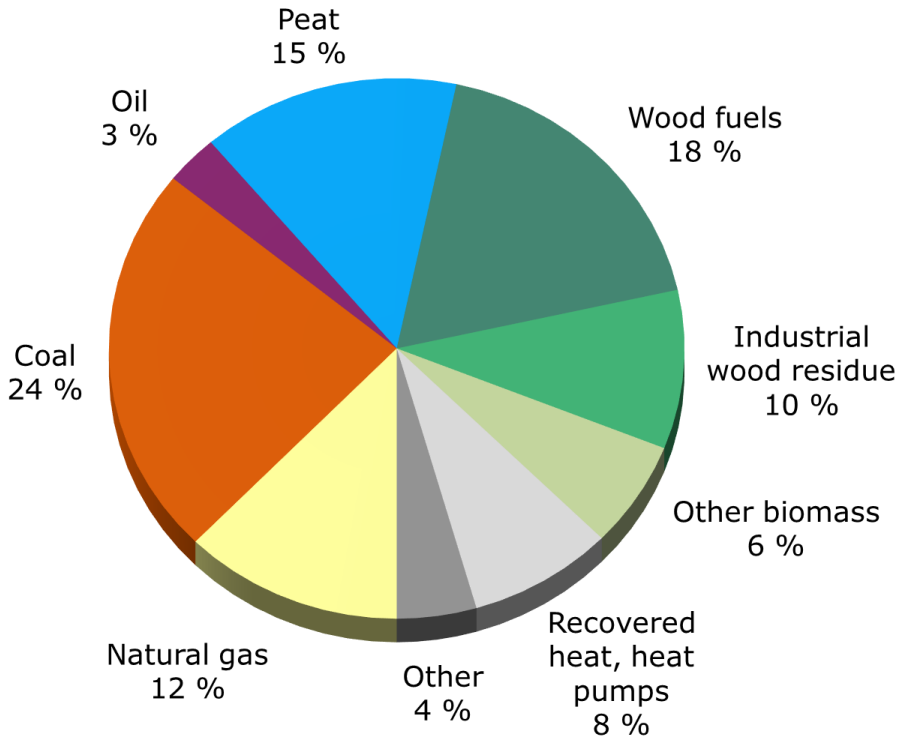

Figure 5. District heating production fuel mix in Finland 2016 (Finnish energy 2017).

Production units are divided into base load, medium load and peak load units. Base load units are meant to cover the continuous stable part of the network demand. Base load units have low heat production costs and high usability for which reason CHP and solid fuel boilers belong to this category. Peak load units, in comparison, are used at the side of base load units during the peak load hours. Peak load units should allow quick start-ups and have low cost per production power. The fossil fuel fired heat only boilers serve often this purpose. The medium load units belong between the peak and base load units by possessing characteristics from both. In addition, reserve unit exists to produce heat during the maintenance breaks and operational breakdowns (Koskelainen et al. 2006).

The environmental benefits from the demand response can be explained by considering afore presented production fuel mix, different heat production units and consumption profiles. The varying load is met by utilizing base load, medium load and peak load units. By balancing the network load by affecting the demand side with DR actions, the need for fossil fuel utilizing peak load units decreases. Adapting the load to the production in DR benefits also the increasing use of intermittent RES heat generation technologies such as solar and RES electricity driven heat pumps because the intermittent production can be balanced by adapting load.

3.1.3 District heating markets and pricing

Electricity and district heating markets differ in numerous ways. In electricity markets the customer can choose where to buy electricity from the open whole-sale markets. The distribution and production markets are separated. In district heating, typically the same heating company acts both as producer and distributor, and in one region only one company sells heat because the building of multiple DH networks in the same area is not economically

feasible. The isolated market without competitors mean that the local heat company has a natural monopoly in the markets. The natural monopoly could lead to abuse of the customers by overpricing because the customers can't change the heat provider. To prevent this the district heating markets are controlled and supervised by the Finnish Competition and Consumer Authority which defines the common principles to protect the customers. This authority supervises the DH pricing according to competition act (FINLEX 948 2011). The pricing policy in DH companies is required to result in reasonable and unbiased prices which means that the prices must be justified by the production costs and the same type of customers must be treated even-handedly (Sarvaranta et al. 2012).

Price of district heating is based on bilateral agreements between the DH company and the consumer. The price varies greatly in different district heating networks. The size of the network and the properties of the production units: fuel mix, age, maintenance and profit expectations affect the prices. The customer price is divided into three parts: connection charge, power charge (sometimes called basic charge) and energy charge. The connection charge is one-time payment which is paid when the property is connected to the DH network. Power charge is dependent on the connection power requested by the customer. The charge can be defined based on either agreed maximum power (kW) or the maximum water flow (m^3/s). Often the power charge is divided into size-based categories to divide the DH production costs fairly between larger and smaller consumers. The energy charge is paid for the consumed energy (€/MWh). In most of the district heating companies in Finland, the energy charge is constant throughout the year. Some companies use seasonal pricing. The charges are charged at least in three instalments. Commonly the energy charge is read using the remote energy meters (Sarvaranta et al. 2012, Koskelainen et al. 2006).

3.1.4 Pricing models for demand response

In demand response perspective its essential that the economic benefits are shared between the district heating producer and consumer. For this purpose, new pricing models need to be developed into district heating markets. Commonly the pricing models in DR are categorized into incentive-based and price-based programs (Goldman et al. 2010). In incentive-based programs the DH companies provide incentives for the customers to attend in the load control. The customer accepts that the DH producer is allowed to control and authorise the end-user's consumption according to the agreement or the end-user needs to reduce the load to predefined amount upon company's request. In price-based programs the district heating price is developed so that it reflects the production costs and load in the network. During the peak demand and high production cost time the price is high and during the low peak and low cost vice versa. Dynamic district heating price is the most sophisticated price-based pricing program where the price is defined before the use for instance day-ahead. In dynamic pricing, the customers who attend in DR, adjust their load according to the DH price (Shan et al. 2016, Palensky, Dietrich 2011, Kärkkäinen et al. 2003).

In this thesis, DR is investigated based on dynamic district heating pricing although such pricing is not yet available in Finnish district heating markets. However, discussion about developing price programs supporting demand response utilization have been running in recent years. In Stockholm and Copenhagen, there exists already experiments in open district heating markets with different pricing models some of which would support DR. In Stockholm, open two-way district heating markets are mainly meant to allow third-party supply of excess heat into the district heating network. Such third-party heat producers

compose mainly from datacentres and supermarkets which produce significantly excess condensing heat (WSP Sverige 2017). In Copenhagen, the pricing is based on the cost optimizing the production of multiple district heating producers in the same network. Also, in Finland, the excess heat from the industry is utilized in some DH networks by making bilateral contracts between the DH company and the industry. However, open DH network is not yet tested in Finland (Pöyry Management Consulting Oy 2016). Developing market models for the DH demand response requires open discussion between the customers and producers. Customers should be also able to understand the principle of price formation (Sarvaranta et al. 2012).

3.1.5 Smart thermal grids

Term smart grid is extensively used in the research of power grids. It means that intelligent controls, measurements and communication technologies are integrated into the traditional power systems to allow smart monitoring, analysis and control of supply and demand. Storage systems, decentralized power production and increasing amount of RES are also included in smart power grids (ABB 2016). The properties that change the traditional power grids to smart power grids are quite similar to those that can change the traditional DH network to smart thermal grid. Some properties that would transform traditional DH network to smart thermal grid are listed in Table 3.

Table 3. Properties of smart thermal grids (IEA 2018).

Property	Purpose
Flexible	- Short-term: adaptation to energy supply and demand - Medium-term: adaptation by adjusting temperature levels in existing networks and by installation of new distribution micro-networks - Long-term: adaptation by alignment of network development and urban planning
Intelligent	- Planning and operation - End-user interaction with the energy system (demand side management)
Integrated	- Urban planning and networks – electricity, sewage, waste, Information and communications technology (ICT), etc.
Efficient	- Optimization of technologies and cascade usage
Competitive	- Cost-effective, affordable
Scalable	- Neighborhood-level or city-wide application
Securing energy supply	- Use of local renewable energy sources

3.2 Concept of demand response

Demand response is part of a broader concept called demand side management (DSM). DSM can be defined as a set of methods which try to improve and optimize the energy system by changing the time pattern and/or magnitude of the load at the side of energy consumption. Traditionally the energy system management (electricity, district heating, district cooling) has focused on optimizing the energy generation and distribution. By allowing also the energy end-users to participate in the energy network management by using the DSM (end-

users act as prosumers), the efficiency of the energy network can be further improved (Palensky, Dietrich 2011, Gellings 1985).

The demand side management can be categorized to long-term strategies and short-term strategies. In long-term DSM the consumers load is modified permanently whereas in the short-term DSM the load is changed temporarily (Sarasti 2017, Alimohammadisagvand et al. 2018). The short-term DSM is also called demand response (DR). More specific definition for the demand response is given by the U.S. Department of Energy which defines demand response as:

"Changes in electric usage by end-use customers from their normal consumption patterns in response to changes in the price of electricity over time, or to incentive payments designed to induce lower electricity use at times of high wholesale market prices or when system reliability is jeopardized." (Shan et al. 2016).

As can be noted from this definition, demand response is traditionally linked to control of loads in the electricity grids. The definitions and concept of demand response in the field of district heating is however quite similar and they can be used interchangeably.

Traditionally six different DSM strategies are identified based on the manner they are modifying the customers load profiles (Figure 6). Figure 6 shows that peak shaving, valley filling and load shifting belong to the short-term DSM strategies and conservation, load building and on-site generation belong to the long-term DSM.

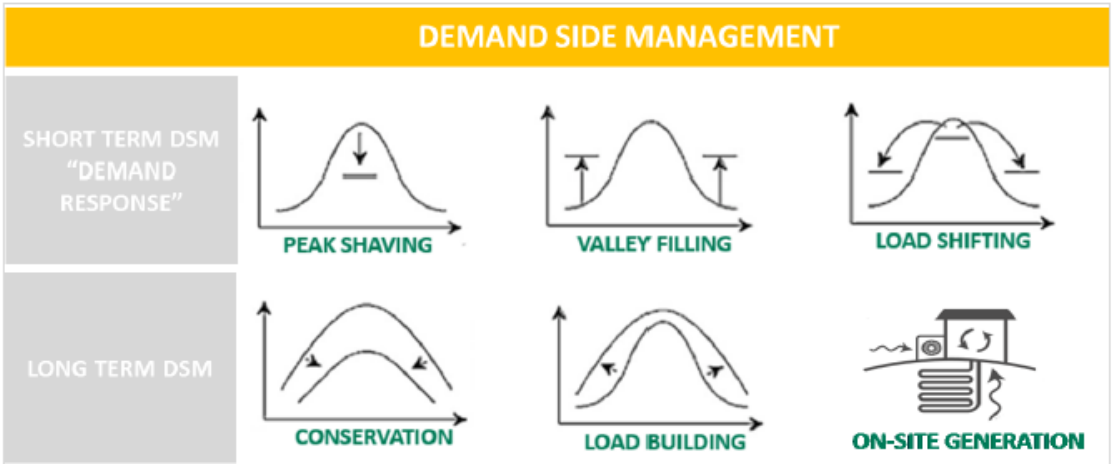

Figure 6. Demand side management strategies (Sarasti 2017).

In peak shaving and valley filling the load profile is modified from its extremes. In peak shaving the peak loads are reduced by limiting the utility's load during the peak load hours. In comparison, in the valley filling the load is constructed during the off-peak hours. The load shifting combines the peak clipping and valley filling by shifting loads from the peak hours to off-peak hours. Load shifting is widely regarded as the most effective load management technique. The pricing model used in both valley filling and peak shaving is incentive based whereas in load shifting the price based model is used (Logenthiran et al. 2012).

Load conservation is a strategy where the customers load is reduced permanently for example by improving the customers (buildings) energy efficiency. Load building refers to general increase of the load. One goal in load building is that by increasing the load of one energy source the load and usage of another energy source can be reduced. This concept may be evident in electrification of transport wherein the buildings electricity consumption is increased due to charging of EVs but at the same time the use of fossil fuels in transport sector is reduced (Gellings 1985). The last long-term DSM strategy, on-site generation, refers to reduction of load in the energy network by producing part of the load at the site of consumption (Shan et al. 2016).

In the building level, distinction needs to be made between the terms energy efficiency and demand response, which are often mixed up. The term energy efficiency refers to reducing the energy consumption by maintaining equal or improved quality of service. Improving the energy efficiency results in permanent reduction in energy consumption. In comparison in demand response the load is controlled temporarily according to the changes in the energy network and the DR actions may not lead to energy savings. Instead, demand response actions aim to reduce the CO_2 emissions and production costs of the whole energy system. Coordination between the energy efficiency and demand response projects is important so that each stakeholder from policymakers and energy companies to utility owners know is the project targeting in DR or energy efficiency improvements or both (Goldman et al. 2010). In this thesis, the focus is in DR, and thus further discussion about the energy efficiency improvements is excluded.

3.3 Earlier studies of demand response in buildings

Earlier studies in the field of demand response have focused on electricity. Some of them are reviewed here although the scope of this thesis is in demand response of district heating. The reason is that regardless of the energy form, the concepts and control strategies in the DR utilized in the buildings are similar.

(Alimohammadisagvand 2018)) studied the influence of demand response actions on thermal comfort, energy consumption and cost in Finnish residential houses having geothermal heat pump or direct electricity heating system. DR was used to control both thermal storage tank temperature setpoints and space heating setpoints. The result from his doctoral dissertation revealed that the maximum heating electricity cost saving for utility owners with different DR control algorithms was 12-15%. The results from the simulations showed that thermal comfort in zones was maintained in acceptable level which was evidenced by checking that the recommendations from the standard EN 15251 was fulfilled.

(Le Dreau, Heiselberg 2016) focused also in the DR actions in residential buildings. The space heating setpoint in two residential houses (one passive house and one older house build in 80s) was modulated with different strategies composing of decreased setpoint periods (heat conservation) during cheap electricity spot prices and increased setpoint periods (heat loading) during expensive spot market hours. They found out that the demand response potential regarding (thermal comfort and power shifting) by utilizing the thermal mass of the building was dependent on the building properties. There doesn't exist one heating setpoint modulation strategy that could be used throughout the entire building stock. Different modulation strategies in both building types led to cost savings between 3-10%.

(Logenthiran et al. 2012) studied the DR of electricity in smart grid containing loads from three different customer areas: residential customers, commercial customers and industrial customers. They pointed out that the loads in these different consumers vary significantly. The electric loads in residential customers are characterized by short durations of operation and small power consumption. The power consumption of devices owned by commercial customers are slightly higher. Industrial sector differs from the residential and commercial sector by having the smallest number of controllable devices but the largest consumption ratings and longest consumption times. The obtained operational cost savings for the residential, commercial and industrial customers were 5.0%, 5.8% and 10%, respectively.

Both studies by (Greensfelder et al. 2011) and (Korkas et al. 2016) considered the DR response in buildings during HVAC cooling operation. Greensfelder et al. found out that remarkable HVAC cost savings can be achieved by optimizing the precooling of the thermal mass combined with information of real-time electricity prices and weather data. Optimization of precooling of three different office buildings (in respect of size, thermal mass and internal gains) in four cities in USA (Chicago, New York, Houston and Los Angeles) resulted in cost savings ranging from 0% to 14%.

Korkas et al. developed a two-level supervisory closed loop feedback strategy to optimize space cooling operation in the microgrid composed of three buildings, a photovoltaic array, a wind turbine and electricity storage battery (Korkas et al. 2016). At the lower level the DR control optimized the space cooling in each building of the microgrid in respect of cost and thermal comfort. At the upper level centralized controller supervised and updated the local controllers with the aim of minimizing the aggregate energy cost and thermal discomfort of the entire grid. Study showed that two-level supervisory controller managed to decrease the cooling cost of the studied buildings without sacrificing the thermal comfort of the occupants.

Recently also research in demand response of district heating has been emerging. One major difference between these two energy forms is that the number of controllable loads in the electricity grid is much higher than in the district heating network. The possible loads to be controlled in district heating network include typically the space heating, domestic hot water heating and ventilation heating loads. However, the DHW load is generally excluded from the DR actions since the load is varying too rapidly and the quality of water needs to be secured (Kärkkäinen et al. 2003). In addition to controllable loads in the buildings, the loads in industrial processes can be used for demand response purposes. Moreover, short-term thermal energy storages (other than buildings thermal mass) such as hot water storage tanks, phase change materials and varying temperatures of the DH network can be utilized in the demand response (Kensby et al. 2015).

Kärkkäinen et al. studied the peak limiting demand response of district heating in three case building, two in Jyväskylä, Finland and one in Mannheim, Germany (Kärkkäinen et al. 2003). The first case building in Finland had hydronic radiator heating system and another had hydronic floor heating system. The load was controlled by adjusting the inlet water temperature curves of space heating systems and by using in-line correction factor for supply air temperature curve which was exhaust air temperature compensated in both buildings in Finland. In comparison the case building in Mannheim was served by air based heating system. The pilot tests were performed in the case buildings to find out the peak load reduction potential in the local district heating networks. The result from Jyväskylä cases

showed that the total heat load could be reduced by 20-25% during 2-3 hours load reduction period. The study assumed that if similar peak load shaving is performed simultaneously in large number of buildings the equal 25% peak shaving could be obtained in the local DH network. This benefits the DH network for instance by increasing the capacity factor of CHP which increases the network efficiency. The use of emission intensive heat only boilers decrease and so does the number of inefficient start-ups of those plants. The maximum temporal variation in the room air temperature was ±2 °C in these case buildings. The Pilot test in Mannheim resulted in minor peak load shaving of 4.1% mainly because of the air based heating system. The peak load shaving resulted in substantially increased energy usage and for this reason no economic benefit was gained.

In research conducted by Kensby et al., pilot tests for five residential buildings was performed to study the potential of buildings to act as thermal energy storage in the DH network (Kensby et al. 2015). Both the thermal comfort and the capacity of heat storage were evaluated. The studied buildings had hydronic radiator heating systems, the specific heat consumption was approximately same in each building (150 kWh/m^2). Buildings differed from each other by having different mass of structures. The heat loading and conservation was performed by adjusting the outdoor temperature signal for the radiator inlet water temperature curve in 21-hour cycles for 52 weeks. Five different cycles were tested and with the highest deviation from the normal temperature curve, as much as 0.1 kWh/m^2 could be stored in the heavy weight building with indoor air temperature variations smaller than ±0.5 °C.

A company called Valor Partners Oy studied the demand response control of district heating and one of their objectives was to evaluate the benefits that DR could bring to DH companies and to DH customers.

The following benefits were found for the DH companies (Valor Partners Oy 2015):

- minimized procurement and production costs
- fewer start-stop cycles of production due to more stable load in the network
- more efficient heat production and lower costs due to increased capacity factor of CHP
- efficient production due to high usage (capacity factor) of production units
- heat production according to electricity prices in CHP, heat pumps and electric boilers
- lower investment cost due to more efficient heat production during peak load hours
- lacked need for network expansions.

The following benefits for DH customers were mentioned (Valor Partners Oy 2015):

- decreased yearly heating cost due to dynamic heating according to DH prices. Load is increased during cheap hours and reduced during expensive hours. (dependent on pricing)
- decreased yearly heating cost due to decreased heating energy consumption (not always present)
- better quality of service due to emerging business and pricing models.

- In addition to these (Kensby et al. 2015) mentioned that the security of heat supply increases since the buildings can store heat and utilize it if the heat delivery is interrupted.

In addition to previous studies, several master's and one licentiate thesis have dealt with the demand response of district heating (Jokinen 2013, Kontu 2015, Salo 2016, Martin 2017, Sarasti 2017, Salmi 2017, Sihvonen 2017). The three most relevant in the scope of this thesis are reviewed shortly.

Sarasti studied the demand response potential in the Espoo district heating network in Finland (Sarasti 2017). The demand response was implemented by adjusting the radiator temperature setpoints according to dynamic price data using model predictive controller. The results from the apartment building simulations were expanded to the whole Espoo DH network. Sarasti found out that the DR yield 7% cost savings for the simulated apartment buildings. If every apartment building in the Espoo DH network would utilize DR, the average peak power in the network could be cut by 11-56 MW.

In Salo's thesis, the thermal mass of heavy weight buildings was studied as a short-term thermal energy storage to offer platform for DSM implementation (Salo 2016). Within an artificial DH network developed in Salo's thesis, the building owners got the variable heating energy savings of 11% during the heating season. The cost saving was obtained by shifting part of the buildings load from the expensive DH price hours to inexpensive DH price hours. No energy savings were implemented. The benefits for the heat producers were found to be relatively larger than for heat consumers. Some business models were suggested to share the DR benefits more evenly between the stakeholders.

In Martin's thesis the demand response of heating and ventilation was studied in the same case buildings as in this study (Martin 2017). Unlike in this thesis, Martin used rule-based control algorithm to adjust the temperature setpoints of ventilation supply air and space heating units. In addition, the VAV ventilation was investigated where the air flows were controlled according to electricity prices and CO_2 levels. Martin found out that the decentralized DR of space heating yield the biggest cost savings from the single DR implementations. The results showed that yearly heating costs of the building decreased 5.2%.

DR can be utilized also by interconnection between the district heating, district cooling and electricity grids. For instance, power to heat conversion can be used to convert variable renewable electricity to heat in the district heating network with electricity boilers and heat pumps (Salpakari et al. 2016). District heating companies could utilize increasingly the large-scale heat pumps to produce DH during the periods of low electricity prices and CHP during the high electricity prices. This would help stabilizing the electricity network, increasing the variable renewable electricity production and also decreasing the emissions from the DH production (Helin et al. 2018). Also, Kensby suggested that the DH systems could act as balancing force in the electrical grid. When the electricity is cheap, heat pump can be used to produce heat in the DH system and TES can be used to store the available heat. During the expensive hours TES can be discharged, and heat pumps shut down. Strategies like that will be invaluable when the total energy system is optimised (Kensby et al. 2015).

3.4 Demand response control methods

Building automation system (BAS) has a key role in implementation of demand response strategies, because the DR control actions are often implemented by BAS. The purpose of BAS is to:

- execute the adjustment and control of the processes inside the building
- supervise the HVAC operation by acquisition of data and sending alerts
- produce consumption, energy efficiency and indoor environment quality statistics to help the proper maintenance of the building
- provide user interfaces that support the usage of the building (Härkönen et al. 2012).

The development in the BAS systems has based on the general development of ITC technology. This has been evidenced in the increased number of Internet connected devices, increased use of computational units and development of the electronic components. Adding more advanced controllers and data acquisition instruments enables the buildings to become so called smart buildings. In smart buildings, the building technologies can provide a state of indoor environment that support the user's activities and the same time the building operation can be optimized to be energy, emission and cost efficient. Furthermore, the development in the BAS enables the development and use of more sophisticated DR control methods in the buildings (Härkönen et al. 2012, Afram, Janabi-Sharifi 2014). Advanced control methods are also required to combine the demand response actions and increased distributed generation (of heat and electricity) (IEA 2018).

Different controllers and control methods are included in the BAS to control for instance the heating units, cooling units and air handling units. In this subchapter the key terminology related to the building system control is introduced. After that the state-of-the-art control methods are discussed. The function of a model predictive control method MPC, is highlighted since, MPC control method is developed in this thesis to implement the DR actions.

The performance of the DR control methods can be evaluated by using different key performance indicators KPIs. Several KPIs are presented at the end of this subchapter.

3.4.1 Building system control

For the sake of clarity, the terminology used in the building system control is defined before the introduction to different control methods for controlling buildings HVAC systems in chapter 3.4.2. The terms shown in the general feedback control scheme shown in Figure 7 are defined as follows (IEA 2018).

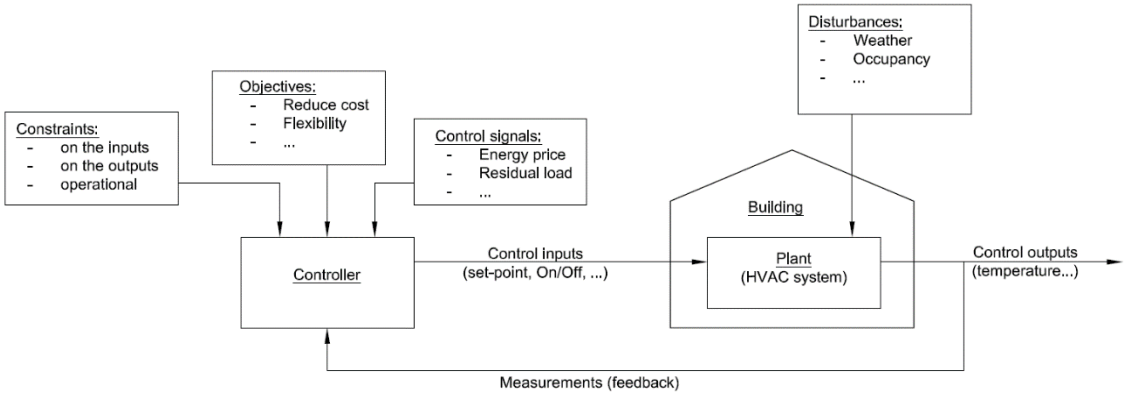

Figure 7. Scheme of building system control (IEA 2018).

Controller is a physical device inside which the control method/algorithm is written. Controller takes as input the feedback from the controllable process, the control objectives, constraints and control signals. Based on the control algorithm the controller sends the control input to the controllable process.

Plant, process or system is the target of control. In the buildings the controllable processes include the HVAC components such as air handling units, district heating heat exchangers and radiators, for example.

Control strategy is a high-level approach to achieve the control objectives. Control method or technique is lower level term. *Control techniques/methods* are used to implement the control strategy. Another term referring to the control methods/techniques is control algorithm. Control algorithm refers to the mathematical presentation of the control method.

Control objectives present the target of the control. The objective may be simple as keeping the process in the desired operational conditions, but it may also consider energy efficiency and costs.

Constraints may be set for control inputs or/and outputs. Constraints define the allowable values for the control inputs or outputs. Almost all building processes have some sort of constraints. The most typical ones deal with the acceptable indoor temperature ranges and CO_2 concentrations.

Disturbances are external parameters that can't be estimated accurately in the control method. For this reason, they often hinder the process to attain the state which is the objective. In the HVAC control the weather and internal gains act as disturbances.

Control input is the signal that the controller sends to the controlled process/plant/system.

Control output is the output parameter from the controlled process that is being controlled.

Control signals compose of data that the controller uses to determine the control inputs. For example, the price data and weather forecast, or measured outdoor air temperature might be used as control signals.

3.4.2 State-of-the-art HVAC control methods

Control methods can be categorized in numerous ways. However, there are two main type of controllers: local/decentralized controls and supervisory/centralized controls. The local controller controls a single component and tries to maintain the controlled process in the desired state (defined by setpoint values). Supervisory control in other hand is used to control the whole building energy system so that the system composing from several local controllers functions smoothly and energy efficiently (Naidu, Rieger 2011).

Control methods used to implement DR can be divided into rule-based and model-based methods. Rule-based control methods make use of the known history and future data. The most typical data that is used are weather and energy cost data which can be relatively accurately predicted in the near future. The rule-based control algorithm evaluates the trend in the cost data and based on the specific rules in algorithm the control input is sent to control the process. In model-based control methods one or several control parameters are predicted by a model that describes the system or part of it. The model-based controls can include for instance prediction of the future heat demand and internal gains (Alimohammadisagvand 2018).

More specific categorization of a state-of-the-art HVAC control methods is shown in Figure 8. Some of these control methods are used only as supervisory control or local control but some may be capable to handle both.

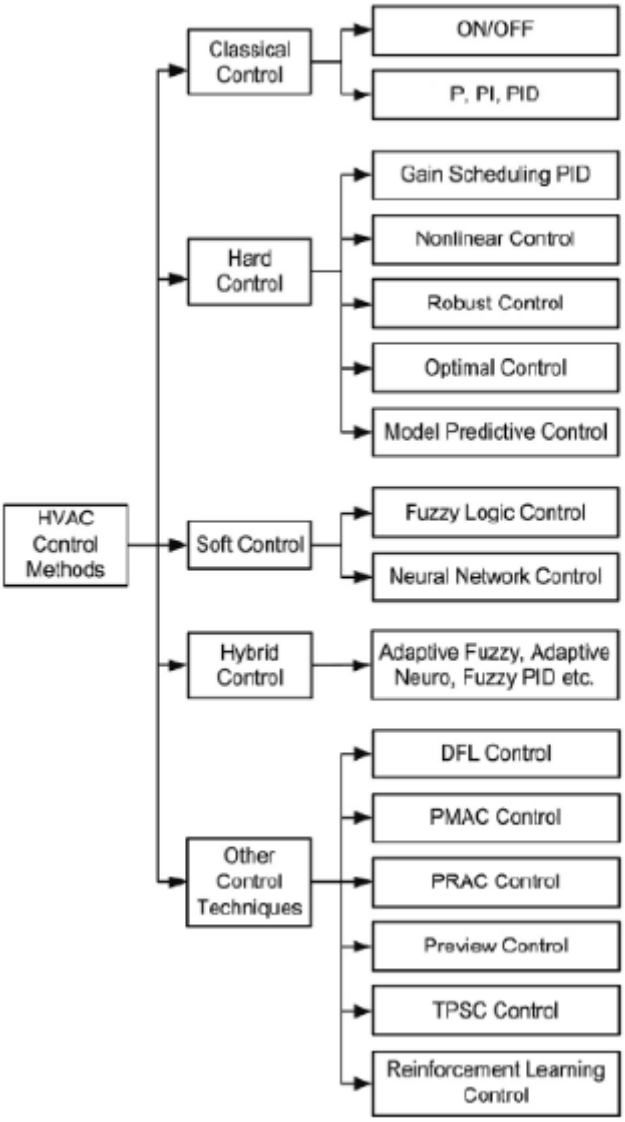

Figure 8. State-of-the-art HVAC control methods (Afram, Janabi-Sharifi 2014).

The most used controls: P, PI, PID and ON-OFF controls belong to classical control group. The principle of on-off control is to keep the process between the upper and lower threshold values by switching the control input ON and OFF. This principle is used in the thermostats. Different PID controllers (proportional–integral–derivative controller) make use of the error physics. The deviation, error, between the setpoint and control output is recorded, and corrections are made to the control input based on the proportion of the error, rate of change of the error and the time the error has persisted. Although the ON-OFF controllers are the most intuitive and easiest to build, they cannot be used to control moving processes with time delays. PID controllers perform well if the operating and tuning conditions (tuning of P, I and D gains) are close to each other. Otherwise the PID controller needs to be tuned every time the operational conditions change which may make the PID cumbersome and time-consuming choice for systems possessing variety of operational conditions (Afram, Janabi-Sharifi 2014).

Gain scheduling control, nonlinear control, robust control, optimal control and model predictive control belong to hard controllers. In gain scheduling the nonlinear system operation is divided into linear regions. The linear regions are controlled by PID controls and each PID controller has been tuned separately and the gains are thus different for each region. The robust controls are developed to control systems that have time-varying disturbances. Model uncertainties and nonlinearities are considered in robust control. The principle in the optimal controllers is that they solve an optimization problem that may deal with energy consumption, control effort and thermal comfort for example. Optimal controls are used for example in passive and active thermal storage control, VAV control and energy optimization of HVAC system (Greensfelder et al. 2011, Korkas et al. 2016). Model predictive control uses a system model to predict the future trends and the decision making in this control method is based on the optimization of cost function. (Kusiak et al. 2011) The MPC control and its benefits are briefly reviewed in the end of this subchapter (Afram, Janabi-Sharifi 2014).

Soft controllers are comparatively new control techniques that include fuzzy logic control and neural network control. Fuzzy logic control is based on logical decision making composed of if-then clauses. Building the fuzzy logic controller requires detailed information about the system operation during different operational conditions. Neural networks such as ANN (artificial neural network) are based on utilizing the historical data of the controlled system. A mathematical model representing the system is constructed that mimics the neural system in human brains. Artificial neural networks are trained to recognize the system conditions based on the historical data and making control decision based on that. To cover wide range of system conditions, extensive amount of historical data may be needed to train the controller (IEA 2018, Afram, Janabi-Sharifi 2014).

Hybrid control are constructed by combining soft and hard controllers. Adaptive fuzzy, Adaptive neuro and Fuzzy PID are couple of examples of hybrid controllers (Dounis, Caraiscos 2009). In addition to all previous mentioned control methods, there are other novel control techniques that are proposed for HVAC control. Perhaps the most promising are the reinforcement learning controllers which use machine learning techniques to learn the behaviour and connections between the process inputs and outputs (Afram, Janabi-Sharifi 2014).

Description of MPC control

As already mentioned, MPC control is based on prediction of the future state of the controlled system by utilizing a build system model. Different modelling approaches for MPC control are briefly introduced next.

The different modelling approaches serve different tasks and phenomena. Selecting the best suitable approach depends on the required quality of the results, what kind of input data is available, and what is the maximal calculation execution time. The high detail of modelling and short time steps results in high quality results, but the calculation time is long and if the input data is coarse the quality of the results is decreased. Longer time steps and lower detail of modelling can be easily used in the normal heating energy demand calculations but for example in the cooling load calculation which are dynamically fast, short time steps are required (Sirén 2016a).

The building models can be grouped roughly to three different groups based on how well the model represents the building: white-box, grey-box and black-box models. White-box models which are also called physical models, are built in detail and they try to capture the thermodynamical behaviour using the principles of building physics. For example, the models build in simulation programs (TRNSYS and IDA ICE) belong to white-box models. Grey box models use simplified physical representation of the building. For example, the heat flows can be described thought simple resistance capacitance network. The blackbox models are based purely on mathematical data-analysis models, which don't include any physical representations of the building. The blackbox models can use either measured building data or data from simulations from which different machine learning algorithms try to capture the thermodynamical behaviour of the building. The physical interpretation of the model is often impossible (IEA 2018).

The building model is utilized in MPC control in predicting the future thermal behaviour of the building and based on that choosing the optimal control strategy. The optimal control strategy is based on optimization of cost function(s). Cost function can incorporate terms dealing with energy efficiency, tracking error, peak power, thermal comfort and RES production. Different constraints can be set for MPC control for example to set acceptable indoor air temperature limits or by determining the system or actuator operational limits. The model in MPC method may include different disturbances. Internal disturbances are caused by the occupant activities, lighting, and equipment use. External disturbances are often linked to weather. Both disturbances are predicted in the model. The weather conditions are predicted by weather forecast and internal disturbances by occupant, equipment and lighting schedules (Afram, Janabi-Sharifi 2014).

Two key variables in the MPC control are the length of prediction and control horizons. The prediction horizon denotes the length of the system operation that is predicted whereas the control horizon refers to the length of time for which the control input is defined. Figure 9 shows the prediction horizon and the predicted control input (control horizon). The length of the control horizon may be equal to prediction horizon or shorter. In Figure 9, the control horizon and prediction horizons are of equal length. The proper choice of these variables is dependent on the system (for example buildings time constant), time scale of the control signals (energy price) and time scale of disturbances (weather data) (Dahl Knudsen, Petersen 2016).

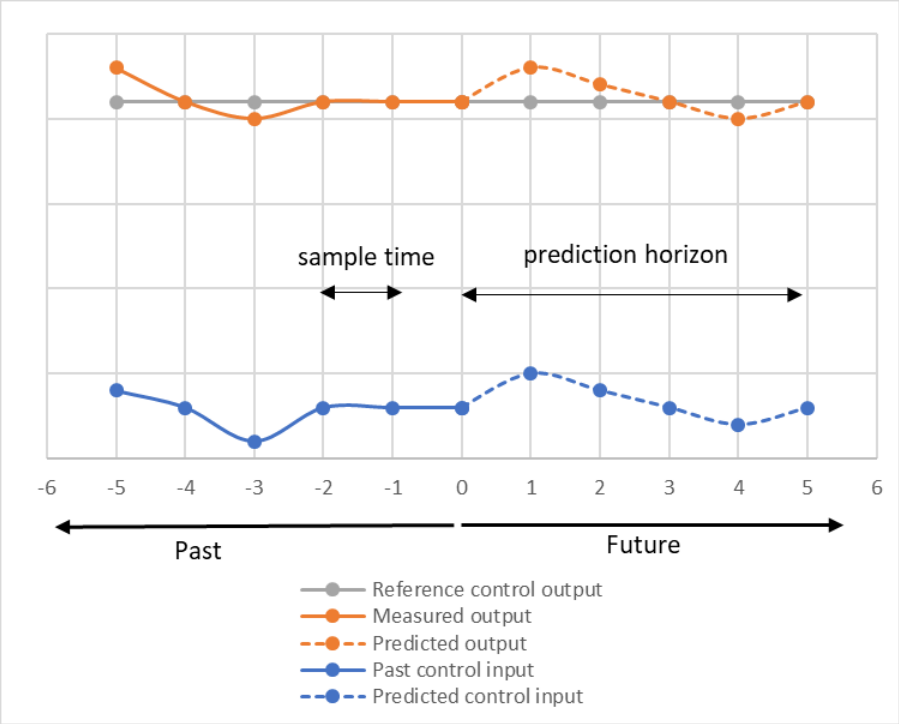

Figure 9. Principle of model predictive control.

3.4.3 Demand response performance indicators

Performance indicators are meant for metering the building and HVAC system performance. Performance indicators enable also comparison of the performance between different buildings and their control and energy systems. For this purpose, the area specific performance indicators are often used.

Traditional performance indicators deal with energy performance and occupant comfort. Metrics for estimating the occupant comfort were already discussed in the chapter 2.3. Energy performance can be characterized for example by the following metrics (Clauß et al. 2017):

- total final energy use, kWh
- total cost of final energy, €
- total primary energy use, kWh
- total net energy use, kWh
- CO_2 emissions, kg.

To evaluate the demand response performance, in addition to energy performance and occupant comfort metrics, the performance indicators that describe the building energy flexibility have been developed (IEA 2018). Energy flexibility, as a concept, can be used to describe the performance of the demand response actions. Energy flexibility can be defined in couple of ways:

- "Energy flexibility can be seen as the **ability** to manage a building's demand and generation according to local climate conditions, user needs and grid requirements." (IEA 2018)

- "It can also be understood as a building **property**, if it is seen as the margin in which the building can be operated while respecting its functional requirements." (Clauß et al. 2017)

- "On the other hand, energy flexibility can be regarded as a **service** which can be provided. In that sense, energy flexibility will allow for demand side management/load control and demand response based on the requirements of the surrounding grids." (IEA 2018)

The key performance indicators to describe the energy flexibility are presented in (IEA 2018). The indicator used in this thesis is flexibility factor, FF, that was first introduced by (Le Dreau, Heiselberg 2016). Flexibility factor describes how well the DR control can shift the energy consumption from expensive periods to cheap energy periods. Flexibility factor gets values between -100% (energy is used only during expensive hours) and 100% (energy is used only during cheap hours). The flexibility factor is calculated with the following equation

$$FF = \frac{\int q_{heating\ during\ low\ price}\, dt - \int q_{heating\ during\ high\ price}\, dt}{\int q_{heating\ during\ low\ price}\, dt + \int q_{heating\ during\ high\ price}\, dt} \quad (5)$$

where

t	time [s]
dt	differential time [s]
$q_{heating\ during\ low\ price}$	heating power at time t when price is low [kWh]
$q_{heating\ during\ high\ price}$	heating power at time t when price is high [kWh].

Le Dreau and Heiselberg defined the high and low heating energy prices based on two weeks historical data as follows:

Low price < 1st quartile of 2-week historical prices

High price > 3rd quartile of 2-week historical prices

The time period that should be used to define the low and high prices is not straightforward. Using shorter time periods when defining the quartiles might be justified because this would prescribe the DR control's ability to react to rapid changes in the energy prices. Martin stated that the time period for defining the price quartiles should be the same as used in the demand response control algorithm (Martin 2017).

4 Methodology in thermal comfort measurement

Demand response of district heating may be implemented by several methods described in chapter 3. Regardless of the method used, it is crucial to assure that the thermal comfort of the occupants is not threatened neither during reduction of heating power (conservation) nor during increased heating power (loading). In this thesis, thermal comfort was examined by measurements with thermal manikin. The objective was to study the effects on the local thermal comfort during the demand response control of space heating. In addition, effort was made to formulate the constraints of thermal comfort for the demand response control.

Experiments were performed in one office room of an educational building at Aalto University campus. Prior to thermal manikin measurements, test smoke visualizations were conducted to examine the upward and downward air flows near the radiator and the cool window surface. After this, thermal manikin was used to measure the equivalent body temperatures in different body segments at varying thermostat setpoints and different window surface temperatures. Additional measurements were carried out to collect information of room air temperature, air humidity, window and radiator surface temperatures and supply and return water temperatures, ventilation air flow rates and supply air temperatures during the measurement periods.

4.1 Measurement room set-up

The thermal comfort with various radiator heating setpoints and different window surface temperatures was studied in one office room with dimensions of 4.2 m (W) x 4.3 m (L) x 2.45 m (H). The measurement setup in the office room is shown in Figure 10. The room had two work stations with adjustable electric tables, chairs and common office furniture. The elevation of the tables was set to be equal to the window bottom frame (at the height 78 cm from the floor). In the office room, there were two large windows (1.8 m (W) x 1.55 m (H) and 1.9 m (W) x 1.55 m (H). Under those windows, there were two water radiators. The thermal manikin used in the experiment was installed in front of the table 2 further from the door (see Figure 10). The layout and the orientation of the room is also shown in Figure 10.

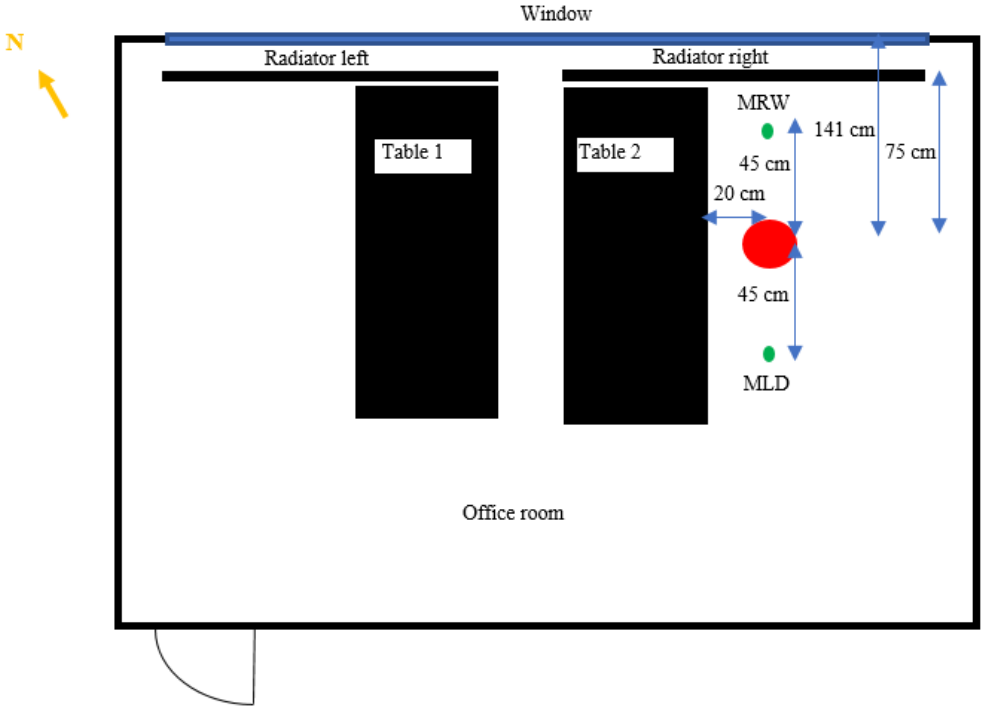

Figure 10. Measurement setup in the office room. Location of the thermal manikin (red dot) and the vertical temperature masts (green dots). MRW and MLD denotes manikin right window and manikin left door sides, respectively.

The heating was provided with a water radiator system. Radiators (Purmo Compact 21) were manufactured by Purmo. The model number 21 denotes that the radiators composed of one convector fin and two radiator plates. Height and width of the radiators were 300 mm and 1600 mm, respectively.

Water radiator heating power was controlled with Fourdeg's electronic IoT thermostat valves. The setpoint temperature for the thermostat valves could be set remotely or by the user. When remote control was applied, demand response algorithm developed by Fourdeg could be used. In the algorithm, marginal district heat costs from the local heat distributor Fortum were used to calculate the optimal control signal for the valves (Salo 2018).

The constant air volume (CAV) ventilation system was used and the air handling unit (AHU) was running continually 24/7. Air distribution was based on mixing ventilation where two supply diffusers (model THB 160, Halton) supplied air in the room (Halton 2018). Supply air diffusers were installed in the centre of the ceiling panels and the exhaust valves were installed in the corridor side near the door. Exhaust air temperature compensation was used to control the supply air temperature.

Air flow rates were measured before the thermal comfort measurements were carried out. The supply air flow was verified using pressure gauge that measured the static pressure loss in the supply air diffuser. The static pressure difference is linearly correlated to the air flow following the manufacturer's product data (Halton 2018). The exhaust air flows were

measured with simple rotating vane anemometer. The total supply and exhaust airflows shown in Table 4 constitute to over pressurized room with supply/exhaust airflow ratio 1.5.

Table 4. Supply and exhaust air flows.

Diffuser/Valve	Supply, l/s	Exhaust, l/s
1	23	13
2	19	15
Total	42 (2.5 l/s,m^2)	29 (1.7 l/s,m^2)

4.2 Thermal manikin set-up

Thermal manikin, build by former Helsinki University of Technology (Foda 2012), was used to evaluate the local thermal comfort while the radiator thermostats setpoint was controlled. Manikin used in this study was size of 50 on European male index and it consisted of 24 heated body parts shown in Figure 11. The body parts are named according to Table 5. Compared to Foda's measurements (measurement points in Figure 11), some measurement points were combined to form only one measurement point. Neck and head were combined, ankles were combined to feet and the right and left hip were combined to one point, named abdomen. This results in 20 body parts used in this measurement.

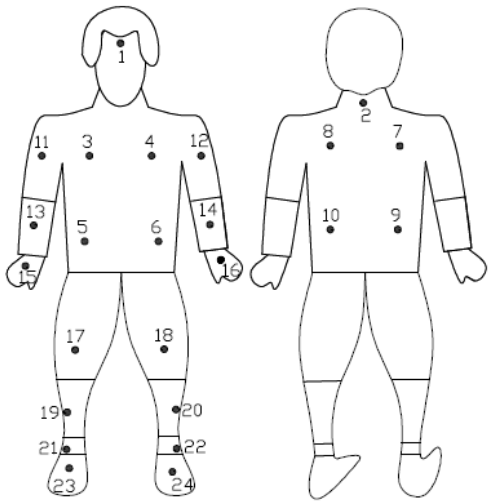

Figure 11. Body parts of the manikin and location of temperature sensors.

Table 5. Manikin body parts.

#	Name of the body part	Abbreviation
1	Head	Head
2	Neck (combined to head)	Head
3	Right chest	R_chest
4	Left chest	L_chest
5	Abdomen (combined left and right hip)	Abdomen
6	Abdomen (combined left and right hip)	Abdomen
7	Upper right back	UR_back
8	Upper left back	UL_back
9	Lower right back	LR_back
10	Lower left back	LL_back
11	Upper right arm	UR_arm
12	Upper left arm	UL_arm
13	Lower right arm	LR_arm
14	Lower left arm	LL_arm
15	Right hand	R_hand
16	Left hand	L_hand
17	Right thigh	R_thigh
18	Left thigh	L_thigh
19	Right leg	R_leg
20	Left leg	L_leg
21	Right ankle (combined to right foot)	R_foot
22	Left ankle (combined to left foot)	L_foot
23	Right foot	R_foot
24	Left foot	L_foot

Manikin was movable: it could stand, sit, move its arms and breathe. In this experiment, manikin was set to sit on an office chair with its hands positioned above the office table. The breathing was not included in this experiment since it was not supposed to have any significant effect on the local thermal comfort.

The water radiator setpoints were controlled according to schedule shown in Table 6. Constant setpoints were chosen to be in ascending order starting from 18 °C and finishing to 24.5 °C. Ascending constant temperature setpoints were used to evaluate the local thermal comfort at varying conditions. The total experiment time was 4 days.

Table 6. Radiator thermostat setpoints during the measurement. After the final time period, the Fourdeg's DR control was turned on to control the setpoints.

Date	Time period	Radiator temperature setpoint, °C
29.3-30.3	18.00 - 12.00	18.0
30.3	12.00 - 18.00	18.5
30.3	18.00 - 24.00	19.0
31.3	00.00 - 06.00	19.5
31.3	06.00 - 12.00	20.0
31.3	12.00 - 18.00	20.5
31.3	18.00 - 24.00	21.0
1.4	00.00 - 06.00	21.5
1.4	06.00 - 12.00	22.0
1.4	12.00 - 18.00	22.5
1.4	18.00 - 24.00	23.0
2.4	00.00 - 06.00	23.5
2.4	06.00 - 12.00	24.0
2.4	12.00 - 18.00	24.5
2.4	18.00 ->	DR

Labview was used as a platform to build the control tasks and measurements. Control mode was ON-OFF type meaning that heating foils inside the manikin were either ON or OFF. Timestep of control was 50 ms and deviation ± 0.05 °C. Skin surface temperature was measured in 1 min interval. The control algorithm of the manikin was developed by Ehab Foda (Foda 2012).

The manikin had normal office environment clothing. The clothing consisted of under shirt, shorts, denim trousers, long sleeve shirt and calf-length cotton socks. The clothing level was measured according to (EN ISO 9920 2007) resulting in clothing level of 0.6 clo = 0.155 m^2K/W. The surface heat transfer coefficients for each body part were determined in the Foda's doctoral thesis (Foda 2012). The clothing used in this experiment was similar to that when determining the heat transfer coefficients, thus the same heat transfer coefficients were used. The manikin was controlled by the constant surface temperature mode (CST) in which case the influence by the environment is shown in the required heating power to keep the temperature constant in each body segment. The heating powers at each time step were used to calculate the corresponding equivalent temperatures.

Data measured with the thermal manikin included the skin surface temperature, the setpoint for constant surface temperature control (CST), equivalent temperature and heating power. Skin temperature and setpoint temperature were equal all the time since CST control was used. The equivalent temperature was used to evaluate the change in thermal comfort of the manikin.

4.3 Thermal environment measurements

In addition to the thermal manikin measurement, separate test smoke visualizations were conducted a week before the manikin measurements to detect the air flow pattern near the window surface with low and high thermostat setpoints. It was assumed that the cool window surface could result in downward convective air flows that might direct towards the manikin and cause draught. The downward air flows are also known as downdraughts. Test smoke was released near the window surface at different heights to see the air flows. While one person was releasing the test smoke another person used camera to record the airflows. The test smoke used in this experiment was Dräger air current tube CH25301 (Dräger 2018).

During the thermal manikin experiment, additional measurements were performed to obtain information about the indoor thermal environment conditions. The additional measurements included vertical temperature difference, air temperature and relative humidity, window surface temperature, radiator inlet and outlet pipe surface temperatures and supply air temperatures. In addition, Fourdeg's thermostat data which consisted of spindle position, thermostat setpoint and room air temperature at the thermostat was obtained from the Aalto Smart Campus server.

Vertical temperature difference describes the thermal environment at close vicinity to the manikin. The vertical temperature difference was measured from the both sides of the manikin at four heights 10 cm, 60 cm, 100 cm and 130 cm above the floor level. Four Tinytag plus 2 (model: TGP-4500) temperature and humidity loggers were attached into two measurement masts. The measurement inaccuracy for temperature was less than 0.5 °C between temperatures 5 °C – 40 °C and for relative humidity ± 3% when temperature was 25 °C (Geminidataloggers 2018). Measurement masts were then positioned on right and left sides of the manikin (measurement points MRW and MLD in Figure 10) at the distance of 45 cm from the manikin's head. Thermal manikin and the temperatures measurement masts are shown in Figure 12. Time interval of 1 minute was used in the measurements.

Figure 12. Manikin and temperature measurement rods.

Air temperature was measured with Tinytag plus 2 temperature and humidity logger that was attached to the wall at the height of 1 meter from the floor. The direct solar radiation did not have any effect on the logger measurement, because the window orientation was towards north-east. That is why no solar protection was installed on the measurement sensor. The window surface temperature was measured with a thermoelement. Measurement point was at the middle of the window glass at the height of 10 cm above the frame. Supply air temperature was also measured with a thermoelement which was installed inside the supply air diffuser and the data was collected with datalogger. The time interval of 15 minutes was used with room air temperature, window surface temperature and supply air temperature measurements.

The water radiator inlet and outlet water temperatures were measured with thermoelements attached to the surface of the radiator inlet and outlet pipes. The thermoelements were covered with insulation to minimize the surface heat loss. The measured data was collected with dataloggers using time interval of 15 min. The measured inlet and outlet water temperatures were used to calculate the radiator heating power which can be used to assess the energy consumption of the radiators during the test.

Radiator heating power was approximated using the equation 6 from the standard (Purmo 2018, SFS-EN 442-2 2015)

$$P = P_n \left(\frac{\frac{T_m - T_p}{ln\left(\frac{T_m - T_h}{T_p - T_h}\right)}}{\frac{}{\Delta T_n}} \right)^n \cdot w \qquad (6)$$

where

P_n radiator model and height dependent nominal power with nominal over temperature 49.8 °C, [W/m]

T_m inlet water temperature, [°C]

T_p outlet water temperature, [°C]

T_h room air temperature, [°C]

ΔT_n nominal over temperature (specified by the manufacturer: 49.8 [°C])

n radiator specific exponent

w radiator width, [m].

5 Model predictive control implemented demand response

Model predictive control algorithm was constructed to study demand response of space heating in an educational office building. Target for the control algorithm was to determine optimal control setpoints for space heating that minimizes the heating energy costs, maximizes heating energy flexibility and do not impair the thermal comfort. The results from the thermal manikin experiments were utilized as constraints in the algorithm to prevent local thermal discomfort in workstations near windows.

5.1 Case building

5.1.1 Basic information

Figure 13. The case building Otakaari 4 in Otaniemi campus area (Aalto University 2018).

Educational building, located in Otakaari 4 (Figure 13), in Otaniemi campus area was chosen as a case building for which the model-based control algorithm was developed. This building was constructed in 1966 during the same era as most of the buildings in the campus area. During the lifetime of the building, there has been several renovations, thus only the upper slab and outer walls are of the original construction (Martin 2017). In the most recent renovation the windows were replaced to new energy efficient windows (Aalto University 2015).

Otakaari 4 building has facilities for teaching and university faculty such as lecture halls, office rooms, restaurant and rooms for student organisations. The case study was however limited to the 4th floor which had only office rooms, conference room, small kitchen and corridors. Figure 14 presents the 4th floor layout. The studied floor had the heated net floor area of 586 m^2, the envelope area of 947 m^2 and window/envelope area ratio of 11.5%.

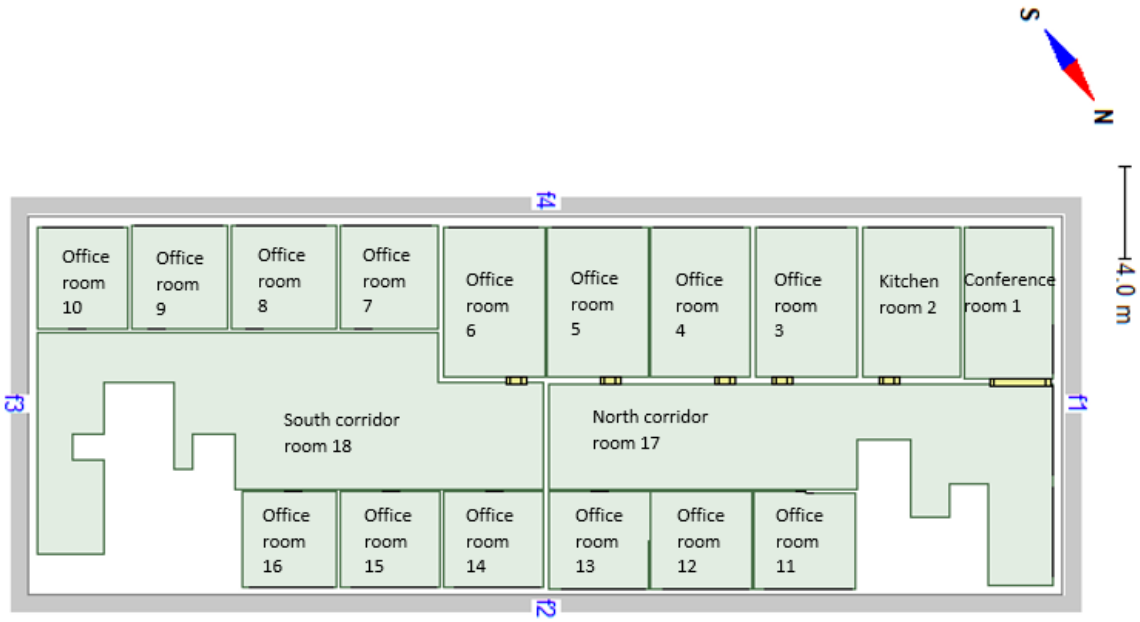

Figure 14. The 4th floor of the case building.

5.1.2 Building structures

The case building was constructed of heavy weight structures that are generally seen well-suitable for demand response implementation. All bearing structures were built of reinforced concrete. The core of the outer walls was reinforced concrete and the façade was brick-faced. The upper slab and the internal slabs were also built using reinforced concrete. The inner walls had two types of structures, one with light gypsum board walls and second with lightweight-blocks. The external floor structure was not taken into account in this study since only the 4th floor was studied.

The new replaced windows were two pane wood-aluminium windows with three-layer glazing and argon filling. In the South-West façade, windows had better solar protection properties than in the other facades. Otherwise the windows had similar properties in the case floor. The office room windows had solar shading blind between the outer panes of the window and they were taken into account in the IDA ICE model. The inner doors were light-weight and the doors between the office rooms and the corridor were kept open during the office working hours 8.00-16.00.

The air leakage rate of 1.6 (n_{50}) at the 50 Pa pressure difference between the inside and outside was used in the simulations. The thermal bridge heat losses were defined according to the guidelines of the Finnish building code D5. The building envelope structure's U-values and the linear thermal bridge conductances are presented in Table 7 (National building code of Finland 2012).

Table 7. The properties of the case building structures.

Structures	U-value W/(m^{2}K)
External wall	0.38
Roof	0.3
Window, South-West	1.1 (g-value 0.38)
Window, North-West and North-East	1.1 (g-value 0.59)
Window frames, All	2.0
Thermal bridges	Conductance [W/(mK)]
External wall / Roof (per meter joint)	0.03
External wall / Internal wall (per meter joint)	0.016
External wall / External wall (per meter joint)	0.06
Window circumference (per meter circumference)	0.04
External floor / Internal wall (per meter joint)	0.017
Roof / Internal wall (per meter joint)	0.0086
External wall, inner corner (per meter joint)	-0.06

5.1.3 HVAC systems and operation

Space heating, domestic hot water and air handling unit's heating coils were heated by local district heating network. The dimensioning inlet/outlet temperatures of the hydronic radiator system and AHU heating system were 70/40 °C. The dimensioning outdoor air temperature in Southern Finland is -26 °C. Domestic hot water consumption was not considered in this study, since it was not part of the demand response scheme.

The control curve shown in Figure 15 was used to control the radiator inlet water temperature at varying outdoor air temperatures. The radiators were manufactured by Purmo and the electronic IoT thermostat valves by Fourdeg. The nominal heating powers for each radiator were modelled in IDA ICE according to the design documents.

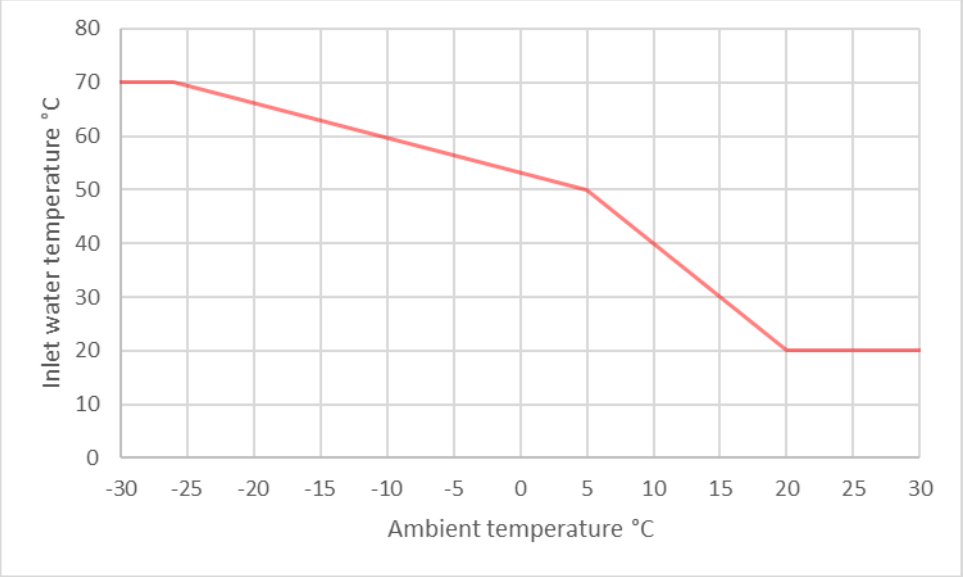

Figure 15. Radiator supply water temperature curve.

Both AHU and space cooling systems were supplied by liquid cooled chiller manufactured by Chiller Oy. In the case floor, only one cooling convector supplied space cooling in the hallway. Heating and cooling network losses were neglected, and thus they did not constitute any heat gains to spaces. The DH-substation efficiency of 97% was used which is regarded as normal efficiency of substations in larger buildings (National building code of Finland 2012).

The ventilation system in the case building was central supply and exhaust ventilation system with heat recovery. Two air handling units AHU 302 and AHU 303 served the case floor. These AHUs served also other spaces. In IDA model, only the AHU 303 was modelled without sever drop of accuracy since both of the AHUs had similar components and were operated by same automation system settings. The variable air volume VAV ventilation system was used in conference rooms, while other rooms were handled by constant air volume CAV system. The ventilation air flows were modelled in IDA according to design documents. The operation schedule for the AHUs was 00:00-24:00 each day of the year. The supply air temperature was exhaust air temperature compensated according to the control curves shown in Figure 16. The altered supply air temperature curve was created and used in the MPC algorithm simulation cases since then the heating/cooling operations could not contradict with the space heating system.

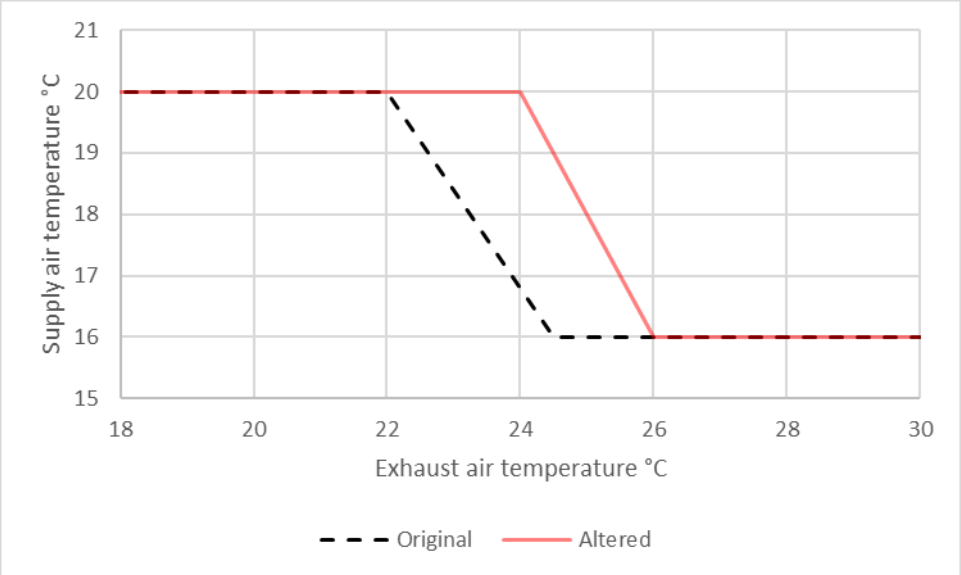

Figure 16. The original and altered supply air temperature curves.

5.2 MPC algorithm for demand response

5.2.1 General process diagram

Figure 17 shows the principle of the simulation approach. First the input data including the weather forecast, marginal district heating price and internal heat load forecast was imported into the model predictive control simulated in the Matlab computational software. The MPC model in the Matlab composed of the calibrated physical building model and a multi-

objective optimization algorithm. The optimization algorithm ran the physical building model several times to find the optimal thermostat setpoints for the chosen prediction horizon. The optimization was repeated so that heating setpoints for entire year were obtained. Once the optimization was finished, the optimal setpoints were exported to IDA ICE building simulation model. IDA ICE simulation was then ran with these setpoints and the room specific temperatures were recorded. Algorithm in IDA ICE environment checked that the room air temperatures remained between the acceptable limits. If these conditions were not met, the algorithm changed the setpoint from the optimized value to the nominal value of 21 °C. This process was repeated for different case studies where the prediction horizon, optimization objectives or input data was altered.

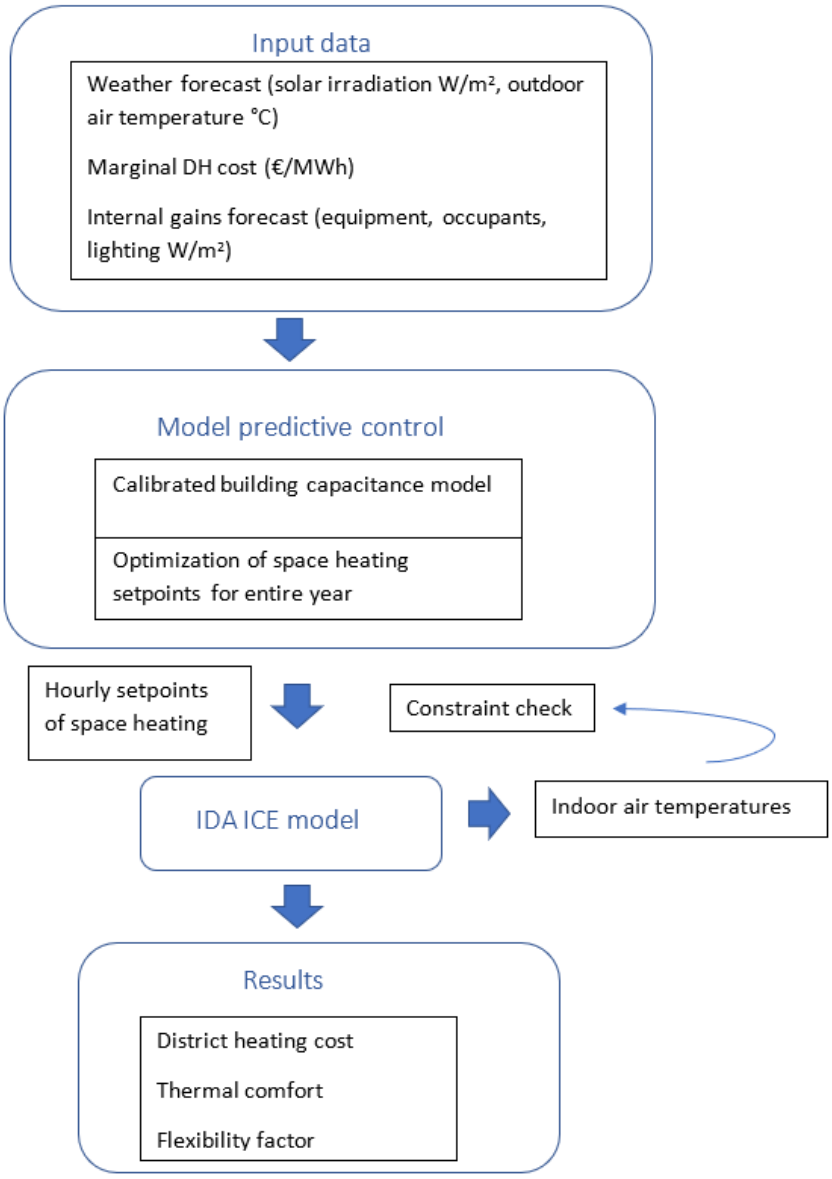

Figure 17. Process diagram of the simulation approach.

5.2.2 IDA ICE and Matlab software

IDA ICE dynamical building simulation software was used for two purposes. Firstly, it was used as a calibration reference model in the calibration of the building capacitance model. Secondly, the IDA ICE model was used to test the performance of the MPC demand response algorithm with different DR cases.

IDA Indoor Climate and Energy 4.8 (IDA-ICE) was chosen as a simulation software because it is an innovative and reliable dynamic simulation program that can be used to analyse the indoor air quality, thermal comfort and energy consumption of buildings. In IDA ICE, the buildings geometry, structures, HVAC systems and building usage can be modelled. The location and the corresponding climate data can also be chosen. The calculation of heat and mass transfer processes are performed in varying time steps for minimized simulation time and maximized accuracy. IDA ICE fulfils the European standard prEN13791 and it has been validated in numerous studies, for example (Vuolle, Sahlin 2000, Kropf, Zweifel 2001, Equa Simulation 2010).

The case floor was modelled in IDA ICE according to the design drawings and known initial building data presented in chapter 5.1. Local zone control macro was used to insert the space heating setpoints given by the MPC algorithm. In addition to inserting the heating setpoints, a small part of the MPC was constructed in IDA as a form of temperature feedback control. In all spaces, the average room air temperature was recorded and if it exceeded the limit of 24.5 °C during any time of the whole year simulation, the MPC setpoint was replaced by normal heating setpoint of 21 °C in that specific room. The purpose of the feedback control was to prevent overheating.

Excluding the room temperature feedback control in IDA, the MPC was built in Matlab (R2018a) computational software. Matlab is a software for technical computing that is mostly used by engineers and scientists. Matlab uses its own matrix-based language that can be integrated to other languages as well. Matlab was chosen for creating the MPC control because the computational model was easy to build using the matrix-based language, and the computationally expensive optimization algorithm could be run efficiently in this environment (Matlab 2018).

5.2.3 Building capacitance model

Building capacitance model was used as a model in the model predictive controller build in the Matlab software. The principle in the MPC control is that the model is used to predict the space heating demand and in other hand calculate the values for the objective functions in the optimization. The optimization in the MPC algorithm tries to find the most optimal space heating temperature setpoints by running the capacitance model of the building.

Simple resistance/capacitance model or shortly RC-model was chosen to be used in the modelling in this study. Since the purpose was to capture only the large-scale changes in the buildings thermodynamical behaviour, the lower level of detail was regarded sufficient for this purpose. The time step for calculation was set to 1 hour because also the weather and DH cost data was hourly based.

RC-model is one of the simplest physical building models. It consists of one or several temperature node points. In this study the two-temperature node point model was used where

the first temperature node point was attached into the centre of the room air volume (T_a in Figure 18) and the second one to the combined (lumped) structure mass node point (T_m in Figure 18). The node points are connected by conductances which describe the heat flows between the nodes. Figure 18 shows the schematic of the RC-model.

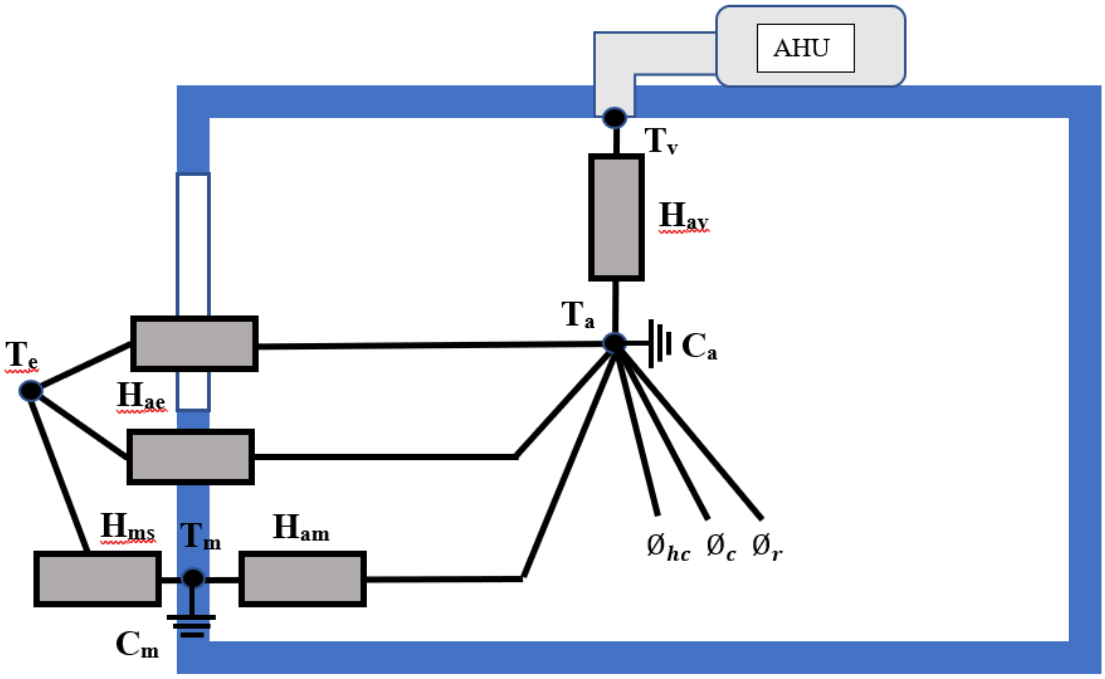

Figure 18. The schematic of the RC-model. Modified from (Sirén 2016a).

Symbol	Description	Unit
C_m	Heat capacitance of the mass node point	J/K
C_a	Heat capacitance of the air node point	J/K
H_{ae}	Combined conductance of the windows and leakage air	W/K
H_{ms}	Conductance between mass node and outdoor air node point	W/K
H_{am}	Conductance between mass node and indoor air node point	W/K
H_{av}	Heat capacity flow through ventilation	W/K
T_e	Exterior/outdoor temperature	°C or K
T_m	Mass temperature node point	°C or K
T_a	Air temperature node point	°C or K
T_v	Supply air temperature node point	°C or K
$\emptyset_{hc}$	Zone heating/(cooling) power	W
$\emptyset_c$	Convective heat loads	W
$\emptyset_r$	Radiative heat loads	W

The energy balance equation for the air and mass temperature node points can be formulated as follows

$$\frac{C_a dT_a}{dt} = H_{av} * (T_v - T_a) + H_{ae} * (T_e - T_a) + H_{am} * (T_m - T_a) + \emptyset_c + \emptyset_{hc} \quad (7)$$

$$\frac{C_m dT_m}{dt} = H_{ms} * (T_e - T_m) + H_{in} * (T_a - T_m) + \emptyset_r \quad (8)$$

where

dT_a	temperature differential of air node point
dT_m	temperature differential of mass node point
dt	time differential.

The two differential equations can be solved numerically by first discretising them using the implicit method (Sirén 2016a) and then solving the required variable (T_a, T_m or $\emptyset_{hc}$) from the discretized equations

$$C_a \frac{T_{a,t} - T_{a,t-\Delta t}}{\Delta t} = H_{av} * (T_v - T_{a,t}) + H_{ae} * (T_{e,t} - T_{a,t}) + H_{am} * (T_{m,t} - T_{a,t}) + \emptyset_c + \emptyset_{hc} \quad (9)$$

$$C_m \frac{T_{m,t} - T_{m,t-\Delta t}}{\Delta t} = H_{ms} * (T_{e,t} - T_{m,t}) + H_{am} * (T_{a,t} - T_{m,t}) + \emptyset_r \quad (10)$$

where subscripts t and t-Δt refer to current time and previous time instance, respectively, and Δt is the length of time step.

Solving the temperatures $T_{a,t}$ and $T_{m,t}$ from equations 9 and 10, respectively and simplifying the equations by replacing on the right hand side the other unknown temperature of the present moment (t) to known temperature of the previous time step (t-Δt), we get the following pseudo-implicit equations:

$$T_{a,t} = \frac{\frac{C_a}{\Delta t} * T_{a,t-\Delta t} + H_{av} T_v + H_{ae} * T_{e,t} + H_{am} * T_{m,t-\Delta t} + \emptyset_c + \emptyset_{hc}}{\frac{C_a}{\Delta t} + H_{av} + H_{ae} + H_{am}} \quad (11)$$

$$T_{m,t} = \frac{\frac{C_m}{\Delta t} * T_{m,t-\Delta t} + H_{ms} T_{e,t} + H_{am} * T_{a,t-\Delta t} + \emptyset_r}{\frac{C_m}{\Delta t} + H_{ms} + H_{am}} \quad (12)$$

Simplifying the equations this way, sacrifices slightly the precision of the exact implicit solution, but compared to other uncertainties in the model the error is insignificant.

The case floor involves several rooms (office rooms, kitchen, corridor, conference room). However, only two office rooms were chosen to be modelled in two separate building capacitance models. The reason was that if every room would have been modelled in one

building capacitance model, the differences between the rooms could have distracted the model and optimization results by balancing each other out. In other hand, the calculation time when modelling only two rooms was much shorter than if every room would have been modelled separately. At least two rooms had to be modelled because the solar heat gains in the rooms at the South-East façade and the North-East façade differ significantly. All in all, the results from these two capacitance models could capture the large-scale thermal behaviour that represents the entire floor.

Modelling only two office rooms makes the choosing of the most representative rooms important. The choice of the modelled rooms was made so that the rooms would represent an average office room in respect of the structures and the external structural surface area, external (solar) heat gains, internal heat gains, air volume and air exchange rate. The chosen rooms are highlighted with red dots in Figure 19.

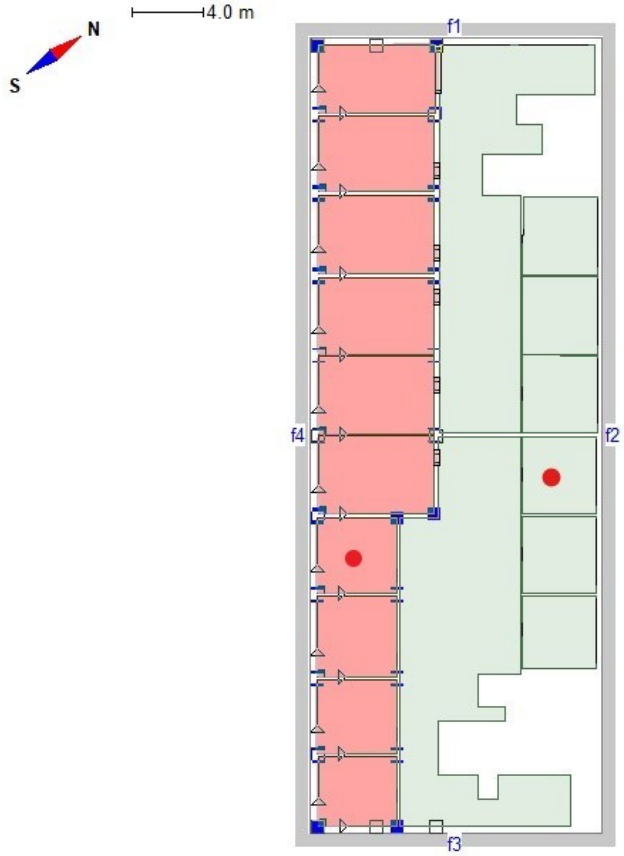

Figure 19. The heating temperature setpoints generated in MPC algorithm with South-West façade solar heat gains (red) and North-East façade solar heat gains (green). The red dot shows the RC-modelled rooms.

As a conclusion, two capacitance models representing two rooms from the different building facades were build. The MPC algorithm was run separately for these two capacitance models. The first run involved the capacitance model of the first room and the second run involved the capacitance model of the second room. Thus, the MPC algorithm produced two heating setpoint series, one for the North-East and another for the South-West side of the

building. These setpoint series were then inserted into the IDA ICE modelled rooms as shown in Figure 19. Heating temperature setpoints from the MPC algorithm ran with the South-West and North-East side rooms are shown in red and green colours, respectively. The corridors have the same setpoints as in the North-East façade since the solar heat gains in corridors and North-East side rooms are closer to each other compared to corridors versus South-West side.

5.2.4 Calibration of the capacitance model

When modelling a building with RC-model, all of the heat conductances and heat capacitances expressed in heat balance equations 7-8 need to be determined. In this study, the IDA ICE simulation results were used to calibrate the conductances and capacitances in the RC-model so that the thermal behaviour in RC-model matched with the results from reference model built in IDA ICE. The RC-model calibration was performed using the methodology developed by Kai Sirén.

First, the chosen representative room was modelled in IDA ICE simulation program (calibration reference model) and in Matlab (the simplified RC-model). Geometry, structures, air exchange rate and infiltration air rate were modelled according to the design values (presented in chapter 5.1). No internal gains were used in the models since they are not relevant in the calibration as long as they are constant.

The calibration was divided into two parts shown also in Figure 20:

1. steady-state parameter identification (0-150 h)
2. dynamic parameter identification (150-250 h).

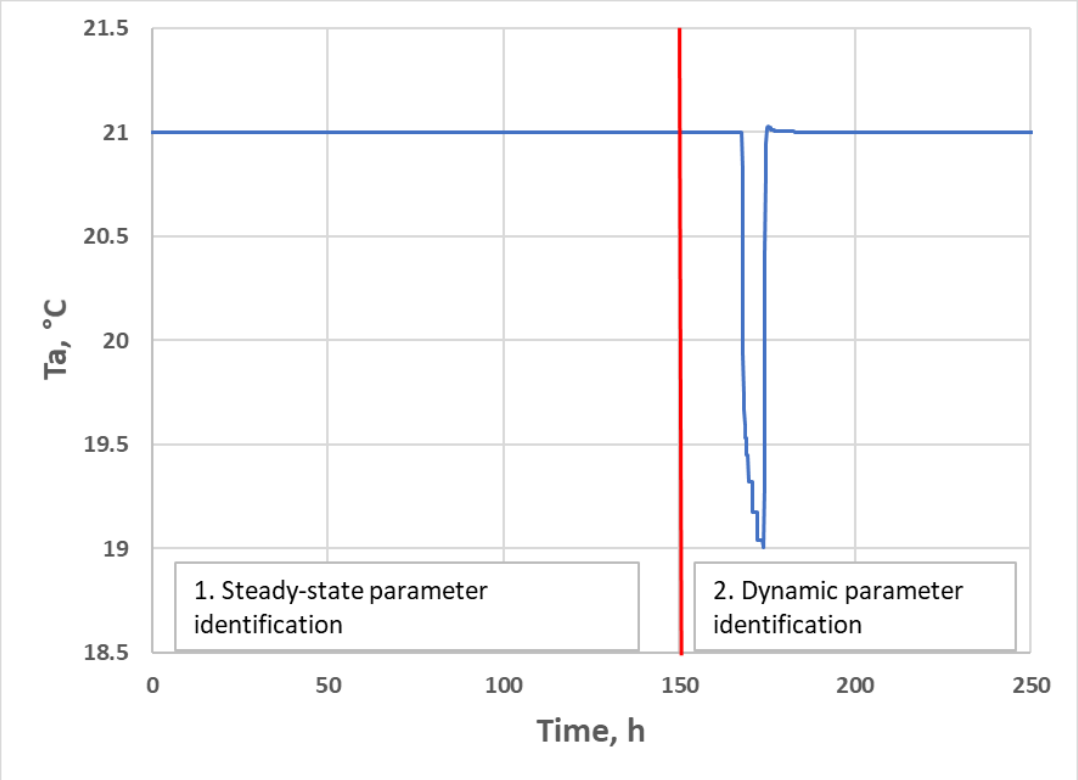

Figure 20. Steady-state and dynamic parameter identification in RC-model calibration with constant T_e=-10 °C.

Steady-state parameter identification

In the steady-state parameter identification, the purpose was to fix the conductance values of the simplified model to make the steady-state air node energy balance in simplified RC model and IDA ICE model to match. Conductance values were searched by running the IDA ICE model with artificial weather file were all the quantities (solar radiation, external temperature, wind) had constant values. For the external temperature, three different values (+10 °C, 0 °C, -10 °C) were used to get an average for the phenomena that are outdoor temperature dependent such as heat transfer coefficients and window U-values.

First, the IDA ICE model with constant values was ran long enough so that the building reached steady-state condition from which the conductance values and the heat capacity flows could be determined. IDA ICE has a dynamic startup simulation of 14 days, and for this reason the air temperature seen in Figure 20 has already reached steady state at the beginning of actual simulation time. All other conductances except H_{am} and H_{ms} could be inserted straight from IDA model to the RC-model. The conductances (H_{am} and H_{ms}) on both side of the mass node point had to be combined to one conductance (H_{ams}) in steady-state identification phase because the division between these can only be determined in the dynamic parameter identification. The combination of conductances was performed following the thermal resistance series connection (analogy to electrical circuits). The correct value for H_{ams} was searched so that the error in heating powers resulting from air node energy balance between the IDA ICE and the RC-model at the three different outdoor temperatures was at the minimum.

Dynamic parameter identification

The dynamic parameter identification was conducted after the conductances were determined in the steady-state parameter identification. In the dynamic parameter identification, the purpose was to determine the air and mass heat capacities (C_a and C_m) and to identify the division of the conductance H_{ams} into its components H_{ms} and H_{am}, which were combined in the steady state parameter identification. The dynamic behaviour was investigated by inserting a time-dependent change during the simulation in one of the dynamical variables in the modelled system (external temperature, solar radiation, internal loads or heating power). Since the RC-model was intended to forecast heating demand, the heating power was chosen as a variable where the time-dependent change was made. The room air temperatures in RC-model and IDA model were then compared and used for parameter identification.

The duration and the magnitude of the change in the heating power is important in the investigation of the dynamic behaviour of the building. In this calibration a six hour decrease in the heating power was used. The heating power was changed by changing the heating setpoint for the six-hour period. First the building model was simulated with the heating setpoint temperature of 21 °C for 14 days. This way the case room was in steady-state before the dynamic interruption. After this, heating was turned OFF for six hours. After the six-hour period, heating was turned back ON with the setpoint of 21 °C. The IDA ICE reference simulations were again performed in three different outdoor air temperatures (+10 °C, 0 °C, -10 °C) and the room air temperatures and heating powers were recorded.

In the dynamic parameter identification, three parameters (H_{am}, C_m, C_a) were to be determined based on the IDA reference simulations (not straight from IDA model) and thus a different identification method had to be used. In dynamic parameter identification the room air temperature between the models was used as identification criteria to find values for H_{am}, C_m and C_a. It was required that the air temperature in both models would match with each other during the dynamic change in heating power. Therefore, the dynamic calibration was defined as a minimization problem, where the average absolute differences between air temperatures in IDA model and RC-model from the simulations with three different outdoor temperatures were minimized:

$$Min\left\{F(\boldsymbol{x}) = \frac{1}{n}\sum_{i=1}^{n}|T_{ai}(\boldsymbol{x}) - T_{ari}|\right\} \qquad (13)$$

where

i	computation time step of the calibration period
T_{ai}	room air temperature from the RC-model at the time step i
T_{ari}	room air temperature in the reference model at the same time step i.

The air temperature in RC-model is dependent on vector $\boldsymbol{x}$ containing the parameters to be identified:

$$\boldsymbol{x} = (H_{am}, C_m, C_a)^T.$$

The minimization problem was solved by using a straightforward sequential search algorithm supplemented with a local refinement procedure. Figure 21 presents the indoor air temperatures in the IDA model and in the RC-model after the calibration with constant exterior air temperature T_e = -10 °C. Table 8 shows the calibrated parameter values.

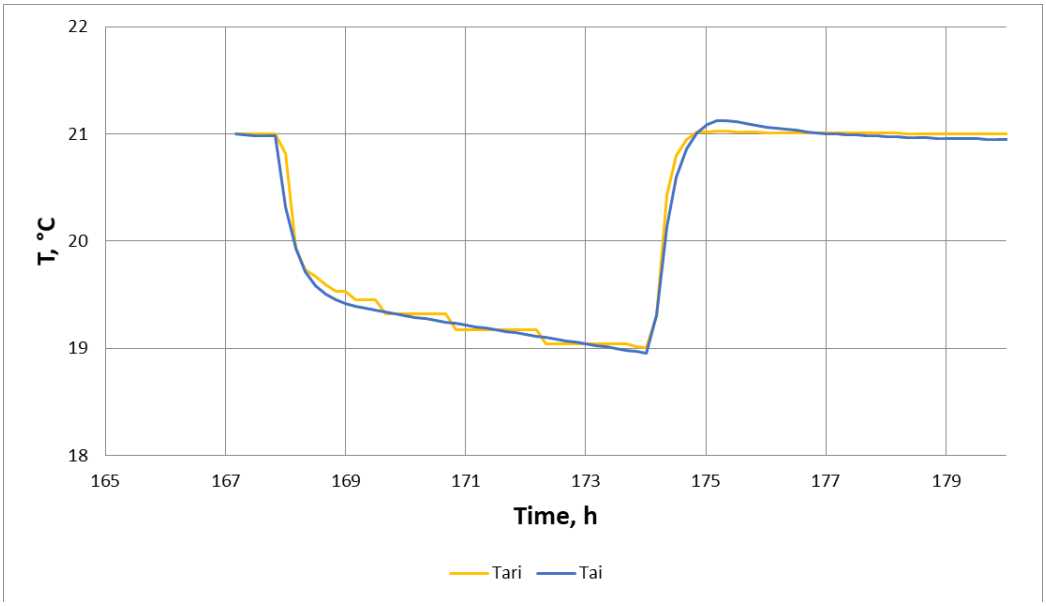

Figure 21. Indoor air temperature in RC-model (T_{ai}) and IDA-model (T_{ari}) after calibration at the outdoor air temperature -10 °C.

Table 8. Calibrated parameter values (with window type 1 described in chapter 5.3)

H_{ams}	H_{av}	H_{ae}	H_{ms}	H_{am}	C_a	C_m
W/K	W/K	W/K	W/K	W/K	kJ/K	kJ/K
10.4	51.8	7.7	10.7	372.2	336.3	19290

Calibrated parameters in RC-model model can be used to study different demand response cases as long as no changes are made to the building structures, geometry, air exchange rate or infiltration air rate. If any of these variables are modified, the calibration must be repeated. In this study, the calibration was performed twice since two window constructions were investigated. Table 9 shows the calibrated parameter values with the window type 2.

Table 9. Calibrated parameter values (with window type 2 described in chapter 5.3)

H_{ams}	H_{av}	H_{ae}	H_{ms}	H_{am}	C_a	C_m
W/K	W/K	W/K	W/K	W/K	kJ/K	kJ/K
9.8	51.8	16.0	10.0	369.6	383.8	16867

5.2.5 Forecasting heating demand with capacitance model

The calibrated RC model was used to forecast the heating demand in the optimization phase of the MPC algorithm. The heating demand with different space heating setpoints trajectories (optimization variable) could be solved in addition to the resulting zone heating energy cost and room air temperatures which were used in the optimization objectives.

The heating demand calculation followed the process diagram shown in Figure 22. First the free-floating room air temperature $T_{a,ff}$ was calculated from the discretized energy balance equation 9 by replacing the air temperature by the free-floating air temperature ($T_{a,t} = T_{a,ff}$). Floating temperature means that the heating was turned OFF, $\emptyset_{\mathrm{hc}} = 0\ W$. If the free-floating air temperature was above the predefined heating setpoint T_{sp}, there was no heating demand and the internal gains and solar radiation kept the room temperature above the required level (Sirén 2016a).

If, however the free-floating air temperature stayed below the heating setpoint temperature the appropriate average heating power demand was calculated from the discretised energy balance equation:

$$\emptyset_{hc} = (H_{ae} + H_{av} + H_{am}) * T_{a,t} - (H_{ae}) * T_{e,t} - H_{av}T_v - H_{am} * T_{m,t} - \emptyset_c +$$

$$C_a \frac{T_{a,t} - T_{a,t-\Delta t}}{\Delta t} \qquad (14)$$

where the air node temperature was set equal to the heating setpoint $T_{a,t} = T_{sp}$.

When heating demand over all the time instances had been computed, the process ended.

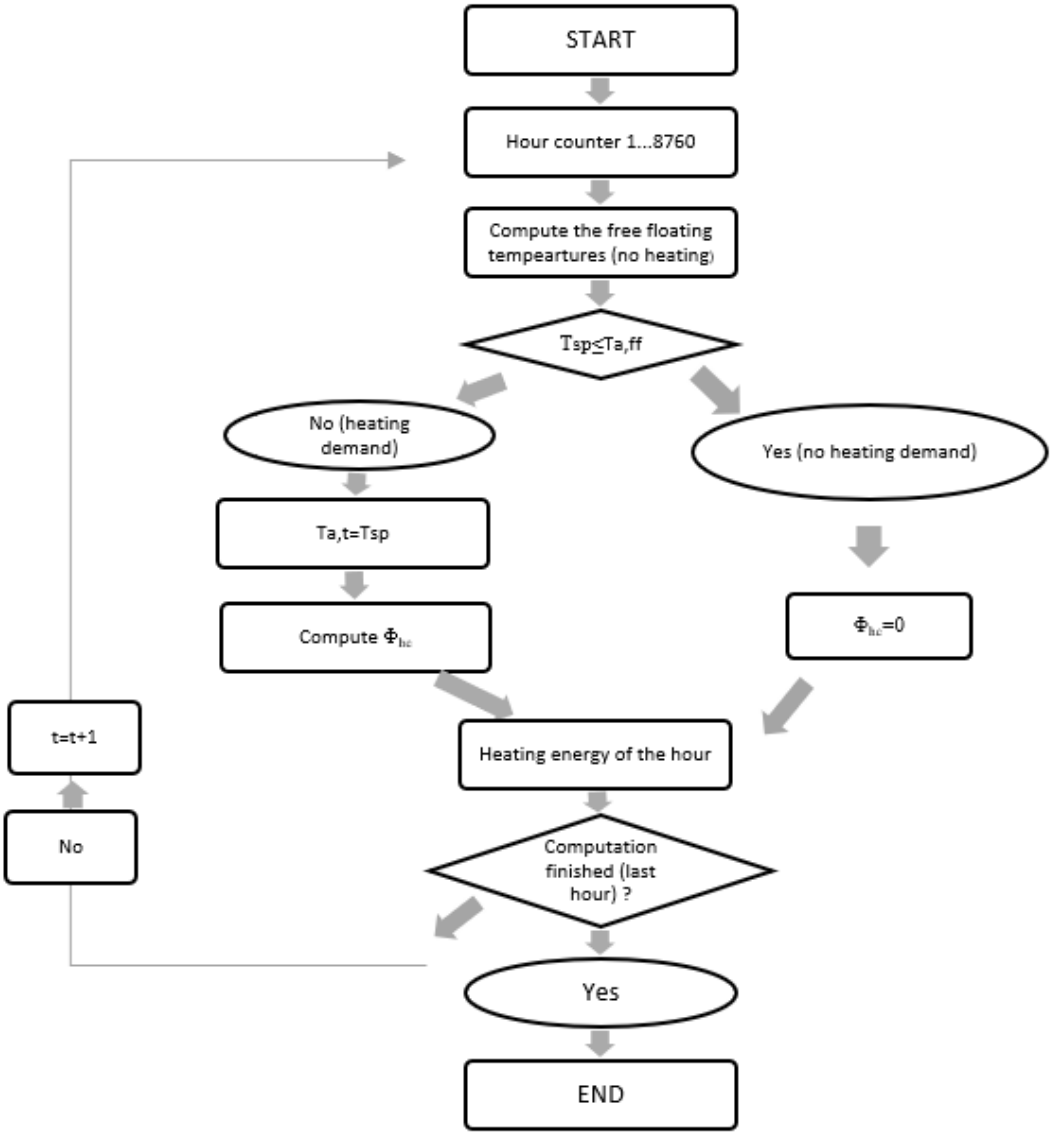

Figure 22. The process of hourly heating demand computation. Modified from (Sirén 2016a).

5.2.6 Optimization of space heating setpoints

In demand response of space heating, the heating power of the local space heating units (radiators) is altered according to the dynamic district heating price. During the high DH prices the heating power is increased (loading) and during low DH prices it is decreased (conservation). The decision when and how much the heating power is changed is made by the control algorithm. In this thesis, the MPC algorithm adjusted the heating temperature setpoints and indirectly the heating powers.

The MPC algorithm solved an optimization problem with one or several objectives and constraints. The calibrated building model (prescribed in the previous chapter) was used in

the optimization to predict the future heating demand and to calculate the values of the objective functions.

Optimization objectives and functions

In this study three objectives were studied with different combinations (heating energy cost, heating energy flexibility and thermal comfort). As demand response is pursuing for cost savings, the first objective was to minimize the total heating energy cost during the examined time period n (prediction horizon). Prediction horizons 12 h and 24 h were used in the study.

$$Min\{F1(\boldsymbol{x}) = \sum_{t=1}^{n} heating\ power(\boldsymbol{x}(t)) * DH\ price(t)\} \quad (15)$$

where

$\boldsymbol{x}$	the space heating temperature setpoints
t	time instance
n	length of the prediction horizon.

Second objective examined was the maximizing of the energy flexibility defined by flexibility factor (introduced in chapter 2). Flexibility factor describes how efficiently the building can utilize the low cost (off-peak demand) energy compared to high cost (peak demand) energy. The flexibility factor was calculated with future district heating prices over the prediction horizon used in the case at hand. This objective was formulated as follows

$$Max\{F2(\boldsymbol{x}(t)) = flexibility\ factor\} \quad (16)$$

where

$\boldsymbol{x}$	the space heating temperature setpoints
t	time instance.

The third objective tried to maintain appropriate level of thermal comfort in the spaces. This optimization problem was defined by minimizing the deviation of the calculated room air temperature from the zone reference temperature. As reference temperature, the room air temperatures from the Finnish Indoor climate classification (category S2) was used (FiSIAQ 2008).

$$Min\left\{F3(\boldsymbol{x}) = \sum_{t=1}^{n} \left(T_a(\boldsymbol{x}(t)) - T_{ref}(\boldsymbol{x}(t))\right)^2\right\} \quad (17)$$

where

$\boldsymbol{x}$	space heating temperature setpoints
t	time instance
n	length of the prediction horizon
T_a	air temperature
T_{ref}	reference air temperature.

Four different combination of objectives were studied:

O1: Min (F1)
O2: Max (F2)
O3: Min (F1) and Min (F3)
O4: Max (F2) and Min (F3).

The last two optimization problems dealt with two objectives which resulted in multi-objective optimization problem (MOO). The objective function F3 contradicted with both F1 and F2 since keeping the room air temperature near the reference temperature throughout the year requires in general more heating power and the heating can't follow the varying DH prices. In MOO problems, there exists a trade-off between the different optimal solutions and it is decision maker's choice how to value the objectives and make the decision.

Variables

The space heating setpoints (trajectory of setpoints) acted as decision variable in each optimization function. The number of decision variables (size of vector **x**) depended on the length of the prediction horizon (12 h or 24 h). Setpoints were defined to be continuous and the range of allowable values was case specific, and it varied by seasons.

Constraints

Constraints are used to define the feasible search space for the decision variables and the feasible solution space for the objective functions. Optimization problem may have one or several constraints but need not to have any constraints (Sirén 2016b). The optimization problem in this study concerned two origins of constraints. Firstly, the maximum heating power from the radiators set a physical constraint to the problem. Another type of constraint considered in this study was result from the local thermal comfort requirements. The thermal manikin measurements investigated the draught risk in workstations near the windows during the DR implementation (see chapter 4). The result from these measurements (see chapter 6.1) was set as constraint in the optimization to assure no draught would occur.

In order to prevent draught, the minimum heating power was defined whenever the window inner surface temperature dropped below the restrictive temperature specified by the thermal manikin measurements (see chapter 6.1). The window inner surface temperatures were not calculated in the RC-model. Instead separate IDA ICE simulations were performed where the window surface temperatures were recorded and then exported to the MPC control algorithm. Constant minimum heating setpoint of 20 °C was used to capture the worst-case scenario. The window surface temperature constraint for the time instance i was written as follows:

$$if\ window\ surface\ temperature(i) \leq restrictive\ surface\ temperature$$
$$then$$
$$radiator\ power(i) \geq minimum\ power\ (case\ specific)$$

Two different cases were studied. In the first one, the minimum heating power was set to 30% from the nominal instantaneous heating power and in the second case 50% from the

instantaneous nominal heating power was set as minimum. This limitation was used only in some of the studied cases, which are described in chapter 5.3.

The maximum heating power from the radiators is not constant, since it depends on the inlet water temperature which again depends on the outdoor air temperature according to the heating curve. The maximum heating powers were first calculated using the steady state performance calculation of the radiators (Stephan 1986, Seppänen 1995). This calculation method solves quite accurately the steady-state radiator powers with different inlet water temperatures. The inlet water temperature control curve of the building was used with the radiator product data in the calculations (see Figure 15). However, it was noticed that this constraint was too strict for the optimization problem. For this reason, the maximum heating power was defined so that based on the RC-model, during each hour, the setpoint temperature could be increased by 1 °C.

The maximum heating power constraint at the time instance i was defined as:

$$heating\ power(\boldsymbol{x}(i)) \leq maximum\ radiator\ power(i)$$

Choosing the optimization algorithm

Optimization can be defined as "an attempt of finding the best available solution(s) from a set of goal(s) and limitations" (Tutum 2010). Since there exists a huge number of different optimization problems, also several optimization algorithms have been developed. In general, the optimization problems can be divided into single-objective optimization and multi-objective optimization depending on the number of objective functions to be solved (Deb 2008). In the case of single-objective optimization one single global optimum solution can be found. In multi-objective optimization, there is generally no single solution that can be regarded as the best solution since in MOO problems there is commonly a trade-off between the objectives: no solution is the best with respect of all objectives. This means that several solutions are found that are regarded equally optimal. These solutions are called pareto-optimal solutions.

The optimization problem determines what kind of optimization algorithm should be chosen. In this thesis, multi-objective optimization algorithm (NSGA-II) was chosen to solve the foredetermined optimization problems (Deb et al. 2002). The optimization code that was implemented in Matlab by Tutum was used (Tutum 2010).

The detailed description of the NSGA algorithm is excluded from this thesis, but the general principle is presented. NSGA belongs to evolutionary algorithms (EA) which tries to mimic evolution and natural selection. The NSGA algorithm starts by creating an initial random population of individuals having specific decision variable values and resulting in solutions of different quality. The initial population is used to breed children (next generation) that outperform their parents by having a set of decision variable values that lead to more optimal solutions. The best individuals of the previous generation survive for the formulation phase of the next generation. The formulation phase can be executed in different ways but in general it includes three steps:

1. Fitness evaluation of the parent solutions
2. Breeding of good fitness parents to produce children (cross-over operator)
3. Increasing the diversity by mutation.

The parameters required for the NSGA optimization are the size of population, number of generations, cross-over probability and mutation probability (Holland 1992).

The difference of EAs to classical preference-based methods of solving MOO problems is twofold. Firstly, the classical preference-based methods use predefined preference vector to determine the relative importance of different objectives in MOO problems. This converts the multi-objective optimization back to single-objective optimization. The difficulty in this approach lies in the determination of the preference vector before the optimization. In EAs the target in solving MOO problems is to find as many different trade-off solutions as possible. It is then decision-makers choice how he/she put weight to different objectives and chooses the best solution. This makes EAs more complex but also more objective to choosing the preferable solution. In this study, weight was put to the cost savings and energy flexibility by choosing the pareto solution that was optimal in the respect of cost (O3) or flexibility (O4). Another difference between EAs and classical methods is that EAs produce a population of solutions after each optimization round whereas the classical methods find only single optimized solution. This makes EAs much more efficient in finding the optimal solutions (Deb 2008).

Optimization parameters and computational time

The number of generations and the size of one population was defined by running test optimization rounds. The population size of 64 was always used but the number of generations was changed between cases. Constant number of generations could not be used since there were huge differences between the computational complexity and computational expenses between the cases studied. With computationally cheaper cases the number of generations was set to 64 and with computationally more expense cases it was increased to 128.

The probability for mutation and crossover were chosen according to (Palonen et al. 2013). Palonen et al. suggested that crossover probability should be between [0.8-1]. In this study value 0.9 was used. The mutation probability is often chosen so that in each individual solution, one variable is exposed to mutation. Palonen et al. suggested mutation probabilities between [$1/n_c$ and $1/10*n_c$] where n_c is the number of decision variables. Value $1/10*n_c$ was chosen to be used in this study.

The MPC algorithm was used to optimize the heating setpoint for the entire year. The length of the control horizon defined the total number of optimization rounds needed since in one optimization round only the setpoints over the control horizon were determined. The number of optimization rounds with different lengths of control horizon are shown in Table 10. The calculation time increases linearly when the control horizon is increased. The length of the prediction horizon defines the number of variables in one optimization round. The increase of optimization variables leads to exponentially increasing computational time.

Table 10. Number of optimization rounds / Number of variables in optimization

	Control horizon (hours)			
Prediction horizon (hours)	1	6	12	24
12	8760/12	1460/12	730/12	-
24	8760/24	1460/24	730/24	365/24

5.2.7 Input data in MPC control

Weather forecast is one of the key input data for the model-based DR algorithms. In this study, the weather data that describes the average climate conditions (test reference year weather data TRY Helsinki Vantaa 2012) was used both in the MPC algorithm and in the IDA ICE simulations. Thus, it was assumed that the forecasted weather in the MPC algorithm was realized perfectly with 100% accuracy in the IDA ICE simulations.

The TRY weather data was generated so that for each month the monthly weather (between years 1980-2009), which is closest to the average climate conditions was chosen. The climate conditions consisted of outdoor temperature, humidity, solar irradiation, wind speed and wind direction. In Finland, the test year data was generated for three climate zones. Since the examined building is in the southern region, corresponding test weather data was used (Jylhä et al. 2011).

Moreover, since the weather data represents roughly the 30 years average climate conditions, the MPC results show the potential of DH demand response in this specific climate. The district heating marginal cost data was also generated using the same test year weather data. This is important since the marginal DH cost is highly dependent on the weather conditions, especially on outdoor air temperature.

The chosen weather data was used both in the MPC control algorithm and in the IDA ICE models. However, in the MPC control and more specifically in the RC-models, only the solar irradiation and external temperature were used compared to the more detailed IDA ICE models which used also wind speed, wind direction and relative humidity. Solar heat gain was given as input data for the RC-models. The solar heat gain was estimated by running a simulation of the RC-modelled rooms in IDA ICE and logging the solar heat gains. Calculating solar heat gains in IDA eased the building of the RC-models considerably because otherwise the solar heat gains should have been calculated inside the RC-models. This is challenging task because several variables including sun position, angle and path, window and shading properties should have been taken into account. These variables can easily be set into IDA ICE model for which reason this method was used.

The Nordic electricity markets define the hourly electricity price for one day ahead. However, in district heating there doesn't yet exist such markets in Finland that would define the price and thus support the DR actions. Lacking the real hourly DH market price, the price for district heating had to be formulated. In this study district heating marginal cost generated by Rinne was used. He generated the hourly marginal cost of DH in respect of fuel prices that are used to produce the district heat in Finland. The yearly DH marginal prices are shown in Figure 23 (Rinne 2017).

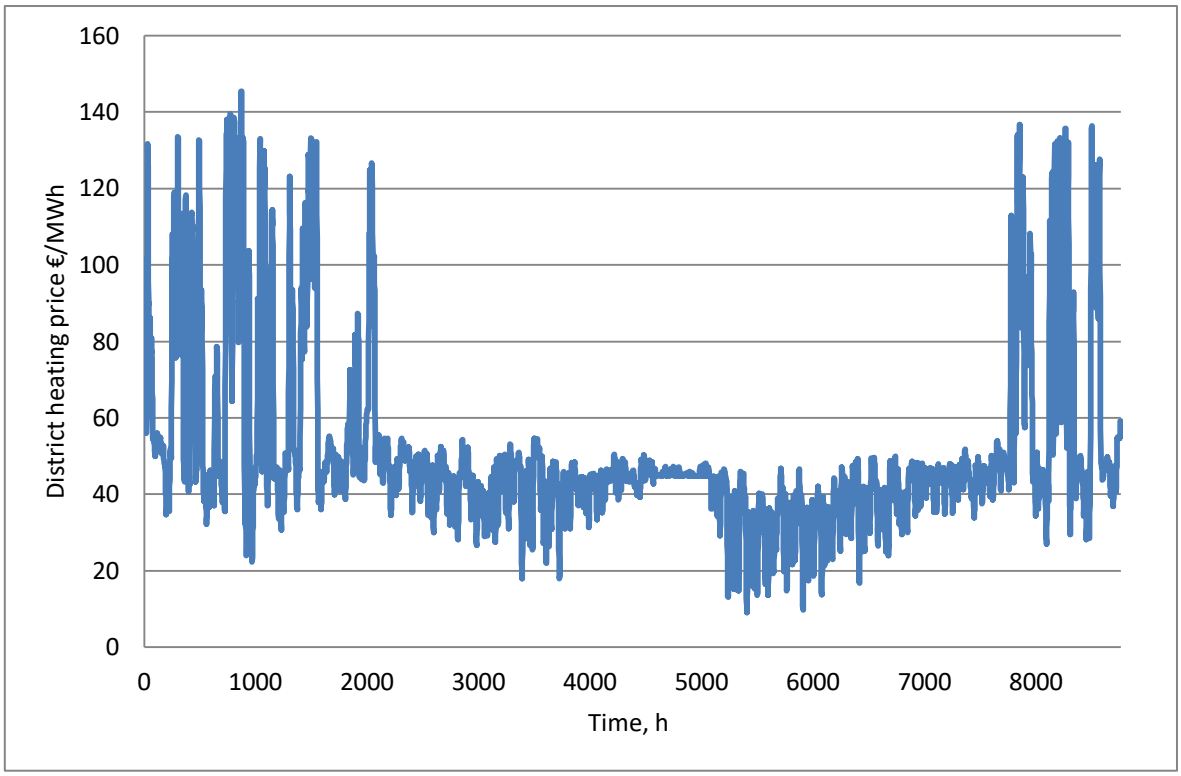

Figure 23. Dynamic district heating price (Rinne 2017).

Acceptable temperature setpoint range for space heating was categorized to three groups according to seasons: midseason, summer and winter. Purpose for the limited setpoint range [20 °C - 21 °C] during summer was to prevent overheating of spaces. During the winter, same limited setpoint range was used because it was figured out that the MPC algorithm did not find solutions which would include higher setpoints temperatures. Furthermore, the optimization did not find any feasible solutions if the space heating setpoint range was too wide during the low outdoor air temperatures. The maximum radiator power was limited by the optimization constraint and, thus setpoint trajectories including high setpoint temperatures did not give any feasible solutions because this constraint could not be passed.

During the midseason, the first idea was to use the same range [20 °C - 24.5 °C] as Martin used in his master's thesis (Martin 2017). However, after running several test optimization rounds, it was realized that the heat loading with setpoint values over 23 °C were seldom obtained. Reason for this is twofold. Firstly, the maximum heating power was not enough to reach such temperatures when the outdoor temperature was low. Secondly, having high setpoint for long enough was against the second objective of keeping the air temperature close to the reference temperature. As a result, temperature setpoint range of [20 °C – 23 °C] for the midseason space was chosen to be used in most of the cases.

Internal heat gains for the representative rooms were estimated to calculate the heating need for each hour. In this study similar internal heat gains were used as in the Martin's study since the case building is the same (Martin 2017). Lighting level was determined according to light's product information. In office rooms, one occupant had two screens and one laptop computer. Values for heat gains were checked from Fujitsu product data (Fujitsu 2014, Fujitsu 2011). Occupancy rate 40% was chosen to be studied since it is close

to the estimated use of the building. Furthermore, in the Martin's thesis it was revealed that the occupancy rate did not have significant effect on DR results and therefore only one occupancy rate was studied in this thesis.

The maximum 100% occupancy was estimated by calculating the number of workstations in each office room. Heat gain from one occupant was set to be 126 W which corresponds to normal office activity level with metabolic rate of 1.2 MET and for an average size person. Schedule for all the internal gains was the normal office hours between 8.00 in the morning and 16.00 in the afternoon. The internal gains for each room are shown in Table 11. The rooms used in the RC-models are highlighted.

Table 11. Internal heat gains in the 4th floor (Martin 2017).

Internal heat gain	Description		Comment	Usage/Occupied hours
Lighting	7.5 W/m^2		Measured value	08 - 16
Equipment	50 W/occupant		Equals a laptop and screen	08 - 16
Occupancy	100%	40%		
Room	Persons			
1 Conference	4	4	126 W/person	09-11, 12-13, 14-16
2 Kitchen	0	0		Unoccupied
3 Office	4	2	126 W/person	08 - 16
4 Office	4	2	126 W/person	08 - 16
5 Office	1	1	126 W/person	08 - 16
6 Office	4	2	126 W/person	08 - 16
7 Office	3	2	126 W/person	08 - 16
8 Office	3	0	126 W/person	08 - 16
9 Office	3	1	126 W/person	08 - 16
10 Office	2	1	126 W/person	08 - 16
11 Office	2	0	126 W/person	08 - 16
12 Office	2	1	126 W/person	08 - 16
13 Office	2	0	126 W/person	08 - 16
14 Office	2	1	126 W/person	08 - 16
15 Office	2	0	126 W/person	08 - 16
16 Office	2	1	126 W/person	08 - 16
17 Corridor	0	0		Unoccupied
18 Corridor	0	0		Unoccupied

5.3 Simulation cases

The studied cases were grouped to reference cases (Table 13) and demand response cases (Table 14-15). Demand response cases were divided to cases where the optimization

objectives were investigated (Table 14), parameter analysis cases (Table 15) and finally the cases where the local thermal comfort was examined with two different window constructions (Table 16).

The reference cases were used to evaluate the potential of demand response. Four reference cases R1-R4 were simulated with constant setpoint of heating 21 °C (cases R1 and R2) and 20 °C (cases R3 and R4). Two values for setpoints were examined so that the DR cases could be compared to the scenario where heat is only conserved (setpoint 20 °C). Cases R1 and R3 had the original window construction type 1 and the cases R2 and R4 had the window type 2.

Optimization objective and parameter analysis was conducted to find out the preferable combination of optimization objectives and optimization parameters. Four different combination of objectives were studied in the cases O1-O4 (described in section 5.2.6). In addition to objectives, the length of the prediction horizon was studied.

The parameter analysis cases C2.1 and C2.2 studied the feasible range for the midseason setpoint range used in the optimization and the case C1 studied the influence of the AHUs supply air temperature. Different supply air temperature control curves were investigated because the risk for simultaneous heating and cooling was tried to be avoided.

In the window cases B1 to B5 the effect of two different window constructions on the DR potential was examined with and without the local thermal comfort limitation. The first window type was chosen to be the same as in the actual building. Therefore, the results from the thermal manikin measurement are valid for comparison for this type of window. The second window type was chosen based on the construction year of the building. The type 2 windows are much poorer in respect of energy efficiency. The properties of studied window types are presented in Table 12. Two types of window surface temperature limitations were examined as described in chapter 5.2.6. In the first one the minimum power of the space heating was set to 30% of the maximum power whenever the window surface temperature dropped below the restrictive temperature (see results from the thermal comfort measurements chapter 6.1). In the second one 50% of the maximum power was required.

Table 12. Two window types studied in the simulation cases.

Window type	**U-value W/m^{2}K**	**g-value**
Window 1	1.0	0.55
Window 2	2.6	0.73

Table 13. The reference cases without demand response.

Case	Window type (see Table 12)	Temperature setpoint range, [°C]			Supply air temperature curve (see Figure 16)
		Winter ($T_{avg,out}$[1] < -10 °C)	Midseason (-10 °C < $T_{avg,out}$ < 0 °C)	Summer ($T_{avg,out}$ > 0 °C)	
R1	Window 1 (U=1.0 W/m^{2}K)	Constant 21	Constant 21	Constant 21	altered
R2	Window 2 (U=2.6 W/m^{2}K)	Constant 21	Constant 21	Constant 21	altered
R3	Window 1 (U=1.0 W/m^{2}K)	Constant 20	Constant 20	Constant 20	altered
R4	Window 2 (U=2.6 W/m^{2}K)	Constant 20	Constant 20	Constant 20	altered

[1] $T_{avg,out}$ = 24 h sliding average outdoor air temperature

Table 14. Demand response cases – investigating optimization objectives.

Case	Optimization objectives	Prediction horizon, [h]	Window type (see Table 12)	Temperature setpoint range, [°C]			Supply air temperature curve (see Figure 16)
				Winter ($T_{avg,out}$[1] < -10 °C)	Midseason (-10 °C < $T_{avg,out}$ < 0 °C)	Summer ($T_{avg,out}$ > 0 °C)	
O1.2	MIN(F1)[2]	12	Window 1 (U=1.0 W/m^{2}K)	[20-21]	[20-23]	[20-21]	altered
O2.2	MAX(F2)[3]	12	Window 1 (U=1.0 W/m^{2}K)	[20-21]	[20-23]	[20-21]	altered
O3.2	MIN(F1) MIN(F3)[4]	12	Window 1 (U=1.0 W/m^{2}K)	[20-21]	[20-23]	[20-21]	altered
O4.2	MAX(F2) MIN (F3)	12	Window 1 (U=1.0 W/m^{2}K)	[20-21]	[20-23]	[20-21]	altered
O2.3	MAX(F2)	24	Window 1 (U=1.0 W/m^{2}K)	[20-21]	[20-23]	[20-21]	altered
O3.3	MIN(F1) MIN(F3)	24	Window 1 (U=1.0 W/m^{2}K)	[20-21]	[20-23]	[20-21]	altered
O4.3	MAX(F2) MIN (F3)	24	Window 1 (U=1.0 W/m^{2}K)	[20-21]	[20-23]	[20-21]	altered

[1] $T_{avg,out}$ = 24 h sliding average outdoor air temperature
[2] F1 = Minimize heating energy cost
[3] F2 = Maximize heating energy flexibility
[4] F3 = Minimize thermal discomfort

Table 15. Parameter analysis – changing supply air temperature curve and heating temperature setpoint ranges.

Case	Optimization objectives	Prediction horizon, [h]	Window type (see Table 12)	Temperature setpoint range, [°C]			Supply air temperature curve (see Figure 16)
				Winter ($T_{avg,out}$[1] < -10 °C)	Midseason (-10 °C < $T_{avg,out}$ < 0 °C)	Summer ($T_{avg,out}$ > 0 °C)	
C1	MAX(F2)[2] MIN (F3)[3]	24	Window 1 (U=1.0 W/m^{2}K)	[20-21]	[20-23]	[20-21]	original
C2.1	MAX(F2) MIN (F3)	24	Window 1 (U=1.0 W/m^{2}K)	[20-21]	[20-24.5]	[20-21]	altered
C2.2	MAX(F2) MIN (F3)	24	Window 1 (U=1.0 W/m^{2}K)	[20-21]	[20-21]	[20-21]	altered

[1] $T_{avg,out}$ = 24 h sliding average outdoor air temperature
[2] F2 = Maximize heating energy flexibility
[3] F3 = Minimize thermal discomfort

Table 16. Window cases. Case O1.2 was chosen as reference case and its equal to B1.

Case	Optimization objectives	Prediction horizon, [h]	Window type (see Table 12)	Window surface temperature restriction	Temperature setpoint range, [°C]			Supply air temperature curve (see Figure 16)
					Winter ($T_{avg,out}$[1] < -10 °C)	Midseason (-10 °C < $T_{avg,out}$ < 0 °C)	Summer ($T_{avg,out}$ > 0 °C)	
B1	MIN(F1)[2]	12	Window 1 (U=1.0 W/m^{2}K)	No	[20-21]	[20-23]	[20-21]	altered
B2	MIN(F1)	12	Window 1 (U=1.0 W/m^{2}K)	30% [3]	[20-21]	[20-23]	[20-21]	altered
B3	MIN(F1)	12	Window 2 (U=2.6 W/m^{2}K)	No	[20-21]	[20-23]	[20-21]	altered
B4	MIN(F1)	12	Window 2 (U=2.6 W/m^{2}K)	30%	[20-21]	[20-23]	[20-21]	altered
B5	MIN(F1)	12	Window 2 (U=2.6 W/m^{2}K)	50% [4]	[20-21]	[20-23]	[20-21]	altered

[1] $T_{avg,out}$ = 24 h sliding average outdoor air temperature
[2] F1 = Minimize heating energy cost
[3] The minimum power is set to 30% of the maximum power during the hour at hand
[4] The minimum power is set to 50% of the maximum power during the hour at hand

6 Thermal comfort field measurements and demand response simulation results

The results from the thermal manikin measurements and MPC implemented demand response are presented in this chapter. Thermal manikin measurements investigated the local thermal comfort in workstations adjacent to windows. The results from the manikin measurements were further studied in the MPC implemented DR as a constraint for the DR control. The demand response results are analysed in the perspective of DR potential: energy cost savings, energy flexibility and thermal comfort.

6.1 Results from thermal manikin field measurements

6.1.1 Measurement periods for analysis

The thermal manikin measurement results are presented and analysed using seven measurement periods with different thermostat setpoints. These measurement periods were chosen from the entire measurement data so that the room air temperature had reached steady state conditions after the setpoint change. In addition, the window surface temperature data was used to choose periods that would represent both cold and warm window surfaces. The exhaust air temperature compensation was used to set the setpoint for the supply air. The measured supply air temperatures were between 18.5 – 19.5 °C during the whole measurement. The chosen measurement periods are shown in Figure 24 and the description of the respective room air temperature setpoint, room air temperature, window surface temperature, outdoor air temperature and radiator valve spindle position are presented in Table 17. During the periods P1 and P2, the water radiators heating was OFF, and the downdraught was examined with cold and warm window surfaces, respectively. During the other periods the heating power was gradually increasing. All the data presented in Table 17 are calculated time averages over each measurement period.

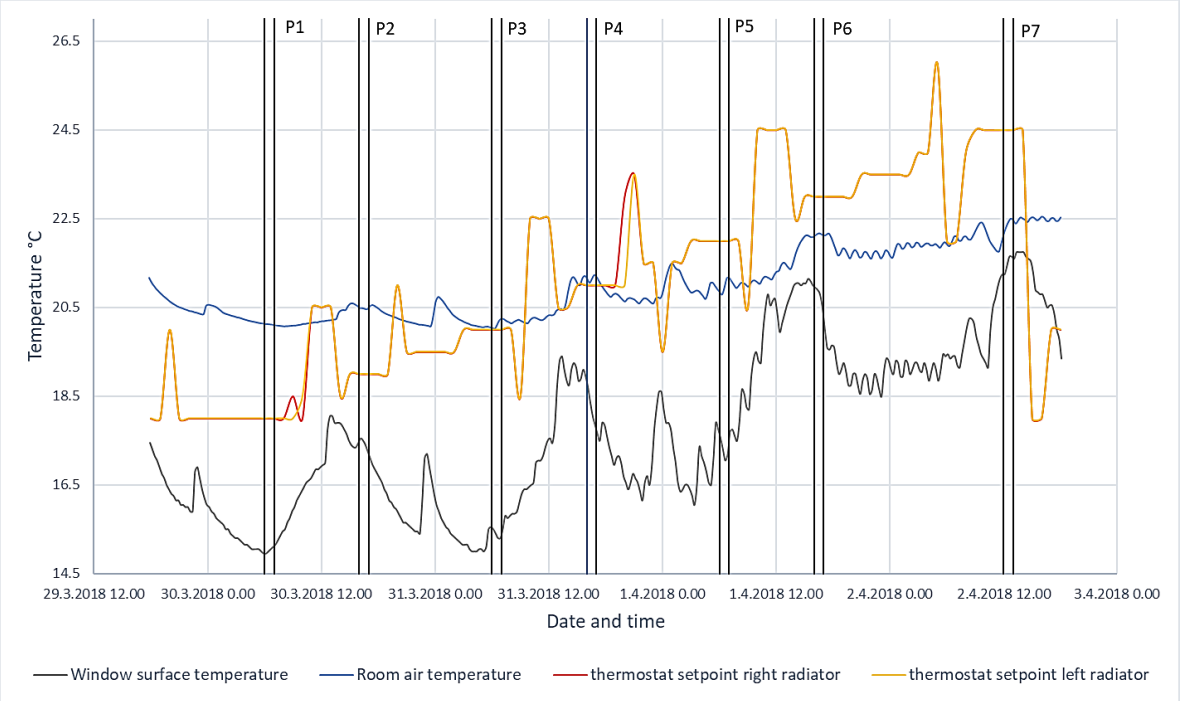

Figure 24. Window surface temperature, room air temperature and radiator thermostat setpoint temperature for left and right radiator. The chosen measurement periods for analysis are shown with grey vertical lines.

Table 17. Chosen measurement periods and time-averaged variables.

Period	Date and time	Room air temperature setpoint [°C]	Average room air temperature [°C]	Average supply air temperature [°C]	Average window surface temperature [°C]	Average outdoor temperature [°C]	Spindle position [%]
P1	30.3 6.00-7.00	18	20.1	18.6	15	-7.0	0
P2	30.3 16.00-17.00	19	20.5	19	17	1.9	3
P3	31.3 6.00-7.00	20	20.1	18.7	15	-6.1	11
P4	31.3 16.00-17.00	21	21.1	19.3	18	2.1	15
P5	1.4 6.00-7.00	22	20.9	18.9	17	-3.7	12
P6	1.4 16.00-17.00	23	22.1	19.4	21	1.7	16
P7	2.4 12.00-13.00	24.5	22.3	19.3	22	-0.1	18

6.1.2 Manikin equivalent temperature

Manikin based time-averaged equivalent temperatures compared to room air temperature are shown in Figure 25. The difference between the equivalent temperature and room air temperature is presented for each body part. Positive differences predict that the occupant would feel warmer than the reference room temperature at the particular body part. Negative differences at the body parts in contrary indicate that the occupant would sense cold.

The rate of change of the relative equivalent temperature was greatest in the lower right back, both chests, right hand and upper right back. The relative increase of body temperatures on the right-hand side of the manikin was expected and obvious because the radiators were located on that side.

The equivalent temperature difference between the left and the right hand was noticeable. With low thermostat setpoints and no heating of water radiator the right hand was remarkably cooler than the left hand. When the setpoint was adjusted to over 20 °C and the radiator valves were opened, both hands were nearly at the same temperature. This indicates that in the right side, which is facing towards the window, the cold window surface was causing downdraughts. Downdraughts were not evidenced when the setpoint was increased and the heating of the radiator was introduced. This phenomenon is further studied in the chapter 0 were a local thermal comfort restriction is determined.

The heating effect of the water radiator was clearly seen on the right foot and thigh facing the radiator. Equivalent temperature was higher in these body parts compared to the corresponding left side body parts in each period. However, the left leg was for some reason warmer than the right one during each period. The equivalent temperatures in left and right lower back were much lower than in the other body parts. There is no clear explanation for that low temperatures. One possible explanation is calibration error in those specific body parts.

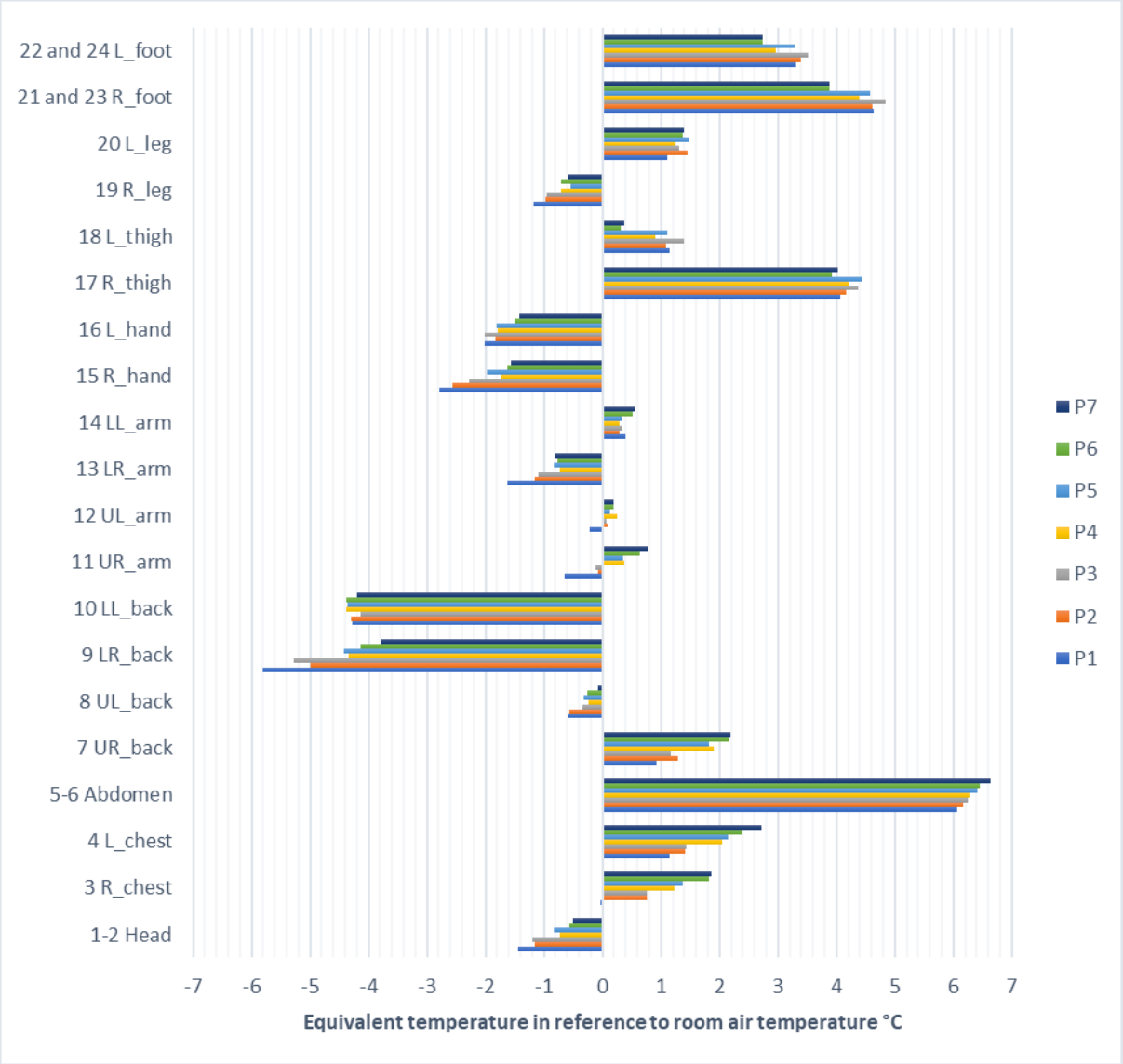

Figure 25. Equivalent temperature minus room air temperature at seven measurement periods in different body parts.

The body parts can be divided into warm, neutral and cold body parts when the corresponding equivalent temperatures are compared to the reference room temperature. Difference of one Celsius degree was regarded as a limit for division. This method of division is not standardized and was purely done for the sake of analysis. It should not be used for the thermal sensation evaluation.

If the difference was greater than 1 °C and positive, the specific body part was kept warm and if negative (vice versa) the specific body part was cold. If the absolute difference was less than 1 °C, the body part belonged to the neutral group. The division of the body parts is shown in Figure 26. The lower back, hands, head and lower right arm were relatively cooler than the rest of the body. The feet, thighs, chest, abdomen, upper right back and left leg were in turn relatively warmer. Rest of the body parts belonged to the neutral temperature group.

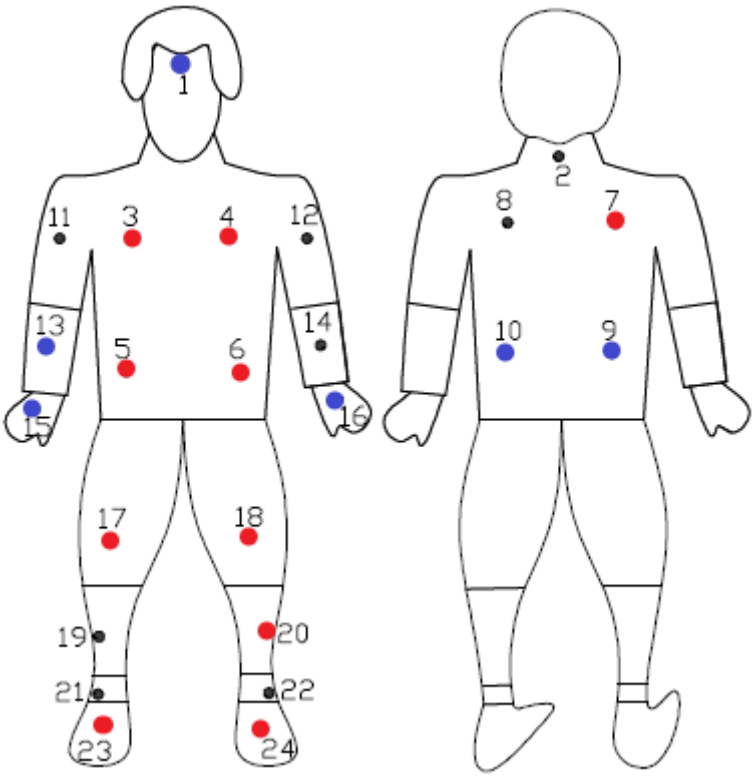

Figure 26. Division of body parts to hot (red), neutral (black) and cold (blue) body parts according to difference of manikin equivalent temperature and room air temperature. Neck and ankles were not included in the measurement and instead of two, only one measurement point for abdomen was used.

The local thermal sensation can be evaluated using the comfort zone diagram created by (Nilsson 2007). Nilsson divided thermal sensation into five comfort zones shown in Table 18. Thermal sensation for each body segment can be estimated with equivalent temperature limits that correspond to borders of mean thermal votes suggested by Nilsson. Thermal comfort zones are useful because now the equivalent temperatures can be interpreted in thermal sensation scale. The thermal comfort zones are different for each body segment and thus the thermal sensation can be assessed for each body segment separately. Comfort zones are constructed using the correlation equation 18

$$T_{eq} = T_{sk} - R_T * (a + b * MTV) \qquad (18)$$

where

T_{sk}	skin temperature [°C]
R_T	clothing thermal resistance [m^{2}K/W]
a and b	linear regression coefficients
MTV	mean thermal vote.

The values for clothing thermal resistance and the correlation coefficients are body segment specific. MTV ranges are used according to Nilsson specification.

Table 18. Thermal sensation scale and corresponding comfort lines according to Nilsson (Nilsson 2007).

Thermal vote range	**Thermal sensation**	**Comfort lines of thermal manikin**	
+1.5 to +3.0	Too hot	hot	thermal vote = 1.5
+0.5 to +1.5	Hot but comfortable	h comf	thermal vote = 0.5
-0.5 to +0.5	Comfort	-	-
-1.5 to -0.5	Cold but comfortable	c comf	thermal vote = -0.5
-3.0 to -1.5	Too cold	cold	thermal vote = -1.5

The measured manikin body segmental equivalent temperatures are shown in Figure 27 with Nilsson's comfort zone lines. Comparing different measurement periods, it can be seen that both window surface temperature and radiator thermostat setpoint affected the equivalent temperature. Even if the thermostat setpoint was increased, if the window surface temperature was low, the equivalent temperatures did not increase.

Most of the body parts ended up in the lower part of the comfortable zone. Hands, lower arms and legs where in the acceptably cold zone. The thermal sensation in these body parts was improved when the setpoint was increased. Abdomen was the only body segment in the hot but acceptable range. Right and left lower back thermal sensation could not be evaluated since, the measurement of the equivalent temperature was regarded as rough measurement error.

However, it should be noted that Nilsson's lines are just a rough estimation of the thermal sensation. The measurement should be evaluated with human subject measurements to get more precise evaluation of the thermal sensation in the measured conditions.

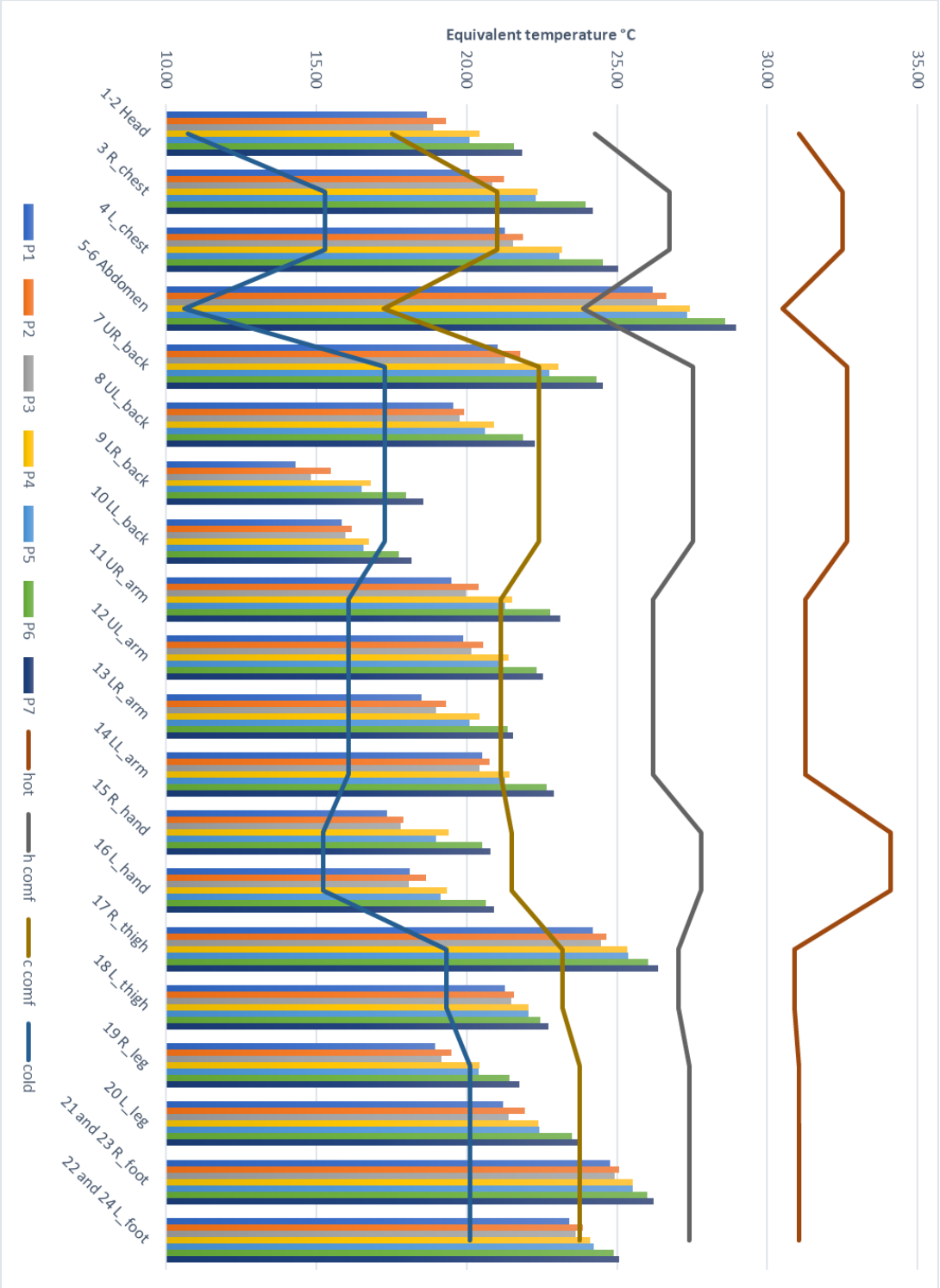

Figure 27. Equivalent temperature and thermal comfort lines (Nilsson 2007) at seven measurement periods.

Time averaged vertical temperatures during the examined periods at 4 measurement heights are shown in the Figure 28 for both measurement locations: MLD (manikin left door) and MRW (manikin right window). Development of the vertical temperature profiles in Figure 28 show that compared to the door side profile, window side profile is on the colder side in

period P1, nearly identical to door side profile in periods P2-P3 and on the warmer side in the periods P4-P7. This resembles the aggregated air flow pattern, in other words, combination of convection flows and ventilation air distribution in the room space. In the condition, where the window is cold, and no heating is applied, the average temperature close to the window is colder. When the water radiator heating is introduced, it prevents the downdraughts from the window. When the heating power was increased, the convection flow of the water radiator is strong enough to create large eddy in the room space that transfers the warm air towards the corridor side.

The form of the temperature profile did not change significantly between the measurement periods. In each period, the temperatures at the middle measurement heights 60 cm and 100 cm were higher than those at the floor (height of 10 cm) and head (height of 130 cm). This might be caused by the combining influence of the radiator and the window temperature. At the middle measurement heights, there exist fully mixed conditions in both side of the manikin. The window side temperatures were affected more in periods P4-P6 where the thermostat setpoint was increased since the radiators were located on that side. The temperature close to the floor level was low due to the effect of the convection flows. The reason, why the room air temperature at the head height was slightly lower than e.g. at the chest height, could be due to the effect of long wave radiation between the cold window and the measurement probes and due to the effect of the ventilation air movement in the room space.

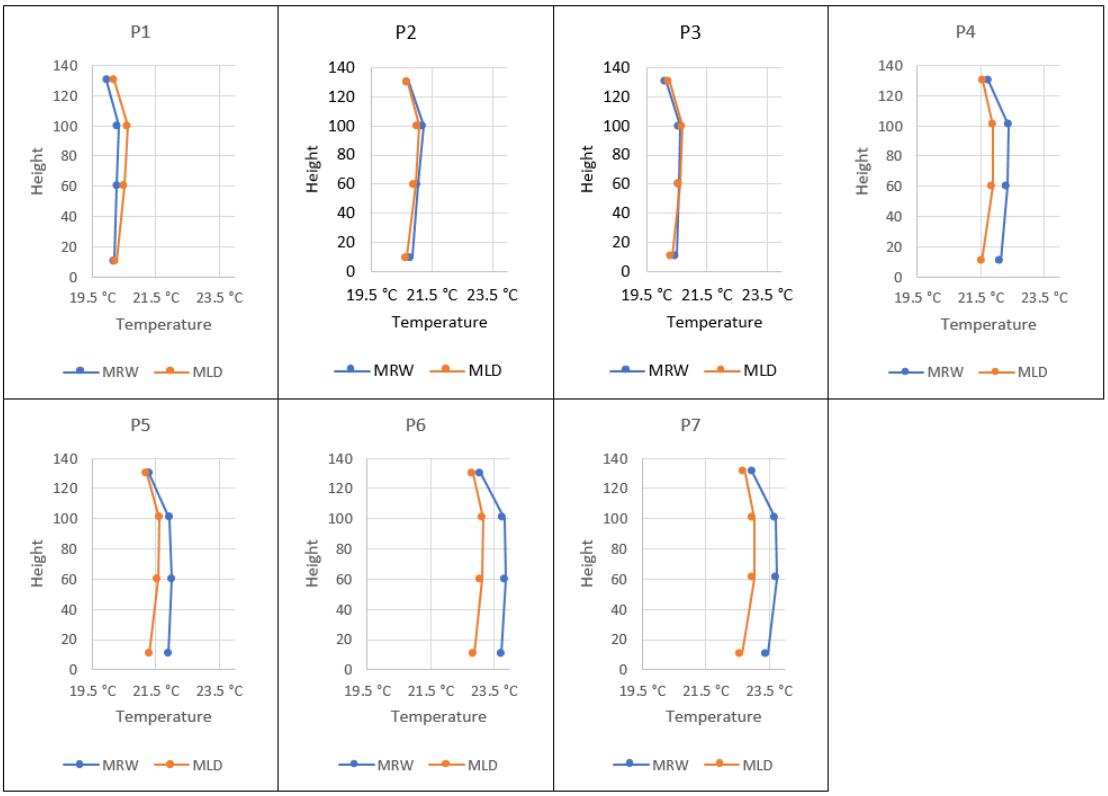

Figure 28. Air temperatures at 4 measured heights at both sides of the manikin during the chosen 7 periods.

The calculated time-averaged water radiator heating powers (using the equation 6) are shown in Table 19. It should be noted that the water radiator power generally increases when the room air temperature setpoint increases during the periods P1 to period P7. However, the average radiator power during the period P2 was higher than in the period P3. This is unexpectable, since the setpoints and spindle positions in the periods P2 and P3 were 19/20 °C and 3%/11%, respectively. Reason for this contradiction is probably that the radiator power had increased just before the beginning of the period P2. Heat conserved into radiator during this radiator power peak hasn't yet dissipated and it affects the heating power during period P2. In addition, it must be noted that the inlet water temperature was measured after the thermostat valve, in which case the measured inlet water temperature is highly dependent on the valve's spindle position.

Table 19. Calculated radiator heating power for the right (manikin side) radiator.

Period	Date and time	Room air temperature [°C]	Radiator inlet temperature [°C]	Radiator outlet temperature [°C]	Radiator power [W]
P1	30.03.2018 6-7	20	19	20	0
P2	30.03.2018 16-17	20	28	23	61
P3	31.03.2018 6-7	20	24	22	32
P4	31.03.2018 16-17	21	26	24	41
P5	01.04.2018 6-7	21	32	27	134
P6	01.04.2018 16-17	22	40	32	230
P7	02.04.2018 12-13	22	44	32	254

6.1.3 Smoke visualizations

Separate test smoke visualizations were conducted a week before the thermal manikin measurements. Two test smoke cases were studied. The case 1 was with the low thermostat setpoint (19 °C) that resulted in cool radiator surface temperature. The case 1 represents possibly conditions were downdraughts might be evidenced. The case 2 was with high thermostat setpoint (23 °C) and hot radiator surface temperatures. The case 1 was performed first. After the visualizations the setpoint was increased and time lapsed so that the radiator surface temperature reached steady state, after that the case 2 was performed.

The radiator surface temperatures and window surface temperatures were measured with a thermoelement before and after the first test smoke visualization and before the second test smoke visualization. Table 20 shows the surface temperatures in the cases 1 and 2. In the case 2 the left radiator was warmer than the right because the radiator inlet water pipe is first connected to the left radiator before continuing to the right radiator. In the case 1 this difference couldn't be detected since the thermostat valves were closed and both radiators were at almost equal temperature.

Table 20. Test conditions during the test smoke visualizations.

	Case 1		Case 2	
Radiator surface temperature °C	*before*	*after*	*before*	*after*
Left radiator	21.4	21.7	45.9	not measured
Right radiator	21.6	21.9	41	not measured
Window surface temperature °C, at height:	*before*	*after*	*before*	*after*
10 cm	19.7	20.1	20.6	not measured
50 cm	20.1	20.5	21.3	not measured
100 cm	20.8	20.7	21.7	not measured

Smoke visualization with low thermostat setpoint 19 °C (case 1, closed valves) and high thermostat setpoint 23 °C (case 2, open valves) are depicted in Figure 29 and 30, respectively. Both figures show sequence of snapshots taken from the videos. In the case 1, it can be seen that the test smoke released above the table flowed quite horizontally towards the manikin. As the test smoke moved close enough, the plume generated by the manikin, turned the test smoke upward and it scattered. In comparison in the case 2, no horizontal air movement can be seen. Test smoke released at the same spot rose immediately and started to scatter. As a result, it can be concluded that with low thermostat setpoint, closed valves and slightly colder window surface in the case 1, the downdraughts developed. In the case 2 with high thermostat setpoint, opened valves and warm radiator, the thermal plume from the radiator prevented the downdraught.

Compared to the manikin equivalent temperature measurement periods P1 to P5, the window temperatures in smoke visualizations in both cases were higher than the lowest recorded temperatures in the manikin measurement. However, even as high window surface temperatures as in the smoke visualizations was evidenced to generate convective downward airflows. From the local thermal comfort perspective, the difference is that the relatively higher window temperatures in smoke visualizations produce airflows with lower speed and higher temperature which aren't as probably causing draught. As the window surface temperature decreases and at the same time, radiator heating is turned OFF, the draught risk increases.

Figure 29. Smoke visualization (case 1) with low thermostat setpoint (19 °C).

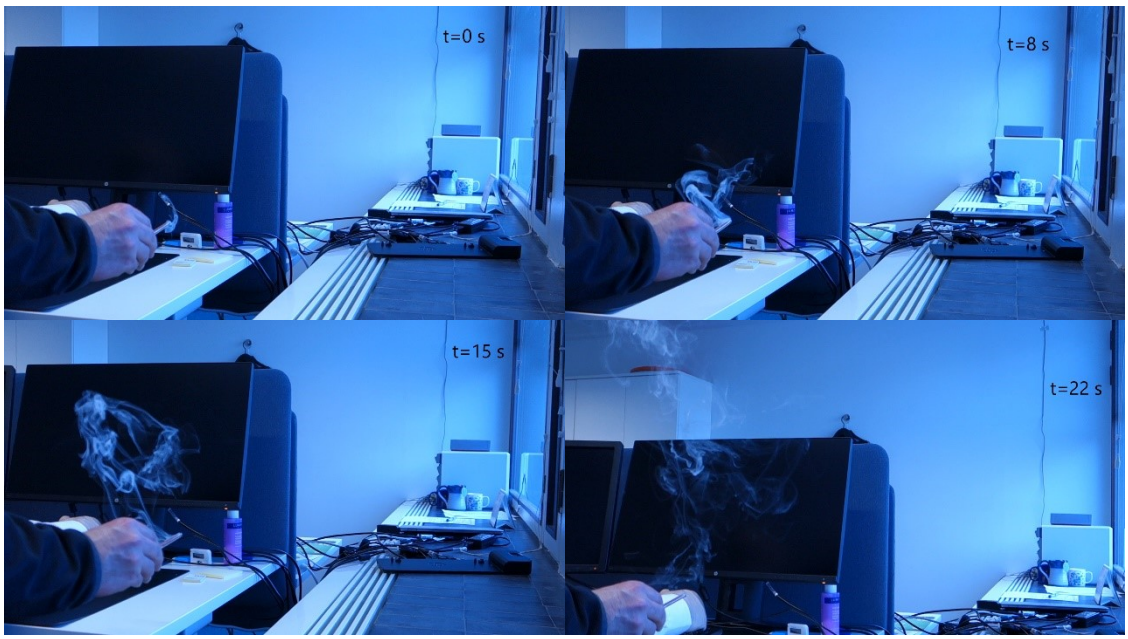

Figure 30. Smoke visualization (case 2) with high thermostat setpoint (23 °C).

6.1.4 Restrictions to DR control algorithm

Test smoke visualizations showed that the cool window surface generates downward air flows that may cause draught. When the radiator power was increased the upward plumes prevented the downward airflow. This phenomenon was further examined by measuring the equivalent temperatures with the thermal manikin. This measurement revealed that the cool window during the reduced radiator power could have a significant effect on the local thermal sensation especially on uncovered body parts e.g. hands and arms.

Usually the draught is also felt in the ankles and feet. Explanation why the equivalent temperature did not drop in these body parts during low thermostat setpoint and window surface temperature was probably result from the geometry of the work station. The window table and the electric tables were almost attached to each other which prevented the downward airflows path below the table. Instead the downward airflows were directed along the table surface towards the hands and arms of the manikin were the draught was sensed.

Objective of this measurement was to identify the conditions where the local thermal comfort was decreased significantly. Since both window surface temperature and radiator setpoints were considered when choosing the examined periods, the restrictive conditions should consider these both.

The downdraughts and thus the local thermal comfort was most significantly sensed in the right hand and lower right arm which were uncovered and facing the window. In order to formulate the restrictive conditions, the equivalent temperatures in the right hand is analysed in Figure 31 - 33. Figure 31 depicts the period P1, Figure 32 period P2 and Figure 33 period P3. The thermostat setpoints and window surface temperatures in the P1, P2 and P3 periods were 18/19/20 °C and 15/17/15 °C, respectively. In addition, the thermostat valve was closed during the periods P1 and P2, but it was opened during the period P3 (Table 17).

Figure 31 shows that the equivalent temperature of the right hand is lower than that of the left hand during the period P1. This indicates that the downdraughts from the window caused convective heat loss in the right arm. In Figure 32 (P2) and Figure 33 (P3), the difference of the equivalent temperature between the right and left hand first decreases and then balances out. It can be deduced that thermostat valves should be forced to open and heating turned ON when the window surface temperature is 15 °C or less. Figure 32 shows that when the window surface temperature was above 15 °C (in this case 17 °C), although the thermostat valves were closed (see Table 17), no local thermal discomfort occurred. In the beginning of the period P2 right- and left-hand equivalent temperatures differed, but in the end the difference balanced out.

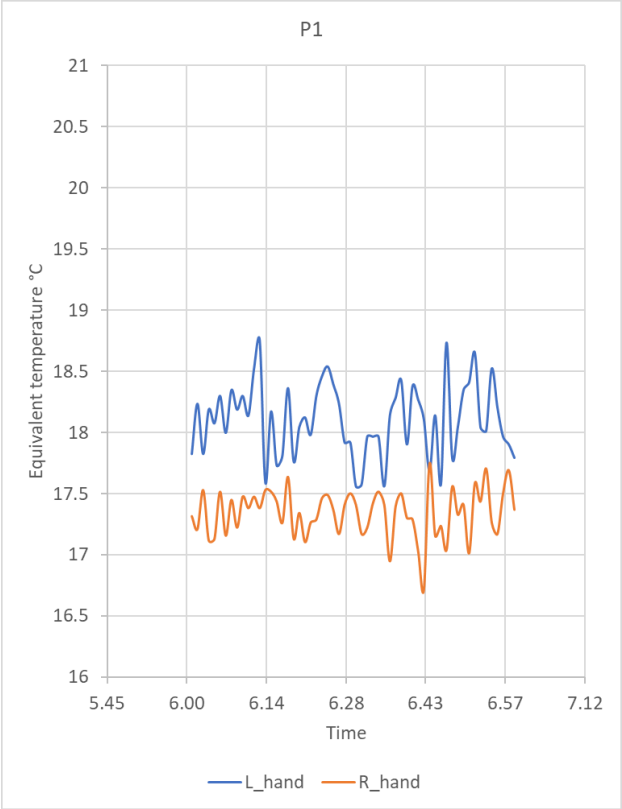

Figure 31. Equivalent temperature of the right- and left-hand during the period P1.

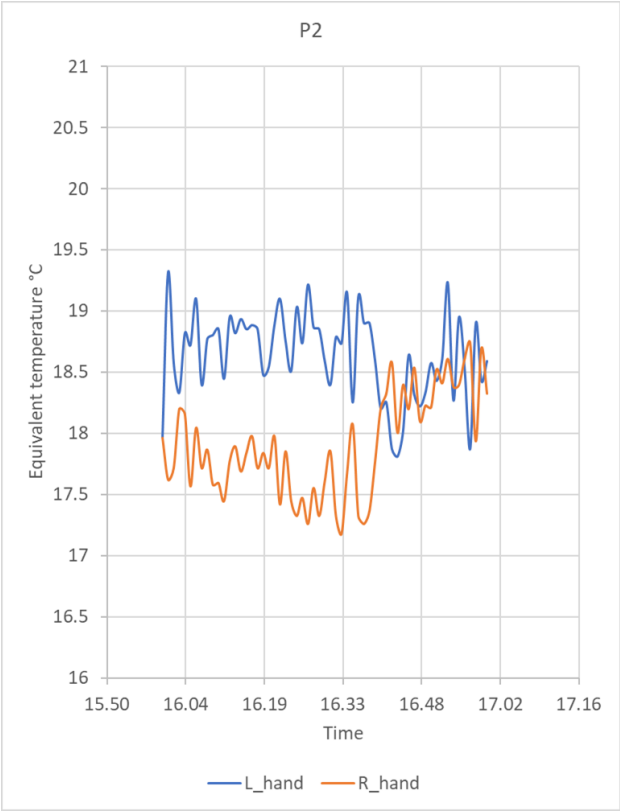

Figure 32. Equivalent temperature of the right- and left-hand during the period P2.

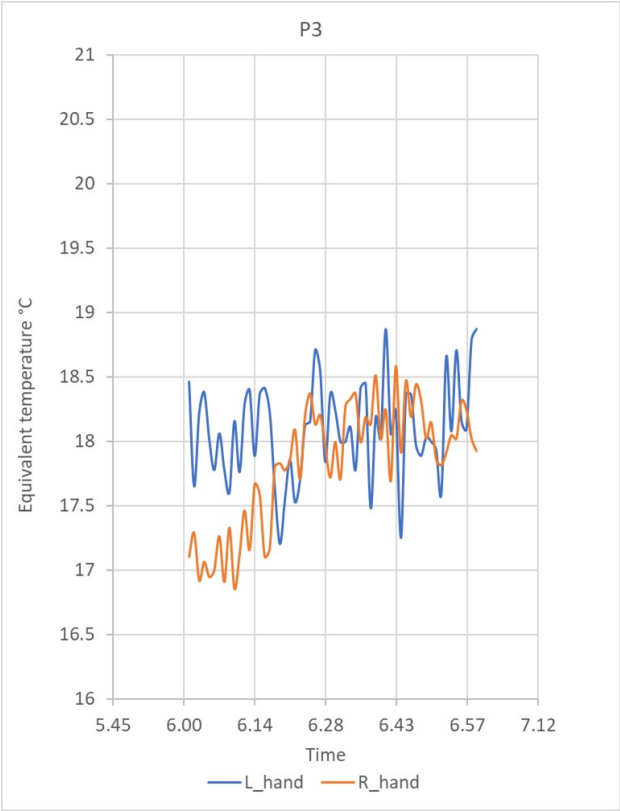

Figure 33. Equivalent temperature of the right- and left-hand during the period P3.

The window surface temperature of 15 °C was found to be the limiting temperature above which the thermostat valves should be opened. The window surface temperature depends on the outdoor air temperature, wind, solar radiation, indoor air temperature, window construction and properties in addition to room conditions like air flow patterns. Using simple heat transfer equation (presented in the appendix), the restriction for window surface temperature can be expanded to cover different windows and outdoor air temperatures. Table 21 shows that with non-energy efficient windows, the outdoor temperature below which the thermostat valves should be opened, are higher. In this simple heat transfer model, solar radiation and transient outdoor wind conditions and indoor air patterns were neglected and only influence of the window glazing's U-value was studied.

Table 21. Exterior temperature when the thermostat valves should be forced open depending on the window U-value. The reference measured period P1 is bolded.

Window surface temperature °C	U-value of the window °C	Exterior temperature °C
15	0.6	-25
15	0.8	-13.8
15	**1**	**-7.0**
15	1.5	2.0
15	2	6.5
15	2.5	9.2

6.2 Results from the DR simulations in IDA ICE

Results from the demand response implementation with the MPC algorithm in an educational office building are presented and analysed in this chapter. The analysis is divided into three main categories. At first, the heating energy consumption and heating cost savings are analysed, secondly the energy flexibility results are examined, and finally the thermal comfort is evaluated.

6.2.1 Energy consumption and cost savings

At first, the total district heating energy consumption and energy cost for all the simulation cases are investigated in Table 22. Both costs and DH consumption are given per heated net floor area allocated form and in the percentages of savings compared to the reference cases R1 and R2. The same data is also shown in Figure 34 and Figure 35 in more representational form of column charts. The DR have no major influence on the electricity consumption and thus these values are not discussed further in this thesis.

The results from demand response cases are compared with results from the reference cases where DR is not used. The heating energy consumption and cost in the reference case R1 with the window type 1 was 128.3 kWh/m^2 and 8.2 €/m^2, respectively. When the space heating setpoint was dropped from 21 °C to 20 °C (the case R3), the heating consumption and cost dropped 5.5% and 4.8%, respectively. The corresponding change between the reference cases with another window type 2 (the cases R2 and R4), was a bit less 4.9% and 3.9%, respectively. The relative change was smaller in the cases R2 and R4 because the heat losses are greater with window type 2. Although the relative change was smaller the absolute

savings were higher. The previous savings in R3 and R4 with only heat conservation are used as reference to savings obtained in the DR cases.

All the demand response cases lead to both cost and energy savings compared to the reference cases with constant setpoint of 21 °C. The cases O2.1 and B1 (which are actually identical cases) achieved the highest cost savings. The energy costs could be decreased by 4.75% compared to the reference case R1. This is close to the savings in the heat conservation reference case R3. Almost as high cost savings was reached in cases O3.2, O3.3 and C2.2.

Demand response cases where the optimization objective was to minimize costs had obviously greater heating cost savings compared to cases where the objective was to maximize heating flexibility. From the cost optimization cases it can be seen that the optimization lead to utilization of heat conservation DR strategy. This means that the heating costs were cut predominantly by decreasing the consumption. However, when optimizing the energy flexibility, the cost savings were lower, but the heating was adjusted more flexibly according to dynamic prices. This can be seen from the ratio of cost and energy savings. In the cost optimized cases the ratio is small but, in the flexibility optimized cases costs were reduced even three times more than the energy consumption. Therefore, the flexibility optimization lead to utilization of the demand shifting DR strategy.

The cases where also the thermal comfort was objective, resulted in slightly lower heating energy and heating cost savings compared to cases where either only heating cost or heating flexibility was optimized. When the prediction horizon was changed from 12 h to 24 h, the heating energy savings dropped but the heating cost savings increased both with cost and energy flexibility optimized cases.

The different allowed midseason space heating temperature setpoints were studied in the cases O4.3, C2.1 and C2.2 where the allowed ranges were [20-23] °C, [20-24.5] °C and [20-21] °C, respectively. Table 22 shows that the case C2.2 with the narrowest setpoint range of [20-21] °C lead to the highest cost savings which were close to the savings with heat conservation in cases R3 and O1.2. This implies that heat loading with setpoints over 21 °C seems not to be feasible. The explanation for this might be that the relatively high air change rate in the rooms prevents the heat loading to the building mass and instead the heat is removed by the exhaust air flow. The air handling units heat recovery will not make a difference since although it transfers part of the heat in the exhaust air to supply air, it won't enhance the heat loading to structures (Martin 2017).

Case C1 was simulated to investigate the influence of the original supply air temperature curve in comparison to the altered supply temperature curve that was used in all other simulation cases. The results from this case should be compared with case O4.3 because beside the supply temperature curve, these cases were identical. The results in Table 22 show that the altered supply air temperature curve does not affect the heating energy nor cost savings.

Two type of windows and two type of window surface temperature restrictions were investigated in the cases B1-B5. The case O1.2 was chosen as the base scenario for which the window construction changes and window surface temperature restrictions were applied.

This case was chosen because it had the highest cost savings when comparing different optimization approaches. The case B1 representing this base point was identical to case O1.2.

The results from the window comparison cases show that the window restriction had neglectable effect on the cost and energy savings with the window type 1 (the cases B1 and B2). With the poorer energy efficiency windows (type 2) the decrease in the cost and energy savings compared to case B3 (without the window restriction) were larger. When 30% minimum heating power from the nominal heating power was required (case B4), the cost and energy savings dropped 0.5 and 0.3%-units, respectively. When the 50 % power requirement was used (case B5), the aforementioned savings dropped by 2.1 and 1.5 %-units.

From the thermal manikin measurements, it was determined that even small heating power during the low window inner surface temperature (below 15 °C) could maintain the acceptable local thermal comfort conditions. Therefore, it may be concluded that the local thermal comfort restriction in demand response has higher influence on the cost savings when the building has non-energy-efficient windows and thus higher heat losses. However, even with the poor windows the DR potential is not dropped dramatically since only small heating power is required to prevent the local thermal discomfort in the workstations adjacent to windows.

Table 22. Annual district heating consumption and cost for all the studied cases. Last column shows the ratio of cost and energy savings.

	CASE	MPC optimization objectives			Window type	$T_{SH\ setpoint}$	DH energy	Cost	DH energy	Cost	Cost and energy saving Ratio
		F1: MIN heating cost	F2: MAX heating flexibility	F3: MIN thermal discomfort	-	°C	kWh/m^2,a	€/m^2,a	%	%	-
Reference cases	R1				1	21	128.3	8.2	0.0	0.0	0.0
	R3				1	20	121.2	7.8	-5.5	-4.8	0.9
	R2				2	21	151.7	9.7	0.0	0.0	0.0
	R4				2	20	144.3	9.3	-4.9	-3.9	0.8
Demand response cases and Paramater analysis	O1.2	X			1	20-23	121.4	7.8	-5.4	-4.7	0.9
	O2.2		X		1	20-23	125.3	7.9	-2.3	-3.1	1.3
	O3.2	X		X	1	20-23	122.3	7.8	-4.7	-4.2	0.9
	O4.2		X	X	1	20-23	126.2	8.0	-1.6	-2.7	1.6
	O2.3		X		1	20-23	125.7	7.9	-2.0	-4.0	2.0
	O3.3	X		X	1	20-23	122.5	7.8	-4.5	-4.6	1.0
	O4.3		X	X	1	20-23	127	7.9	-1.0	-3.0	2.9
	C1		X	X	1	20-23	127.1	7.9	-0.9	-2.9	3.1
	C2.1		X	X	1	20-24.5	127.2	8.0	-0.9	-2.5	3.0
	C2.2		X	X	1	20-21	126	7.8	-1.8	-4.3	2.4
Window comparizon	B1	X			1	20-23	121.4	7.8	-5.4	-4.8	0.9
	B2	X			1[1]	20-23	121.4	7.8	-5.4	-4.7	0.9
	B3	X			2	20-23	144.5	9.3	-4.7	-3.8	0.8
	B4	X			2[1]	20-23	145.3	9.4	-4.2	-3.5	0.8
	B5	X			2[2]	20-23	147.7	9.5	-2.6	-2.3	0.9

[1] Window surface temperature restriction (min 30% from the maximum instantaneous heating power)
[2] Window surface temperature restriction (min 50% from the maximum instantaneous heating power)

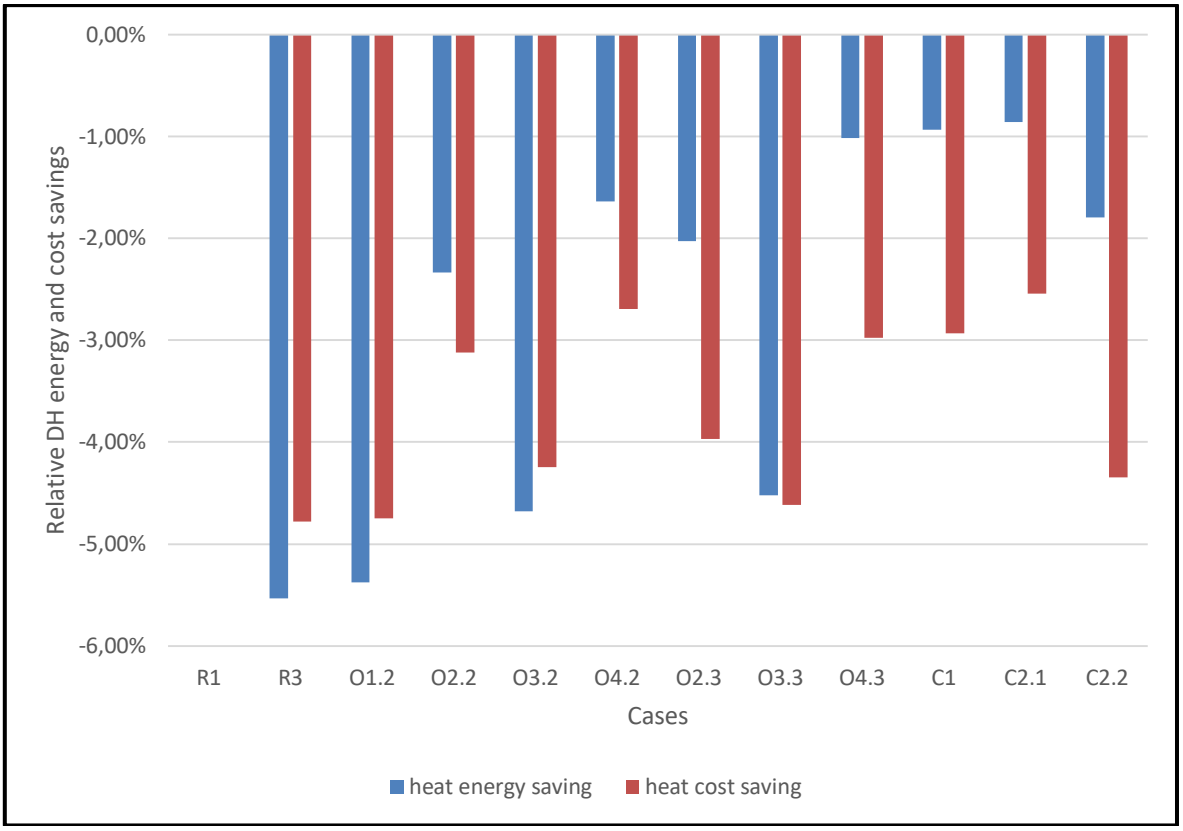

Figure 34. Relative district heating energy and cost savings in the O and C cases compared to the reference case R1.

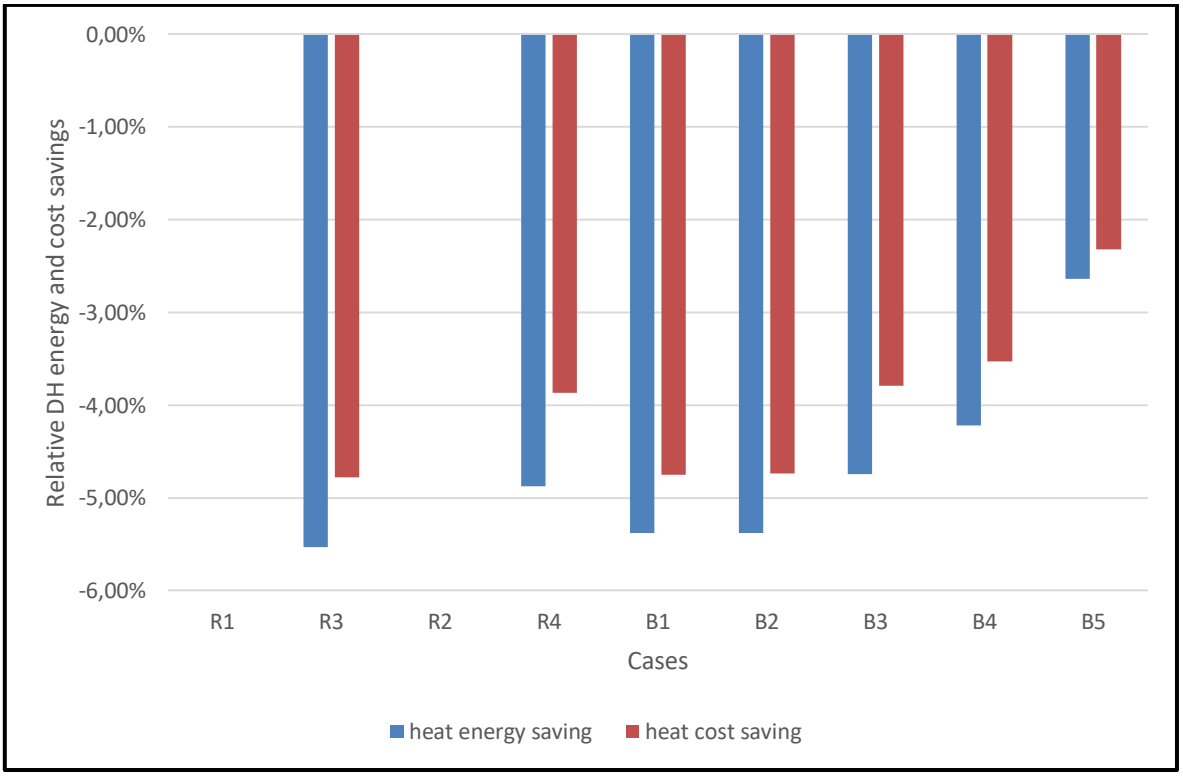

Figure 35. Relative energy and cost savings in the cases R3, B1, B2 compared to the reference case R1 and in the cases R4, B3, B4, B5 compared to the reference case R2.

Figure 36 and 37 present the heating energy consumption and heating cost divided to the hourly district heating price ranges (HDHP), respectively. Only the cases R1, O1.2, O2.3, O3.3 and C2.2 are depicted. Figure 36 shows that cost optimized cases O1.2 and O3.3 decreased the energy consumption in all the price ranges compared to R1. The energy flexibility optimized cases O2.3 and C2.2 used least energy during the top price range. In addition, these cases consumed a bit more heating energy during the 3rd cheapest (30<HDHP<40) price range. Similar notices and trends can be seen in Figure 37 where the simulated costs were divided to price ranges.

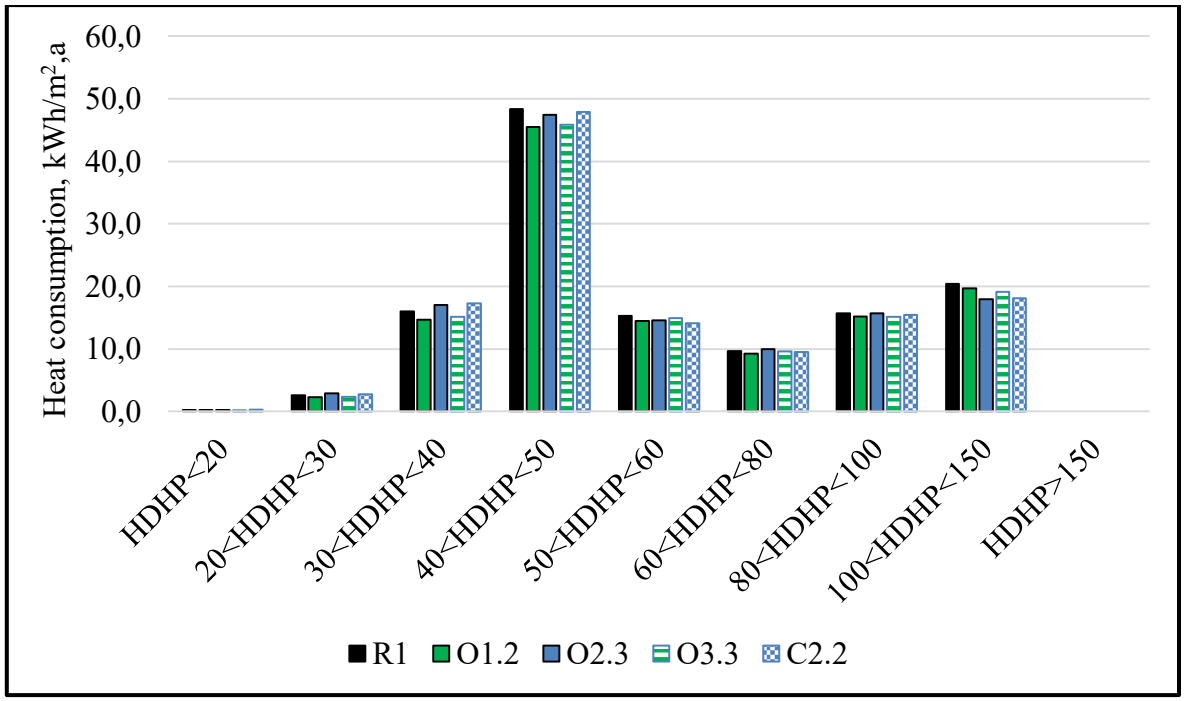

Figure 36. District heating energy consumption divided to hourly district heating price (HDHP) ranges for one reference case R1 and four DR cases.

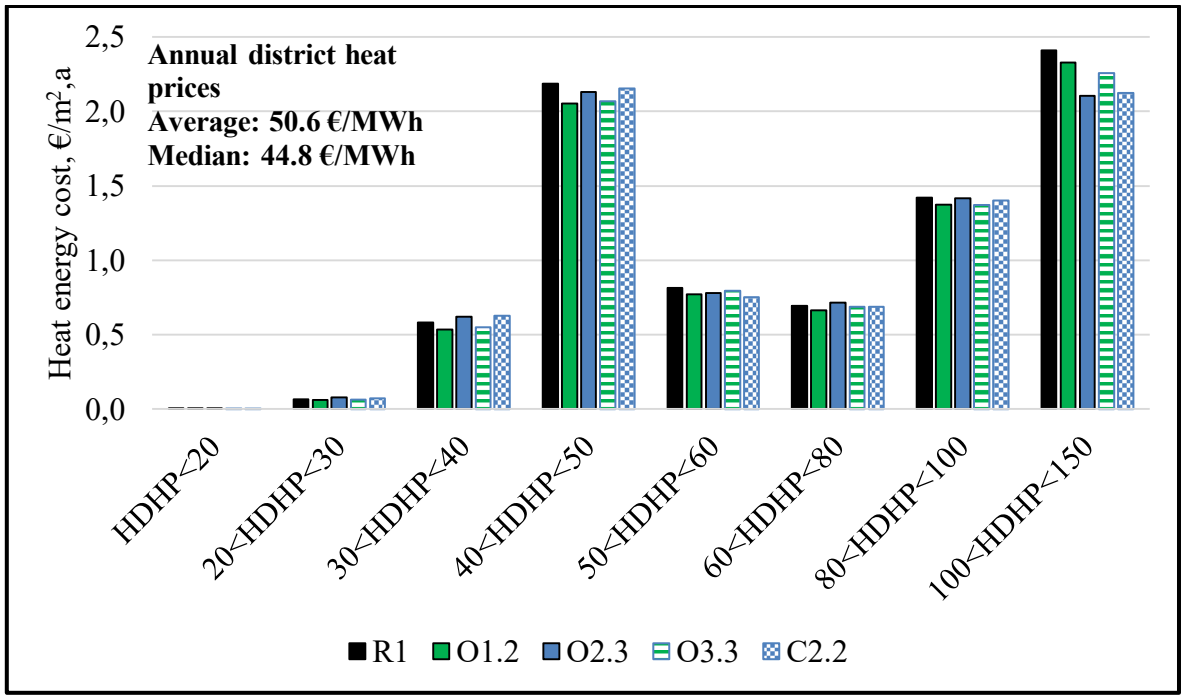

Figure 37. District heating cost divided to hourly district heating price (HDHP) ranges for one reference case R1 and four DR cases.

6.2.2 Energy flexibility

Energy flexibility was investigated by calculating the flexibility factor that was introduced earlier in chapter 3.4.3. Flexibility factor is an indicator that depicts how well the building can share its energy consumption to cheap energy price hours compared to expensive energy price hours. In order to be able to compare all the cases with each other, the flexibility factor was calculated based on 24-hour historical price data in every case.

The flexibility factors for all the cases are shown in Figure 38 and 39. The flexibility factor in the reference cases were a bit under 7%. The highest flexibility factor of 14.2% was obtained with the DR case C2.2. The cases O3.4, C1 and C2.1 had almost as high heating flexibilities. This result is apparent since all the previous cases had energy flexibility as one of the optimization objectives. The cost-optimized DR cases had heating flexibilities only slightly higher than the reference cases. This indicates that the DR control based on cost optimization leads to mainly heat conservation strategy instead of load shifting with higher heating flexibilities.

The cases where both thermal comfort and heating flexibility were optimized resulted in slightly higher flexibility factors compared to the cases where only energy flexibility was optimized. In the other hand, the cases with only energy cost optimization performed better regarding the flexibility factor compared to the cases with both thermal comfort and cost optimization. The longer prediction horizon resulted in higher flexibility factors.

The different midseason temperature setpoint ranges in the cases O4.2, C2.1 and C2.2 did not show major differences in respect of energy flexibility. In addition, the influence from the altered versus original supply air temperature curve seemed not to affect the energy flexibility (the cases O4.3 and C1).

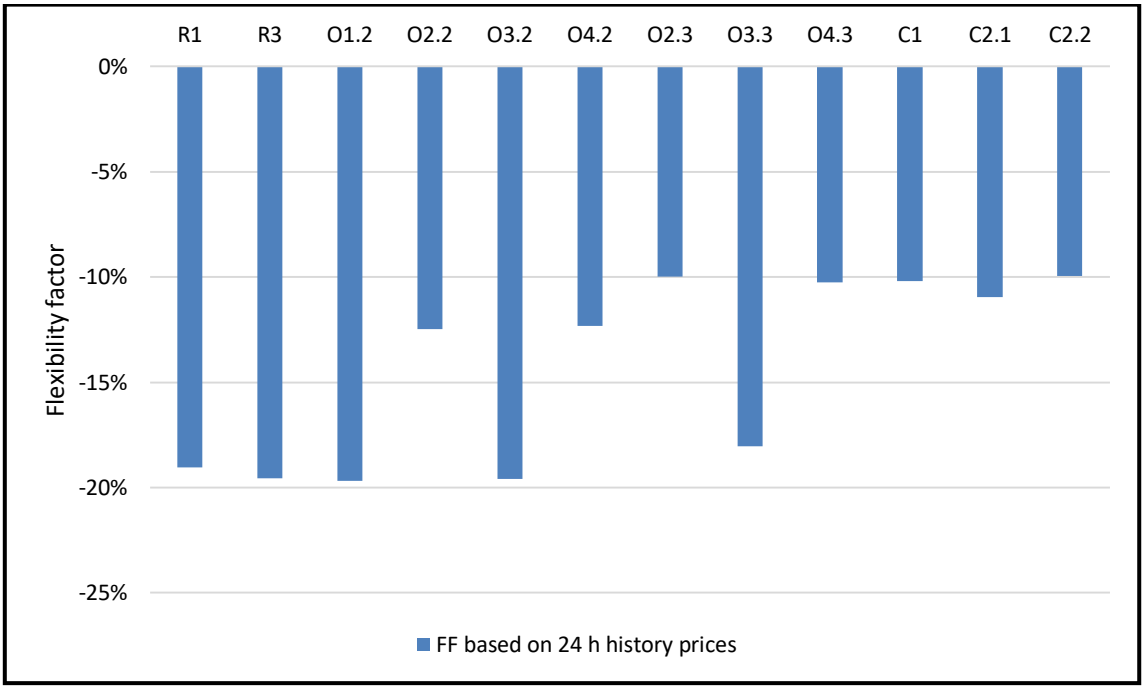

Figure 38. Flexibility factors in the O and C cases calculated based on 24 h historical DH price.

The window restriction had minor effect on the heating flexibility (see Figure 39). Only in the case B5 where the at least 50% heating power from the nominal power was required in the constraint periods, the FF decreased noticeable to under 5% compared to FF close to 7 % in the other cases with window type 2 construction.

Figure 39. Flexibility factors in cases B1-B5 calculated based on 24 historical DH price.

In Figure 40 the flexibility factors calculated from the IDA ICE simulation results and from the calibrated RC-model are compared. The flexibility factors from the RC-model results are calculated separately for the South-West and North-East facades. Generally, it seems that the flexibility factors based on the RC-model results are higher compared to flexibility factors based on the IDA ICE results. This difference might be caused by the level of modelling accuracy in the RC-model. Another trend that is seen from Figure 40 is that the flexibility in the South-West façade is greater than in the North-East façade in all studied cases. One explanation for this could be that the greater solar heat gains in the spaces in South-West façade give more flexibility for the utilization of the buildings thermal mass for the DR purpose.

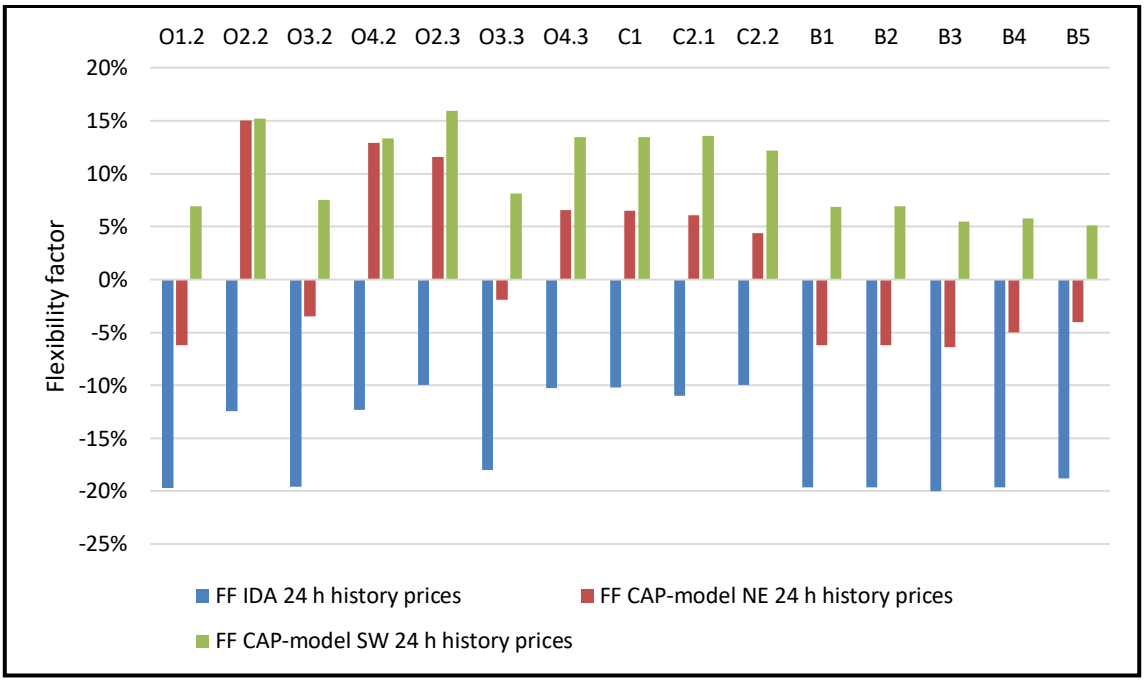

Figure 40. Flexibility factors calculated from CAP-model optimization results (North-East and South-West facades) and IDA-ICE simulation results.

6.2.3 Thermal comfort

Appropriate level of thermal comfort was maintained throughout the year in every DR case. The range of acceptable space heating setpoints guaranteed that the MPC algorithm did not allow setpoints to drop under 20 °C. The temperature of 20 °C is defined as the lowest acceptable operative temperature in occupied spaces according to indoor climate category S2 in the Finnish indoor climate classification (FiSIAQ 2008). The summer time temperatures where not under special interest in this study since only space heating DR was investigated. However, during summer time the maximum heating setpoint of 21 °C guaranteed that no overheating could occur due to demand response.

Thermal comfort is analysed in this thesis by checking the air temperature duration curves of the coldest room in the studied floor in each of the studied cases. In addition, the local thermal comfort where the focus was in avoidance of draught was studied in the window restriction cases B1 to B5.

Indoor air temperature duration curves for the coldest room in the floor (office room 10 in Figure 14) are presented in Figure 41-42. Also, the minimum room air temperatures and cost reductions are shown in these figures. Figure 41 shows the DR cases with the prediction horizon of 12 hours, window type 1 and the corresponding reference cases R1 and R3. The cases with flexibility as one optimization objective (O2.2 and O4.2) resulted in higher indoor air temperatures than the cases where heating cost acted as one objective (O1.2 and O3.2). The duration curves of the cost optimized cases were close to the reference case R3 with constant space heating setpoint 20 °C. This reveals that the cost optimized cases utilized the energy conservation DR strategy. The cases O3.2 and O4.2, where the thermal comfort acted as second optimization objective, resulted in slightly higher indoor temperatures than the cases O1.2 and O2.2 where only heating cost and energy flexibility were optimized, respectively. The effect of the thermal comfort optimization is small because the setpoint

trajectory resulting in lowest energy cost or energy flexibility was chosen from the pareto optimal solutions. Similar conclusion can be drawn from the duration curves with the cases with prediction horizon of 24 hours. Therefore, the prediction horizon has no major influence on the thermal comfort, but it clearly affects the heating cost, energy consumption and energy flexibility as described in previous chapters.

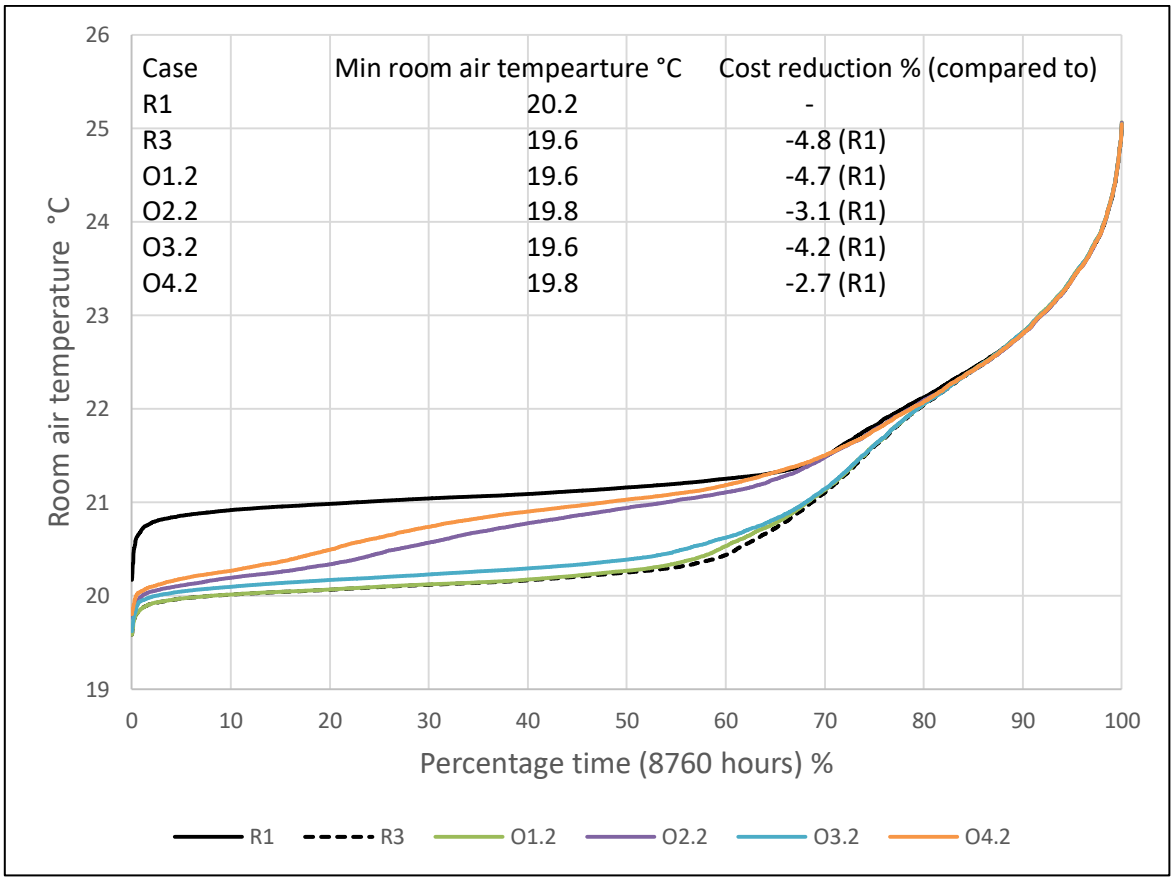

Figure 41. Room air temperature duration curves of the coldest room of the floor (room 10) in the cases R1, R3, O1.2, O2.2, O3.2 and O4.2.

Figure 42 depicts the temperature duration curves of the DR cases O4.3, C1, C2.1 and C2.2 with the prediction horizon of 24 hours and window type 1. The temperature duration curves of the reference cases R1 and R3 are also shown. The difference between the altered and original supply air temperature curves can be investigated by comparing the cases O4.3 (altered curve) and C1 (original curve). Both supply air temperature curves where shown in Figure 16. At the first place, the original curve was modified to guarantee that no concurrent heating and cooling could happen.

The duration curves differ only within the high indoor air temperature range (summer season). The case with original supply air temperature curve has lower temperatures than the case with altered supply air curve. The reason is that with the original curve the supply air temperature was decreased with lower exhaust air temperatures compared to altered curve. In other words, AHU cooling was increased earlier.

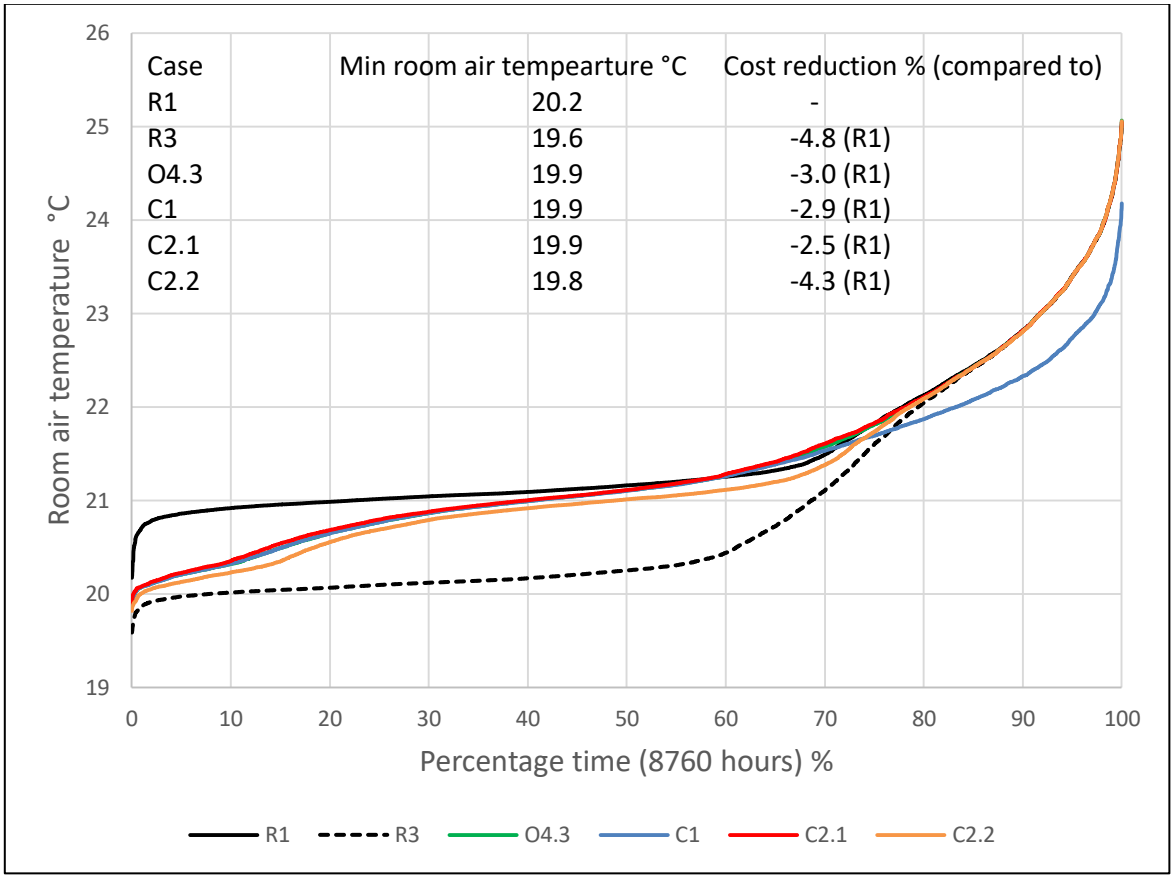

Figure 42. Room air temperature duration curves of the coldest room of the floor (room 10) in the cases R1, R3, O4.3, C1, C2.1 and C2.2.

The varying allowed midseason space heating temperature setpoint ranges were studied in the cases O4.3, C2.1 and C2.2 (Figure 42). The allowed ranges during the midseason (outdoor air temperature between -10 °C and 0 °C) in the cases O4.3, C2.1 and C2.2 were the following [20-23] °C, [20-24.5] °C and [20-21] °C. No major difference is seen in the air temperatures of the coldest room between the different midseason setpoint ranges in Figure 42. Although the heating setpoint was allowed to increase above 21 °C in cases O4.3 and C2.1, the optimization did not lead to increased setpoints and heat loading into the building mass. It can thus be concluded that the heat loading is not feasible in this case building.

The indoor air temperature duration curves of the coldest room are shown in Figure 43 for the window surface restriction cases and the corresponding reference cases. The duration curves from the cases B1 and B2 with the window type 1 are close to each other and thus the 30% power constraint applied in the case B2 had no effect to the indoor air temperatures. The cases with window type 2 (B3, B4 and B5) showed small variations in the indoor air temperatures. B3 without and B4 with 30% heating power requirement were still close to each other but the 50% power requirement during the restricted hours lead to increased indoor air temperatures. The higher heat losses in the cases with window type 2 resulted also in higher indoor air temperatures at the high end part of the duration curve (summer time).

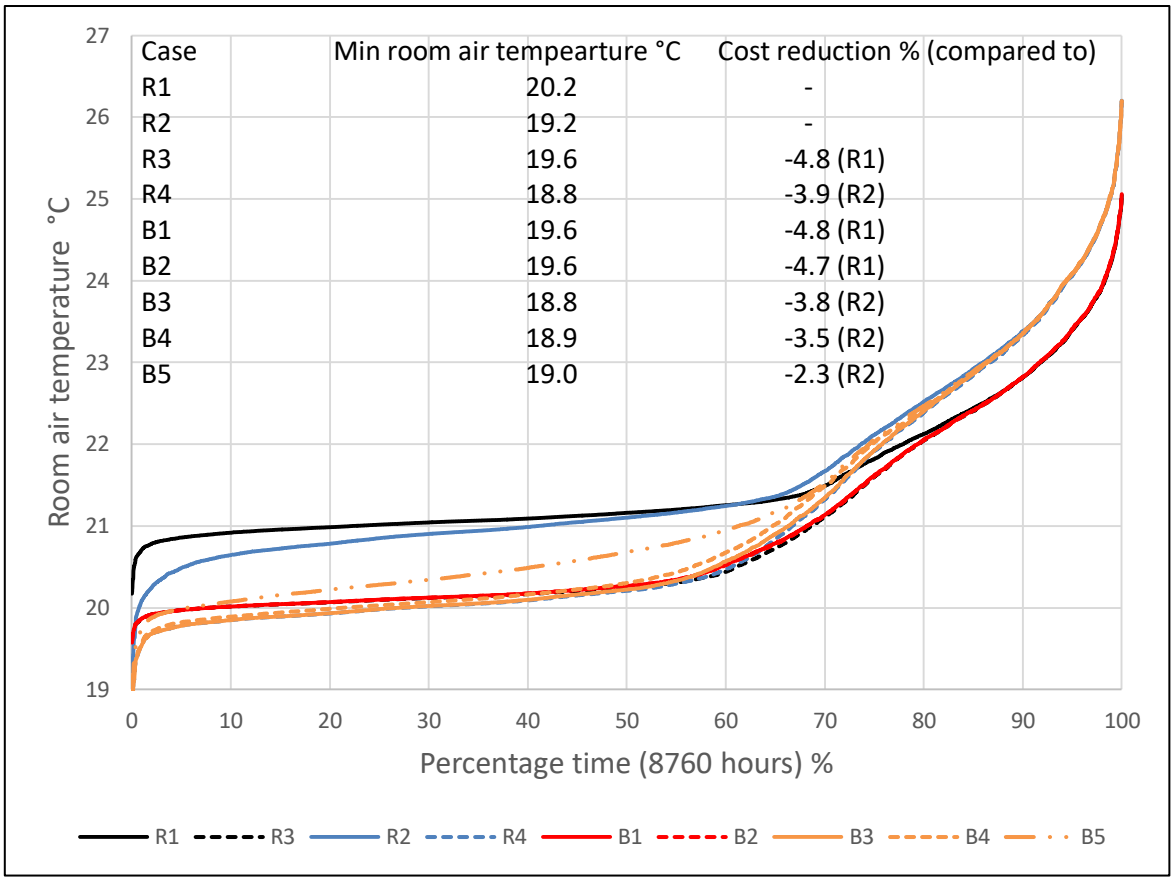

Figure 43. Room air temperature duration curves of the coldest room of the floor (room 10) in the cases R1-R4, B1-B5.

6.2.4 Original and altered supply air temperatures

The differences in the AHU cooling and heating power can further be studied by analysing the Figure 44 where the data from the cases C1 and O4.3 are depicted. The AHU cooling power is greater in the original supply air curve (case C1) during the summer months. This did not affect the demand response potential as was seen in previous chapters, but it succeeds in maintaining lower indoor air temperatures during summer time seen in the duration curves. In addition, no concurrent AHU cooling and space heating occurred with either altered or original supply air temperature curve. For these reasons, the original curve could be used throughout the year or the original curve could be changed for the summer months to have more effective cooling of spaces.

Moreover, it can be noticed that the AHU heating difference occurs only during couple of hours in spring and summer. The difference is due to that in altered supply temperature curve the supply air is heated up to constant setpoint 20 °C with higher exhaust air temperatures compared to original supply air curve. As a result, in the cases with altered supply air curve the share of the AHU heating is slightly larger from the total heating power. This difference is however small, and it did not affect significantly the DR potential in respect of flexibility, cost or energy savings.

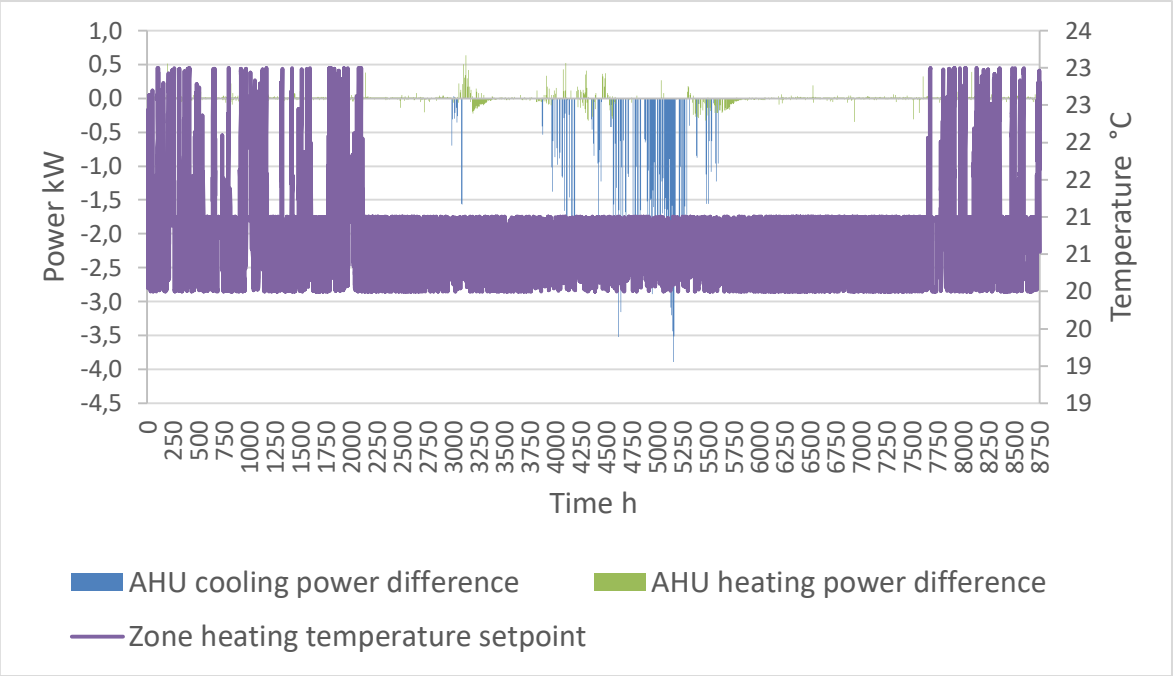

Figure 44. Differences in AHU cooling and heating powers between the two examined supply air temperature curves (original and altered) during entire year.

7 Discussion

7.1 The usability of the MPC algorithm

Implementing space heating demand response with the model predictive control algorithm (MPC) developed in this study succeeded in cutting off the heating energy costs, improving the energy flexibility and maintaining acceptable thermal comfort in spaces. Therefore, the demand response with the MPC has a great potential to achieve the targets of DR in general:

- to decrease the peak load consumption and thus decrease the CO_2 emissions of peak load power plants
- to enable the increasing introduction of RES in the energy system
- to offer cost savings for the building owners and energy companies.

The cost saving potential of the MPC implemented DR is dependent on at least the building characteristics, climate and the local energy markets. In the case building of this study, the maximum heating energy cost savings were only about 5% when compared to the reference case. The relatively low cost savings may have resulted from several issues for example:

- high ventilation air flow rates in spaces and partly air based heating
- thermal characteristics of the case building
- the dynamic DH price model.

Since the ratio of the annual AHU heating and space heating was around 50%, the significance of the actions made by the demand response into the space heating were limited. The high ventilation air flow rates prevented the feasibility of the heat loading to the structures, because the heat was flushed away by the ventilation system.

The significance of the building characteristics (mass of the building structures and the overall heat losses) to the potential of the DR is twofold. In well-insulated passive buildings, the shifted, cut, or increased amount of heat load is limited and thus the potential might be smaller than in the poorly insulated buildings. In other hand, the length of the load change can be longer in well-insulated buildings without sacrificing the thermal comfort. In poorly insulated, low weight buildings the overall heating load is high, and thus large amount of heat can be modulated. However, the modulation can't take long since otherwise the thermal comfort is threatened (Le Dreau, Heiselberg 2016). The case building used in this study had heavy weight structures, but the heat losses through the envelope where moderate. Thus, also the heat losses might have limited the energy cost savings, because the heat could not be loaded feasible as considerable share would have been dissipated thought the envelope. As a conclusion the building characteristics have a significant role in the potential of the DR. However, the significance of the building characteristics is further dependant on the dynamic DH pricing (or other pricing models) and climate.

The dynamic DH price is perhaps the most significant single factor influencing the DR potential. The hourly dynamic prices used in this thesis were based on the marginal production costs of a typical Finnish district heating company. Different dynamic prices would result in different potentials. For example, the rate of price changes is crucial factor. If the prices are changing rapidly, the MPC implemented DR might not be able to adjust the heating loads according the fast-changing prices. In other hand, long stable price periods

make the load modulation useless, because no load shifting based cost savings can be obtained.

The local thermal constraint added to the MPC control algorithm could be used to prevent the draught in workstations adjacent to windows. It was showed that the local thermal comfort constraint had only a small influence on the energy cost savings obtained by the DR. Therefore, the thermal comfort constraint can be used as an important part of the DR control, because it can improve the local thermal comfort without having major influences on the heating energy costs.

7.2 Reliability of the results

The reliability of the results depends mainly on the accuracy of the modelled buildings and the accuracy of the input data inserted to the MPC control. The MPC control itself functioned smoothly once the optimization problem was well described. The accuracy of the building model was decreased by modelling only two rooms from the entire floor. The reason for this was that with two building models both representing one room, the large-scale thermal behaviour could be predicted by having still relatively short simulation times. Modelling each room separately would have taken much more time, though the results might have been better. The chosen building model was simple RC-model. The accuracy of the more sophisticated models would have been better, but the time consumed in the modelling would have been greater and the final difference in the DR potential might have been small. The calibration improved the accuracy of the RC-models and increased the reliability of the results.

The most important input data used in the MPC control were the dynamic DH price, forecast of the internal gains and the weather forecast. All of these have a major influence on the reliability of the DR results. In this study, it was assumed that the weather and the internal gain forecasts were realized in 100 % accuracy. If errors would occur between the forecasted and realized data, the DR potential could be decreased. In the future, analysis should be performed to estimate the influence of the accuracy of the forecasted weather and internal gains to the overall DR potential.

The result from this thesis were of the same magnitude than in the earlier master's thesis written by (Martin 2017) where the rule-based DR was tested with IDA ICE simulations of the same case building. This indicates that the potential of DR in this case building is well-founded and in other hand almost equal potential was found with both rule-based and model-based DR methods.

The differences between the two DR methods: rule-based and model-based methods is mostly in the ease of use and control possibilities they offer. The rule-based control method is easier to define and use, because no building model needs to be created. The MPC control is more complicated and takes more time to create. However, it offers some additional control features because the model can be easily used to add control functions for example the control of the local thermal comfort as was done in this thesis. Once the MPC algorithm is created, the ease of its usage is mainly dependant on the number of modifications that are made to the building that would require updates in the building model. Reinforced learning based control algorithms could be more flexible to changes but even these models need to be updated if the geometry of the spaces is modified.

7.3 Future research topics

The future research could be focused to study the DR control with the MPC algorithm in different building types. Since the buildings differ in numerous ways the results from the studies performed in only one building type can't be expanded to cover all the other building types.

Sensitivity analysis could be performed to study the influence of the accuracy of the input data to the overall DR potential. For example, the influence from the error in the weather forecast and internal gain forecast on the DR potential could be investigated.

To increase the use of DR in buildings, more pilot tests should be performed where the DR is utilized in actual buildings. The MPC control algorithm developed in this thesis could also be tested in real-life buildings, for example in the case building of this study, where the algorithm has already been tested with simulations.

In the end, the breakthrough of the DR utilization in buildings would require that the energy companies would, in co-operating with the building owners and authorities, develop the pricing models that would support the DR utilization and would share the benefits between the stakeholders fairly. Currently, the state of development in the DR of electricity is far ahead compared to the DR of district heating.

8 Conclusions

The main objective of this thesis was to define the potential of space heating demand response in the perspective of local thermal comfort, cost savings and energy flexibility in an educational office building heated by district heating. The case building located in the Aalto University campus area in Finland. The space heating demand response was studied with an MPC control algorithm developed in this thesis. The focus was put to the decentralized space heating demand response because the results from the earlier study in this case building showed that the decentralised control yield higher energy cost savings compared to centralized control. The MPC algorithm was tested with number of demand response cases by performing IDA ICE simulations. The hourly dynamic district heating price based on the marginal costs of heat production in Finland was used in this study.

The second research question dealt with the local thermal discomfort due to draught that could occur during the DR implementation in the workstations adjacent to windows. The hypothesis was that convective downward airflows might developed and cause draught if the window surface temperature is low and at the same time the heating power from the water radiators below the windows is reduced by the DR control. Thermal manikin measurements were conducted to study this phenomenon in one office room in the same case building.

The thermal manikin measurements showed that the draught risk was increased in the workstations adjacent to windows if the window surface temperature dropped below 15 °C while the heating was turned OFF. Therefore, it is suggested that a window surface temperature restriction should be used in the decentralized DR to force the space heating ON whenever the window surface temperature drops below the restrictive temperature of 15°C. The outdoor air temperature limit, when the restrictive window surface temperature is reached, is dependent on the window construction. The outdoor air temperatures below which the radiator heating should be forced on were calculated in this thesis with different window constructions. Furthermore, a window surface temperature constraint with two different heating power requirements were added in the MPC algorithm to investigate the influence of the window surface temperature constraint on the heating energy cost savings and energy flexibility obtained by the DR.

The results from the MPC implemented DR simulation in IDA ICE showed that in all the studied cases the heating energy costs could be reduced compared to the reference case with the constant space heating setpoint of 21 °C. Moreover, the heating energy flexibility described by the flexibility factor was either equal or higher in the DR cases. Acceptable thermal comfort was maintained in all the studied cases.

The studied DR cases included the investigation of different optimization objectives and different lengths of the prediction horizon. The cases where the heating energy cost acted as one objective lead to utilization of heat conservation DR strategy whereas cases including heating flexibility as objective lead to utilization of load shifting DR strategy. The highest heating energy cost savings (-4.7%) was obtained when the total heating energy costs were optimized and the highest energy flexibility (14%) was obtained when the energy flexibility was optimized with the thermal comfort objective. The case with the highest energy flexibility resulted in almost equal cost savings than in the cost optimized case (-4.3%). The

reference case, where heat was conserved by having constant space heating temperature setpoint of 20 °C throughout the year, resulted only slightly higher heating energy cost savings (-4.8%). The longer prediction horizon in the MPC control increased both the energy cost savings and energy flexibility.

Adding the thermal comfort as a second objective resulted in slightly higher indoor air temperatures (and better thermal comfort) compared to cases where only either heating energy costs or heating energy flexibility was optimized. As a result, the heating energy cost savings dropped slightly. When both energy flexibility and thermal comfort was optimized, the energy flexibility increased compared to cases optimizing only energy flexibility. When optimizing both energy cost and thermal comfort the result was opposite, and the energy flexibility decreased slightly compared to cases where only energy cost was optimized.

The optimization with different space heating setpoint ranges (during the midseason) showed that the heat loading was not feasible in the case building. Even if, the setpoints higher than 21 °C were allowed, the cost nor energy flexibility optimization did seldom find it feasible, in respect of optimization objectives, to use setpoints higher than 21 °C. The reason for this is probably the relatively large ventilation air flow rates in the case building. The heat loaded in the structures would be flushed away by the ventilation and thus the heat loading is not feasible.

The acceptable level of thermal comfort was maintained in the studied cases mostly because the space heating setpoint range was set so that it did not allow setpoint temperatures below 20 °C. In addition, the maximum setpoint temperature of 21 °C was set during the summer time to prevent overheating of spaces.

The study of local thermal comfort constraint was performed with two different window constructions and with two different maximum power requirements during the restricted hours. The influence from the window surface temperature restriction on the demand response potential was found to be small. With the better window type, the influence on the energy cost savings and energy flexibility was insignificant with both heating power requirements. With the poorer windows, the influence was neglectable with the lower heating power requirement. With the higher heating power requirement, the energy cost saving, and energy flexibility potential of DR was decreased somewhat. However, the local thermal comfort measurement showed that even small heating power was sufficient to block the convective downdraught and thus maintain acceptable local thermal comfort level in the space. Therefore, it may be concluded that the local thermal comfort restriction in demand response has higher influence on the cost savings when the building has non-energy-efficient windows. However, even with poor energy efficiency windows, the DR potential is not decreased significantly, because only small increase in the heating power is required during the restricted hours.

References

Aalto University. 2018. Otakaari 4, case building. [Online]. [Cited 15.10.2018]. Available from: https://www.aalto.fi/fi/sijainnit/otakaari-4.

Aalto University. 2015. Aalto University campus - architecture and history. [Online]. [Cited 22.8.2018]. Available from: http://www.aalto.fi/fi/about/campus/.

ABB. 2016. An introduction to smart grids. [Online]. Helsinki, Finland: ABB. Available from: https://mycourses.aalto.fi/mod/folder/view.php?id=152677.

Afram, A. and Janabi-Sharifi, F. 2014. Theory and applications of HVAC control systems–A review of model predictive control (MPC). Building and Environment. [Online]. Vol. 72, pp. 343-355. [Cited 25.10.2018]. ISSN 0360-1323. DOI 10.1016/j.buildenv.2013.11.016.

Alimohammadisagvand, B. 2018. Influence of demand response actions on thermal comfort and electricity cost for residential houses. Doctoral Dissertation. Aalto University, Department of Energy Technology. Espoo.

Alimohammadisagvand, B., Jokisalo, J. and Sirén, K. 2018. Comparison of four rule-based demand response control algorithms in an electrically and heat pump-heated residential building. Applied Energy. [Online]. Vol. 209, pp. 167-179. [Cited 25.10.2018]. ISSN 0306-2619. DOI 10.1016/j.apenergy.2017.10.088.

ASHRAE. 2013. ASHRAE handbook : Fundamentals Chapter 9. Inch-pound edition ed. Atlanta, USA: Ashrae. pp. 16. ISBN 9781628705348.

ASHRAE 55. 2004. Thermal environmental conditions for human occupancy. Atlanta: ANSI - American national standards institute & ASHRE - American Society of Heating, Refrigerating, and Air-Conditioning Engineers. pp. 30.

Babiak, J., Olesen, B.W. and Petras, D. 2009. Low temperature heating and high temperature cooling: embedded water based surface heating and cooling systems. Brussels, Belgium: Rehva. pp. 108. ISBN 2-9600468-6-2.

Clauß, J., C. Finck, P. Vogler-Finck and P. Beagon. 2017. Control strategies for building energy systems to unlock demand side flexibility–A review. IBPSA Building Simulation 2017. San Francisco, USA. 7.-9.8.2017. Available from: https://researchrepository.ucd.ie/handle/10197/9016.

Corgnati, S.P. and da Silva, M.G. 2011. Indoor Climate Quality Assessment: Evaluation of Indoor Thermal and Indoor Air Quality. Brussels, Belgium: Rehva. pp. 119. ISBN 978-2-930521-05-3.

Dahl Knudsen, M. and Petersen, S. 2016. Demand response potential of model predictive control of space heating based on price and carbon dioxide intensity signals. Energy and Buildings. [Online]. Vol. 125, pp. 196-204. [Cited 25.10.2018]. ISSN 0378-7788. DOI 10.1016/j.enbuild.2016.04.053.

Dahl, M., Brun, A. and Andresen, G.B. 2017. Using ensemble weather predictions in district heating operation and load forecasting. Applied Energy. [Online]. Vol. 193, pp. 455-465. [Cited 25.10.2018]. ISSN 0306-2619. DOI 10.1016/j.apenergy.2017.02.066.

Dear, R.J., Akimoto, T., Arens, E.A., Brager, G., Candido, C., Cheong, K., Li, B., Nishihara, N., Sekhar, S.C. and Tanabe, S. 2013. Progress in thermal comfort research over the last twenty years. Indoor Air. [Online]. Vol. 23, no. 6, pp. 442-461. [Cited 25.10.2018]. ISSN 0905-6947. DOI 10.1111/ina.12046.

Deb, K., Pratap, A., Agarwal, S. and Meyarivan, T. 2002. A fast and elitist multiobjective genetic algorithm: NSGA-II. IEEE Transactions on Evolutionary Computation. [Online]. Vol. 6, no. 2, pp. 182-197. [Cited 22.9.2018]. ISSN 1089-778X. DOI 10.1109/4235.996017.

Deb, K. 2008. Multi objective optimization using evolutionary algorithms. West Sussex, UK: John Wiley and Sons. pp. 515. ISBN 978-0-470-74361-4.

Dounis, A.I. and Caraiscos, C. 2009. Advanced control systems engineering for energy and comfort management in a building environment—A review. Renewable and Sustainable Energy Reviews. [Online]. Vol. 13, no. 6, pp. 1246-1261. [Cited 25.10.2018]. ISSN 1364-0321. DOI 10.1016/j.rser.2008.09.015.

Dräger. 2018. Air current tube model CH216. [Online]. [Cited 5.6.2018]. Available from: https://www.draeger.com/Products/Content/air-flow-tester-pi-9045536-en-gb.pdf.

EN 15251. 2007. Indoor environmental input parameters for design and assessment of energy performance of buildings addressing indoor air quality, thermal environment, lighting and acoustics. Brussels: European Committee for Standardization. pp. 52.

EN ISO 9920. 2007. Estimation of thermal insulation and water vapour resistance of a clothing ensemble. Brussels: CEN, European committee for standardization. pp. 109.

Equa Simulation, A.B. 2010. Validation of IDA Indoor Climate and Energy 4.0 build 4 with respect to ANSI. ASHRAE Standard. [Online]. pp. 140-2004. [Cited 25.10.2018].

European Commission. 2017. Energy efficiency - Buildings. [Online]. [Cited 13.8.2018]. Available from: https://ec.europa.eu/energy/en/topics/energy-efficiency/buildings.

Fanger, P.O. 1970. Thermal comfort. Analysis and applications in environmental engineering. Copenhagen, Denmark: Danish Technical Press. pp. 244. ISBN 0070199159 9780070199156.

FINLEX 948. 2011. Competition act, english translation. Helsinki: Finnish Competition Authority/Ministry of Employment and the Economy. pp. 17.

Finnish energy. 2018. Energiavuosi 2017 - Kaukolämpö
(Energy year 2017 - District heating). [Online]. [Cited 28.8.2018]. Available from: https://energia.fi/ajankohtaista_ja_materiaalipankki/materiaalipankki/energiavuosi_2017_-_kaukolampo.html.

Finnish energy. 2017. Energiavuosi 2016 - Kaukolämpö (Energy year 2016 - District heating). [Online]. [Cited 28.8.2018]. Available from: https://energia.fi/en/news_and_publications/publications/district_heating_statistics.html#material-view.

FiSIAQ. 2008. Finnish indoor climate classification; Sisäilmaluokitus 2008– tarpeenmukainen sisäilmasto. Helsinki: pp. 22.

Foda, E. 2012. Evaluating local and overall thermal comfort in buildings using thermal manikins; Paikallisen ja kokonaislämpöviihtyvyyden arviointi rakennuksissa lämpönuken avulla. Doctoral Dissertation. Aalto University, Department of Energy technology. Espoo. pp. 187.

Foda, E. and Sirén, K. 2012. A thermal manikin with human thermoregulatory control: implementation and validation. International Journal of Biometeorology. [Online]. Vol. 56, no. 5, pp. 959-971. [Cited 25.10.2018]. ISSN 0020-7128. DOI 10.1007/s00484-011-0506-6.

Frederiksen, S. and Werner, S. 2013. District heating and cooling. 1.th ed. Lund, Sweden: Studentlitteratur AB. pp. 586. ISBN 978-91-44-08530-2.

Fujitsu. 2014. Product data, Display B23T-6 LED. [Online]. [Cited 19.9.2018]. Available from: https://sp.ts.fujitsu.com/dmsp/publications/public/ds-display-b23t-6-led.pdf.

Fujitsu. 2011. Product data, ESPRIMO E9900 E-Star5. [Online]. [Cited 19.9.2018]. Available from: https://sp.ts.fujitsu.com/dmsp/Publications/public/wp-energy-ESPRIMO-E9900-EStar5.pdf.

Gellings, C.W. 1985. The concept of demand-side management for electric utilities. Proceedings of the IEEE. [Online]. Vol. 73, no. 10, pp. 1468-1470. [Cited 25.10.2018]. ISSN 1558-2256. DOI 10.1109/PROC.1985.13318.

Geminidataloggers. 2018. Tinytag TGP-4500, Temperature and humidity data logger. [Online]. [Cited 19.9.2018]. Available from: https://www.geminidataloggers.com/data-loggers/tinytag-plus-2/tgp-4500.

Goldman, C., Reid, M., Levy, R. and Silverstein, A. 2010. Coordination of energy efficiency and demand response. [Online]. California, USA: Ernest Orlando Lawrence Berkeley National Laboratory. Available from: https://pubarchive.lbl.gov/islandora/object/ir:154063/datastream/PDF/view.

Greensfelder, E.M., Henze, G.P. and Felsmann, C. 2011. An investigation of optimal control of passive building thermal storage with real time pricing. Journal of Building

Performance Simulation. [Online]. Vol. 4, no. 2, pp. 91-104. [Cited 25.10.2018]. ISSN 1940-1493. DOI 10.1080/19401493.2010.494735.

Halton. 2018. THB Supply air diffuser. [Online]. [Cited 23.4.2018]. Available from: https://www.halton.com/dh/BAAHbzfOu8Be4KVk_A0Jk39Lb5kT1l4wmYnfK5oVs8gz5yYx414UaIqJ95FwmLivkaKxhqx-bxY9_Dv789i6rYu8gaTiJTWmcMV9F1g/Halton_THB_-_fi.pdf.

Härkönen, P., Mikkola, J., Piikkilä, V., Sahala, A., Sahlstén, T., Sandström, B., Sirviö, A., Spangar, T. and Sulku, J. 2012. Rakennusautomaatiojärjestelmät, ST-käsikirja. 3rd ed. Espoo, Finland: Sähköinfo Ry. pp. 285. ISBN 978-952-231-059-0.

Helin, K., Syri, S. and Zakeri, B. 2018. Improving district heat sustainability and competitiveness with heat pumps in the future Nordic energy system. Energy Procedia. [Online]. Vol. 149, pp. 455-464. [Cited 25.10.2018]. ISSN 1876-6102. DOI 10.1016/j.egypro.2018.08.210.

Holland, J.H. 1992. Adaptation in natural and artificial systems: an introductory analysis with applications to biology, control, and artificial intelligence. Cambridge, UK: MIT Press. pp. 211. ISBN 0-262-08213-6. Available from: https://aalto.finna.fi/Record/vaari.1918563.

Holmer, I. 2004. Thermal manikin history and applications. European Journal of Applied Physiology. [Online]. Vol. 92, no. 6, pp. 614-618. [Cited 22.5.2018]. ISSN 1439-6319. DOI 10.1007/s00421-004-1135-0.

IEA. 2018. EBC Annex 67, Review of applied and tested control possibilities for energy flexibility in buildings. [Online]. International Energy Agency. Available from: http://www.annex67.org/publications/reports/.

IEA. 2015. Building Energy Performance Metrics [Online]. [Cited 13.8.2018]. Available from: https://webstore.iea.org/building-energy-performance-metrics.

ISO 7726. 1998. Ergonomics of the Thermal Environment: Instruments for Measuring Physical Quantities. Brussels: International Organization for Standardization. pp. 59.

ISO 7730. 2005. Ergonomics of the thermal environment. Analytical determination and interpretation of thermal comfort using calculation of the PMV and PPD indices and local thermal comfort criteria. Helsinki: Finnish standards association SFS. pp. 55.

Jokinen, E. 2013. Kysyntäjousto kaukolämmitetyissä kiinteistöissä; Demand response within district heating heated buildings. Master's Thesis. Aalto University, Department of Energy Technology. Espoo. pp. 78.

Jylhä, K., Kalamees, T., Tietäväinen, H., Ruosteenoja, K., Jokisalo, J., Hyvönen, R., Ilomets, S., Saku, S. and Hutila, A. 2011. Rakennusten energialaskennan testivuosi 2012 ja arviot ilmastonmuutoksen vaikutuksista. Helsinki, Finland: Ilmatieteen laitos. pp. 110. ISBN 978-951-697-756-3.

Karjalainen, S. 2008. The characteristics of usable room temperature control; Huonelämpötilan hallinnan käyttöliittymät. Käytettävyyden tarkasteluja toimistoympäristössä. Doctoral Dissertation. Aalto University, Faculty of Information and Natural Sciences. Espoo. pp. [71].

Kärkkäinen, S., Sipilä, K., Pirvola, L., Esterinen, J., Eriksson, E., Soikkeli, S., Nuutinen, M., Aarnio, H., Schmitt, F. and Eisgruber, C. 2003. Demand side management of the district heating systems. VTT Research Notes. [Online]. Vol. 2247, pp. 104. [Cited 25.10.2018]. ISSN 1455-0865. Available from: https://www.vtt.fi/inf/pdf/tiedotteet/2004/T2247.pdf.

Kensby, J., Truschel, A. and Dalenbäck, J.-. 2015. Potential of residential buildings as thermal energy storage in district heating systems - Results from a pilot test. Applied Energy. [Online]. Vol. 137, pp. 773-781. [Cited 28.5.2018]. ISSN 0306-2619. DOI 10.1016/j.apenergy.2014.07.026.

Kontu, K. 2015. District heating and cooling as part of smart energy systems. Licentiate Thesis. Aalto University, Department of Energy Technology. Espoo. pp. 111.

Korkas, C.D., Baldi, S., Michailidis, I. and Kosmatopoulos, E.B. 2016. Occupancy-based demand response and thermal comfort optimization in microgrids with renewable energy sources and energy storage. Applied Energy. [Online]. Vol. 163, pp. 93-104. [Cited 25.10.2018]. ISSN 0306-2619. DOI 10.1016/j.apenergy.2015.10.140.

Koskelainen, L., Saarela, R. and Sipilä, K. 2006. Kaukolämmön käsikirja; Handbook of district heating. Helsinki, Finland: Energiateollisuus ry. pp. 566. ISBN 952-5615-08-1.

Kosonen, R. 2017. Course material: Comfortable and healthy indoor environment. Espoo, Finland: Aalto University.

Kropf, S. and Zweifel, G. 2001. Validation of the Building Simulation Program IDA-ICE According to CEN 13791 “Thermal Performance of Buildings–Calculation of Internal Temperatures of a Room in Summer Without Mechanical Cooling–General Criteria and Validation Procedures”. Hochschule Technik Architektur Luzern.HLK Engineering. [Online]. pp. 24. [Cited 25.10.2018]. Available from: http://www.equaonline.com/iceuser/validation/ICE_vs_prEN%2013791.pdf.

Kusiak, A., Tang, F. and Xu, G. 2011. Multi-objective optimization of HVAC system with an evolutionary computation algorithm. Energy. [Online]. Vol. 36, no. 5, pp. 2440-2449. [Cited 25.10.2018]. ISSN 0360-5442. DOI //doi-org.libproxy.aalto.fi/10.1016/j.energy.2011.01.030.

Le Dreau, J. and Heiselberg, P. 2016. Energy flexibility of residential buildings using short term heat storage in the thermal mass. Energy. [Online]. Vol. 111, pp. 991-1002. [Cited 25.10.2018]. ISSN 0360-5442. DOI 10.1016/j.energy.2016.05.076.

Logenthiran, T., Srinivasan, D. and Shun, T.Z. 2012. Demand side management in smart grid using heuristic optimization. IEEE Transactions on Smart Grid. [Online]. Vol. 3, no. 3, pp. 1244-1252. [Cited 25.10.2018]. ISSN 1949-3053. DOI 10.1109/TSG.2012.2195686.

Martin, K. 2017. Demand response of heating and ventilation within educational office buildings; Efterfrågeflexibilitet inom uppvärmning och ventilation i pedagogiska kontorsbyggnader. Master's Thesis. Aalto University, Department of Energy Technology. Espoo. pp. 124.

Matlab. 2018. MATLAB Documentation - MathWorks Nordic. [Online]. [Cited 11.10.2018]. Available from: https://se.mathworks.com/help/matlab/index.html.

Maula, H. 2017. Effects of Indoor Climate on Occupants' Perception and Work Performance in Office Environment. Doctoral dissertation. Aalto University, Department of Mechanical Engineering. Espoo. pp. 72+54.

McCartney, K.J. and Humphreys, M.A. 2002. Thermal comfort and productivity. Proceedings of Indoor Air. [Online]. Vol. 2002, pp. 822-827. [Cited 25.10.2018]. Available from: https://www.irbnet.de/daten/iconda/CIB6441.pdf.

Naidu, D.S. and Rieger, C.G. 2011. Advanced control strategies for heating, ventilation, air-conditioning, and refrigeration systems—An overview: Part I: Hard control. HVAC&R Research. [Online]. Vol. 17, no. 1, pp. 2-21. [Cited 25.10.2018]. ISSN 1078-9669. DOI 10.1080/10789669.2011.540942.

National building code of Finland. 2012. Part D5, Calculation of power and energy needs for heating of buildings 2012. pp. 74.

Nilsson, H.O. 2007. Thermal comfort evaluation with virtual manikin methods. Building and Environment. [Online]. Vol. 42, no. 12, pp. 4000-4005. [Cited 25.4.2018]. ISSN 0360-1323. DOI 10.1016/j.buildenv.2006.04.027.

Nilsson, H.O. and Holmer, I. 2003. Comfort climate evaluation with thermal manikin methods and computer simulation models. Indoor Air. [Online]. Vol. 13, no. 1, pp. 28-37. [Cited 15.4.2018]. ISSN 0905-6947. DOI 10.1034/j.1600-0668.2003.01113.x.

Ormandy, D. and Ezratty, V. 2012. Health and thermal comfort: From WHO guidance to housing strategies. Energy Policy. [Online]. Vol. 49, pp. 116-121. [Cited 25.10.2018]. ISSN 0301-4215. DOI 10.1016/j.enpol.2011.09.003.

Palensky, P. and Dietrich, D. 2011. Demand side management: Demand response, intelligent energy systems, and smart loads. IEEE Transactions on Industrial Informatics. [Online]. Vol. 7, no. 3, pp. 381-388. [Cited 25.10.2018]. ISSN 1551-3203. DOI 10.1109/TII.2011.2158841.

Palonen, M., M. Hamdy and A. Hasan. 2013. MOBO a new software for multi-objective building performance optimization. Proceedings of the 13th Internationcal Conference of the IBPSA. Chambery, France. 26.-28.8.2013. pp. 2567-2574.

Pérez-Lombard, L., Ortiz, J. and Pout, C. 2008. A review on buildings energy consumption information. Energy and Buildings. [Online]. Vol. 40, no. 3, pp. 394-398. [Cited 25.10.2018]. ISSN 0378-7788. DOI 10.1016/j.enbuild.2007.03.007.

Pöyry Management Consulting Oy. 2016. Kaksisuuntaisen kaukolämmön liiketoimintamallit (Business models for bidirectional district heating). [Online]. Helsinki: Energiateollisuus ry; Sitra. Available from: https://www.sitra.fi/julkaisut/kaksisuuntaisen-kaukolammon-liiketoimintamallit/.

Purmo. 2018. Purmo compact, heat output calculator. [Online]. [Cited 23.4.2018]. Available from: http://www.purmo.com/fi/tuotteet/vesikiertoiset-radiaattorit/paneeliradiaattorit/purmo-compact.htm#tab-lataukset.

Rinne, S. 2017. Dynamical pricing of district heating and electricity in Finland. [Adapted from Kristian Martin's Master's thesis]. [Cited 25.9.2018]. Available from: https://aaltodoc.aalto.fi/handle/123456789/29149.

Salmi, W. 2017. Cost optimised demand response strategies with air-conditioning in office buildings; Ilmastoinnin kustannusoptimoidut kysyntäjoustostrategiat toimistorakennuksissa. Master's Thesis. Aalto University, Department of Mechanical Engineering. Espoo. pp. 74 + 3.

Salo, S. 2018. Fourdeg smart heating, company and service description. [Online]. [Cited 20.4.2018]. Available from: https://fourdeg.com/.

Salo, S. 2016. Predictive demand-side management in district heating and cooling connected buildings; Ennustava kysyntäjousto kaukolämmitetyissä ja -jäähdytetyissä kiinteistöissä. Master's Thesis. Aalto University, Department of Energy Technology. Espoo. pp. 97+6.

Salpakari, J., Mikkola, J. and Lund, P.D. 2016. Improved flexibility with large-scale variable renewable power in cities through optimal demand side management and power-to-heat conversion. Energy Conversion and Management. [Online]. Vol. 126, pp. 649-661. [Cited 25.10.2018]. ISSN 0196-8904. DOI 10.1016/j.enconman.2016.08.041.

Sarasti, J. 2017. Evaluation of load shifting potential in Espoo district heating network using a model predictive approach; Kysynnän siirron potentiaalin arvioiminen Espoon kaukolämpöverkossa malliperusteisella ennustavalla ohjauksella. Master's Thesis. Aalto University, Department of Energy Technology. Espoo. pp. 94+6.

Sarvaranta, A., Jääskeläinen, J., Puolakka, J. and Kouri, P. 2012. Kaukolämmön hinnoittelun nykytila ja tulevaisuuden mahdollisuudet; Current pricing of district heating and the future possibilities. Espoo, Finland: ÅF-Consult. Available from: http://docplayer.fi/1155236-Kaukolammon-hinnoittelun-nykytila-ja-tulevaisuuden-mahdollisuudet.html.

Seppänen, O. 1995. Rakennusten lämmitys. Helsinki: Suomen LVI-yhdistysten liitto ry. pp. 467. ISBN 951-97233-1-5.

Seppänen, O., Fisk, W.J. and Lei, Q.H. 2006. Effect of temperature on task performance in office environment. [Online]. California, USA: Lawrence Berkeley National Laboratory. Available from: https://escholarship.org/uc/item/45g4n3rv#main.

SFS-EN 442-2. 2015. Radiators and convectors. Part 2: Test methods and rating. Helsinki: Finnish standards association SFS. pp. 80.

Shan, K., Wang, S., Yan, C. and Xiao, F. 2016. Building demand response and control methods for smart grids: A review. Science and Technology for the Built Environment. [Online]. Vol. 22, no. 6, pp. 692-704. [Cited 25.10.2018]. ISSN 2374-4731. DOI 10.1080/23744731.2016.1192878.

Sihvonen, S. 2017. Optimization of demand response control strategies in Finnish city-owned buildings; Kysyntäjouston ohjausstrategioiden optimointi suomalaisissa kaupungin omistamissa kiinteistöissä. Master's Thesis. Aalto University, Department of Energy Technology. Espoo. pp. 97+9.

Sirén Kai. 2016a. Course material: A simple model for the dynamic computation of building heating and cooling demand. Espoo, Finland: Aalto University.

Sirén Kai. 2016b. Course material: Building energy optimization - A short introduction to building energy optimization. Espoo, Finland: Aalto University.

Statistics Finland. 2017. Energy in Finland 2017. [Online]. Helsinki, Finland: Statistics Finland. Available from: http://www.stat.fi/tup/julkaisut/tiedostot/julkaisuluettelo/yene_efp_201700_2017_16860_net.pdf.

Stephan, W. 1986. System simulation. Specification: Radiator International Energy Agency, Annex. Vol. 10. [Cited 17.7.2018].

Tanabe, S., H. Zhang, E.A. Arens, T.L. Madsen and F.S. Bauman. 1994. Evaluating thermal environments by using a thermal manikin with controlled skin surface temperature. ASHRAE Transactions. New Orleans, USA. 23.-26.1.1994. pp. 39-48. ISSN 0001-2505. Available from: https://www.scopus.com/inward/record.uri?eid=2-s2.0-0028698624&partnerID=40&md5=03fe4ab54980207736692c7a7638712b.

Tutum, C.C. 2010. Optimization of thermo-mechanical conditions in friction stir welding. Doctoral Dissertation. Technical University of Denmark (DTU), Department of Mechanical Engineering. Copenhagen. pp. 159.

University of California, B. 2017. Center for the Built Environment: Occupant Indoor Environmental Quality (IEQ) Survey. [Online]. [Cited 9.10.2018]. Available from: http://www.cbe.berkeley.edu/research/survey.htm.

Valor Partners Oy. 2015. Kaukolämmön kysyntäjousto, loppuraportti (Demand response of district heating). [Online]. Available from: https://energia.fi/ajankohtaista_ja_materiaalipankki/materiaalipankki/kaukolammon_kysyntajousto_loppuraportti.html.

Vuolle, M. and P. Sahlin. 2000. IDA indoor climate and energy application. Proceedings of Healthy Buildings. Espoo, Finland. 6.-10.8.2000. pp. 523-528. Available from: http://citeseerx.ist.psu.edu/viewdoc/download?doi=10.1.1.16.6574&rep=rep1&type=pdf.

Wargocki, P. and Wyon, D.P. 2017. Ten questions concerning thermal and indoor air quality effects on the performance of office work and schoolwork. Building and Environment. [Online]. Vol. 112, pp. 359-366. [Cited 25.10.2018]. ISSN 0360-1323. DOI 10.1016/j.buildenv.2016.11.020.

World Health Organization. 1990. Indoor environment: health aspects of air quality, thermal environment, light and noise. [Online]. [Cited 23.10.2018]. Available from: http://whqlibdoc.who.int/hq/1990/WHO_EHE_ RUD_90.2.pdf.

WSP Sverige. 2017. Ökad anslutning till Öppen Fjärrvärme, (Increased connections to open district heating network). [Online]. Stockholm, Sweden: City of Stockholm. Available from: http://www.stockholm.se/-/Sok/?q=%c3%96kad+anslutning+till+%c3%96ppen+Fj%c3%a4rrv%c3%a4rme+&uaid=3AF080989574A9811ADCBC136D019B8F:326130333A633738303A363A3232383A3A313438:5248407892962866960.

Appendix 1. A simple heat transfer equation for expanding the window surface restriction to cover different window constructions (Table 21 in chapter 6.1.4).

Heat loss through the window in stationary conditions in measured period P1 (subscript 1) and with examined window situation (subscript 2) are given by equations A1 and A2, respectively. Heat loss equations are formed between the indoor air and the outdoor air temperature node points. Since the conditions are stationary, the equal heat transfer takes place between the indoor air and window inner surface and between the indoor air and the outdoor air temperature node points. The inner heat transfer coefficient is assumed constant and the outdoor heat transfer coefficient is excluded from the inspection.

$$\Phi_1 = A * U_1 * (T_s - T_{e2}) = A * h_i * (T_i - T_{si}) \quad (A1)$$

$$\Phi_2 = A * U_2 * (T_s - T_{e2}) = A * h_i * (T_i - T_{si}) \quad (A2)$$

where

T_{si}	inner window surface temperature [°C]
A	window area [m^2]
T_i	indoor air temperature [°C]
T_{e1}, T_{e2}	outdoor air temperatures [°C]
U_1, U_2	window U-values [W/m^{2}K]
h_i	interior heat transfer coefficient [W/m^2].

The heat transfer rate through the window in the measured period P1 is known. The heat transfer rate with the different window glazings is equal to the measured condition if the indoor air temperature is the same and the window surface temperature is limited to the same value 15 °C. Therefore, the outdoor air temperature with different window glazing can be calculated from the equal heat transfer equations A3 and A4.

$$U_1 * (T_i - T_{e1}) = U_2 * (T_i - T_{e2}) \quad (A3)$$

$$T_{e2} = T_i - \frac{U_1}{U_2} * (T_i - T_{e1}) \quad (A4)$$

When known values from the period P1 are inserted into equation A4 for subscript 1: $U_1 = 1.0 \frac{W}{m^2K}$, $T_{e1} = -7.0$ °C and $T_s = 15$ °C, the window and exterior temperature correlations shown in Table 21 were obtained.